Sea-level change over the northern European continental shelf due to atmospheric and oceanic contributions

Fabio Mangini

Thesis for the degree of Philosophiae Doctor (PhD)
University of Bergen, Norway
2022

UNIVERSITY OF BERGEN

Sea-level change over the northern European continental shelf due to atmospheric and oceanic contributions

Fabio Mangini

Thesis for the degree of Philosophiae Doctor (PhD)
at the University of Bergen

Date of defense: 02.09.2022

Year: 2022

Title: Sea-level change over the northern European continental shelf due to atmospheric and oceanic contributions

Name: Fabio Mangini

Print: Skipnes Kommunikasjon / University of Bergen

Scientific environment

I have carried out this thesis at the Nansen Environmental and Remote Sensing Center (NERSC) in Bergen, Norway, where I was part of the Ocean and Sea Ice Remote Sensing (OSIRS) group. The work was supported by the Research Council of Norway (contract number 272411/F40). I have attended courses provided by the Research School on Changing Climates in the Coupled Earth System (CHESS) and the Geophysical Institute in Bergen. I also joined numerous meetings organized by CHESS and the Bjerknes Centre for Climate Research. I also attended three international conferences, namely the Sea Level Futures Conference in 2018 and the European Geoscience Union (EGU) annual meetings in 2019 and 2020. Finally, at the beginning of 2019, I spent three months at the Department of Meteorology of Stockholm University as a visiting Ph.D. student.

Acknowledgements

Even though the front page of this thesis hosts only my name, more than one person contributed to my Ph.D. Therefore, I would like to take this opportunity to express my gratitude to them.

I would like to begin with Jan Even Øie Nilsen, from whom everything started, for initiating me to such an intriguing yet challenging topic such as sea level. I would like to thank Laurent Bertino for his support, patience, calm, and for always listening to me and being open-minded towards my ideas. I am grateful to Léon Chafik for sharing his passion for oceanography, offering new insights whenever needed, and hosting me in Stockholm. I am also thankful to Camille Li for her significant help on the first paper and for introducing me to the craft of writing.

Even if not officially involved in the project, I feel indebted towards Erica Madonna, for her constant, kind support on the first paper, and Antonio Bonaduce, for his help on the second and third papers and for being there for me every time I needed. I am also thankful for the contribution of Johnny Johannssen and Roshin Raj, who suggested the main idea of the third paper, a project I really enjoyed working on.

I am also grateful to the Nansen Center, not just for its scientifically stimulating environment, but also for its family-like atmosphere, which I liked since I first arrived. In particular, I know I will never work in a place with an admin staff as kind as the one I met here. I am only sorry we are so far apart in the new building!

Finally, I would like to thank my friends, in Italy and abroad, and my family, for sustaining me throughout this journey.

Abstract

Global mean sea level (GMSL) is a key indicator of climate change as it comprises information on different components of the climate system. However, despite its importance for climate and society, GMSL cannot be used for coastal adaptation policies because regional sea-level variations can significantly depart from the global average. Providing accurate estimates of sea-level rise is therefore one of the most important scientific issues that climate change poses, with a large impact for the human population as it is recognized as the main driver for changes in sea-level extremes, influencing the non-linear interactions between processes acting over different temporal and spatial scales in coastal areas.

This thesis addresses different aspects of the sea-level variability over the northern European continental shelf. Paper I uses gridded satellite altimetry data and adopts the jet clusters perspective of the winter-time atmospheric variability over the North Atlantic to reassess the contribution of local winds to the sea-level variability over the northern European continental shelf. By using the jet clusters, Paper I distinguishes itself from the existing literature since the jet clusters provide a physical description of the atmospheric variability in the North Atlantic.

Papers II and III focus on the steric and manometric components of the sea-level over the Norwegian section of the northern European continental shelf and on the sea-level observing system in the region. Paper II first evaluates a coastal altimetry dataset, reprocessed with the ALES-retracker, against the Norwegian set of tide gauges. After showing a good agreement between the two, it exploits the coastal satellite altimetry dataset to reassess the steric component of the sea level over the Norwegian shelf: the paper finds that the estimates of the steric component of the sea-level do not depend much on the choice of the tide gauges or satellite altimetry. Paper III evaluates the sea-level observing system along the Norwegian coast by assessing the ability of a satellite gravimetry mission, the Gravity Recovery and Climate Experiment (GRACE), and of a combination of satellite altimetry and hydrography to monitor manometric sea-level

variations in the region. It then investigates the open-ocean contribution to the inter-annual manometric sea-level variations along the coast of Norway. It shows that, while commonly considered not reliable in the coastal region, GRACE captures the main features of the manometric sea-level change in the area, which on interannual and longer time scales can be attributed to along-slope winds and open-ocean steric changes. Therefore, GRACE can be used to analyze the manometric sea-level variability, such as in sea-level budget studies, especially in those areas of the coastal ocean where in-situ measurements are sparse.

Overall, by focusing on the northern European continental shelf due to its well developed sea-level observing system, this thesis has demonstrated the potential of remote sensing observations in improving our understanding of sea-level variability and change in the coastal ocean.

List of Publications

1. F. Mangini, L. Chafik, E. Madonna, L. Bertino, J. E. Ø. Nilsen. The relationship between the eddy driven jet stream and northern European sea level variability. *Tellus* A, **73**, 1-15 (2021). https://doi.org/10.1080/16000870.2021.1886419.

2. F. Mangini, L. Chafik, A. Bonaduce, L. Bertino, J. E. Ø. Nilsen. Sea-level variability and change along the Norwegian coast between 2003 and 2018 from satellite altimetry, tide gauges and hydrography. *Ocean science*, **18**, 331-359 (2022). https://doi.org/10.5194/os-18-331-2022.

3. F. Mangini, A. Bonaduce, L. Chafik, R. Raj, L. Bertino. Detection and attribution of manometric sea-level variations along the Norwegian coast using GRACE mascon solutions. *Manuscript in preparation*.

Contents

Chapter 1 - Introduction

1.1 Global mean sea-level variations

Global mean sea-level (GMSL) variability is an aspect of climate change with possible significant consequences for society. As such, it continues to attract considerable attention, not only within the scientific community but also among the general public. Despite their uncertainties (MacIntosh et al., 2017), observations provide strong evidence that GMSL has increased during the 20th century (Fig. 1; Church & White, 2011; Jevrejeva et al., 2014; Hay et al., 2015 Dangendorf et al., 2017; Frederikse et al., 2018, 2020), and has accelerated in recent times (Cazenave et al., 2018a; Dangendorf et al., 2019). Climate models further suggest that GMSL will most likely continue to rise over the 21st century (Hu and Bates, 2018), even under very low emission scenarios (Hermans et al., 2021). The projected changes will not only impact coastal ecosystems, but also coastal communities, who might be exposed to coastal erosion, more frequent storm surges, floodings, and saltwater intrusions into the aquifers (Douglas, 2001).

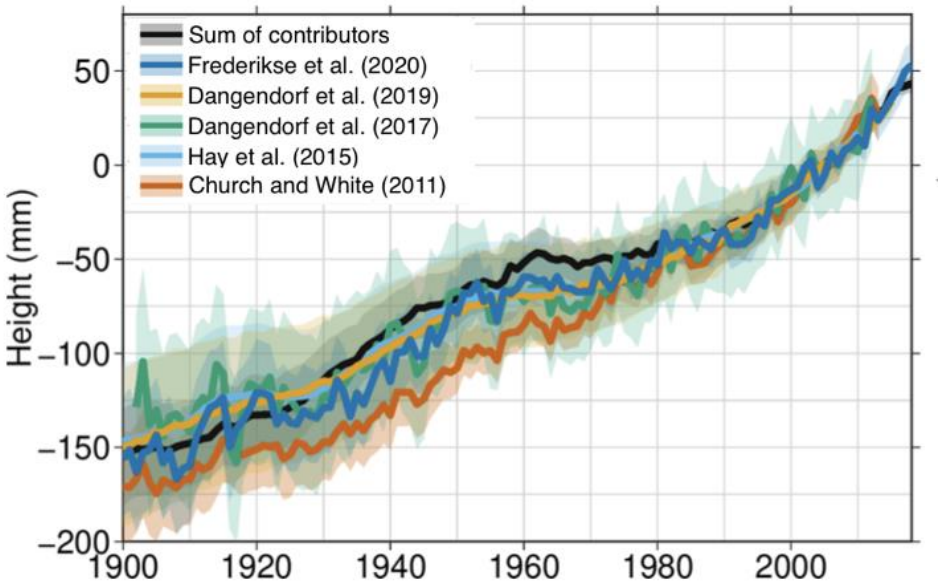

Figure 1: GMSL reconstructions (blue, yellow, green, cyan, and orange lines) and sum of the contributors (thermosteric plus barystatic components) to the GMSL since 1900. Image readapted from Frederikse et al. (2020).

GMSL change results from variations in ocean density and ocean mass. The density-induced and the mass-induced change in GMSL go under the name of steric and barystatic sea-level change, respectively (Gregory et al., 2019). The steric component of sea level primarily results from ocean thermal expansion, whereas the barystatic component of sea level from the melting of land-based ice and variations in terrestrial water storage (Pugh and Woodworth, 2014). Several studies have quantified the different contributions to GMSL change (Gregory et al., 2013; Slangen et al., 2016) to understand the causes behind its variability and to assess the quality of the GMSL reconstructions (Munk, 2002). The research community can now well explain the observed changes since the 1960s (Church et al., 2011), and progress has been made to fully understand the variations during the first half of the 20th century (Frederikse et al., 2020). According to the latest GMSL budget (Frederikse et al., 2020), glaciers explain most of the change since 1900 even though, starting from the 1970s, ocean temperature variation has become the most important driver of GMSL change.

1.2 Regional sea-level variations

While relevant to diagnosing the state of the climate system, the GMSL perspective ignores local sea-level variations. However, when observed from space through satellite altimetry, sea-level trends exhibit a pronounced spatial variability (Fig. 2), and local sea-level variations can significantly depart from the global average (Stammer et al. 2013). Regional sea-level variations are also evident when sea level is measured relative to land (e.g., with tide gauges). For example, in Sweden at Nedre Gävle, sea level has been dropping, relative to land, at a rate of -6.1 mm/year during the last century (Fig. 3). On the contrary, in Tokyo or Bangkok, sea level has been rising at a much faster pace than the global mean sea level, which has been increasing at a rate of 3.1 mm/year over the last two decades (e.g., Nicholls, 2011).

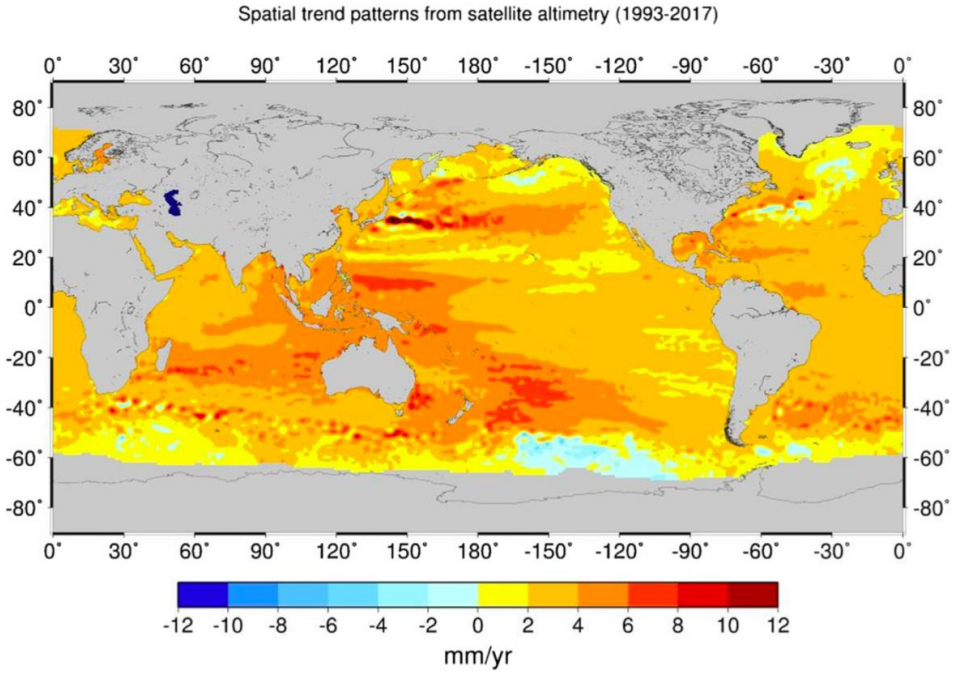

Figure 2: Spatial variation of sea-level trend estimated from satellite altimetry between 1993 and 2017. Being based on satellite altimetry, the sea-level estimates in the figure are not affected by vertical movements of the Earth's crust and do not include the pressure contribution to sea level. Units are mm/year. Image from Cazenave et al. (2018b).

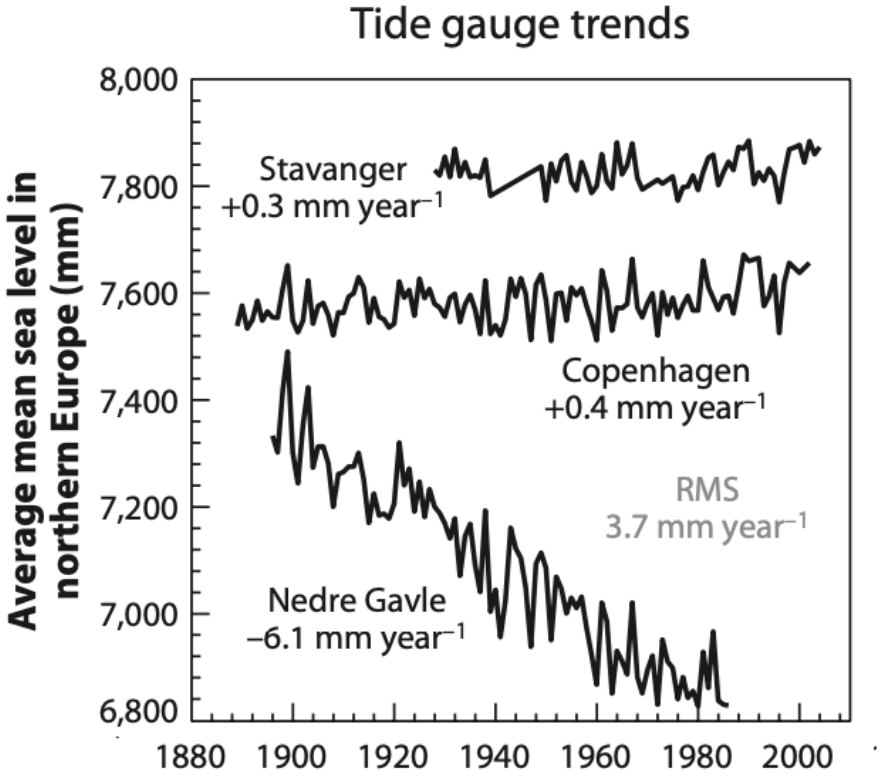

Figure 3: Annual mean sea level, with arbitrary offset, measured by three tide gauges located in northern Europe. The time series, which include the contribution of the atmosphere, ocean, as well sa vertical movements of the Earth's crust, shows that regional sea level can largely depart from the global average. Image from Stammer et al. (2013).

To assess the impact of future sea-level change on coastal regions and implement suitable adaptation strategies, researchers have devoted a considerable effort to understand the processes behind local sea-level fluctuations (Pugh & Woodworth, 2014, Hamlington et al., 2020). This does not only allow them to assess and predict local sea-level variability (Ponte et al. 2019), but also to filter out sea-level variations

at multi-decadal or shorter timescale which, by hiding the secular change, prevent accurate estimates of regional sea-level trends (Dangendorf et al., 2014).
As for the GMSL, regional sea-level variations result from changes in ocean density and ocean mass. The former are known as steric sea-level variations, whereas the latter as manometric sea-level variations (Gregory et al., 2019). Steric and manometric sea-level change occur due to atmospheric variations, as well changes in the ocean circulation, river runoff, glaciers and ice-sheets melting, and in the geoid. Given their importance, all these contributions will be now briefly described.

The atmosphere affects the sea level through changes in winds and pressure (Pugh and Woodworth 2014). Over periods of a few days or longer, pressure variations modify the sea level through the inverse barometer effect (IBE; Fig. 4). The pressure component of the sea level is well known. It does not contribute to the ocean circulation at timescales of a few days or longer. Indeed, as the mean sea level pressure (MSLP) increases or decreases by 1 hPa, the sea level adjusts by dropping or rising by approximately 1 cm. The IBE can be used to assess the pressure contribution to sea level and for validating historical time series of sea level against independent measurements. A strong variability between the two time series at one location gives confidence that they both satisfy a certain level of quality.

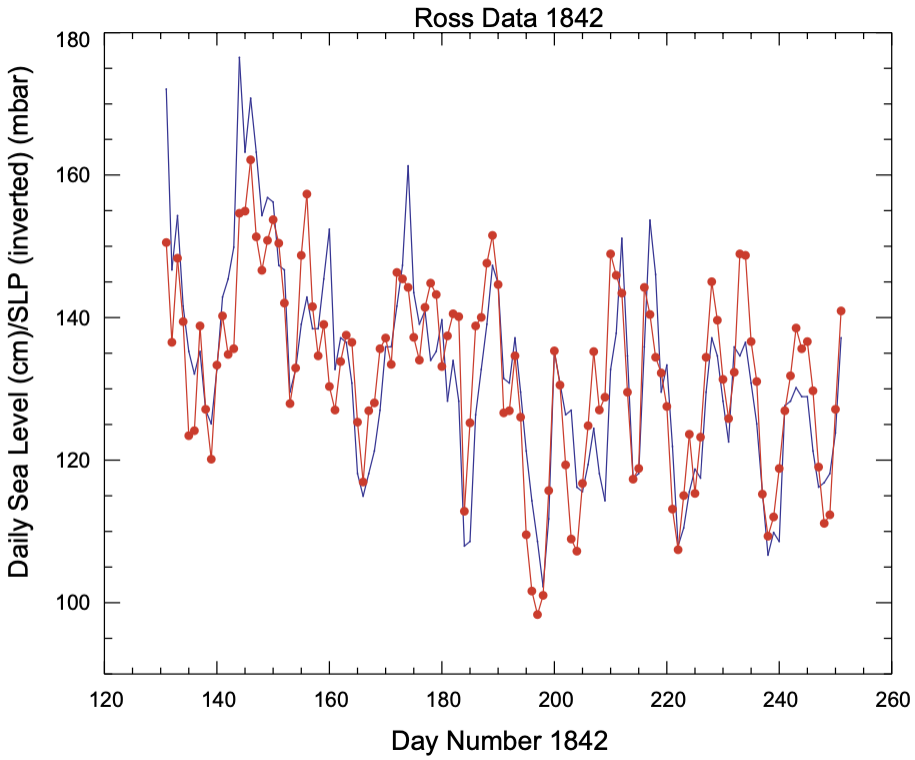

Figure 4: Comparison between the daily mean sea-level (in cm, blue line and dots) and the daily-averaged atmospheric pressure at the sea surface (in mbar, red line and dots) measured in 1842 at Port Louis, in the Falkland Islands. Image from Woodworth et al. (2010).

Winds also contributes to local sea-level change. For example, from a few days up to monthly timescales, Ekman theory can explain part of the wind contribution to coastal sea-level variations (Cushman-Roisin and Beckers, 2010): a stable wind blowing parallel to the continental slope generates a cross-shelf Ekman transport that can affect sea level through a barotropic or a baroclinic response (Chelton and Enfield, 1986). To better understand this contribution, one can consider the case of an along-shore wind blowing with the coast on the right. The barotropic response of the ocean involves winds moving water from the open ocean onto the shelf: by piling water up against the coast, this process increases the sea surface height along the coast (manometric effect). The baroclinic response of the ocean is more complicated. If the ocean is considered

as made of a warm, lighter layer on top of a colder, denser layer, winds move warm surface water onto the shelf and pile it up against the coast. As a result, downwelling occurs, and cooler, denser water near the sea bed is moved offshore (Fig. 5). As warm water occupies a larger volume than the replaced cold water, the height of the water column near the coast increases and a positive sea surface height anomaly occurs (steric effect).

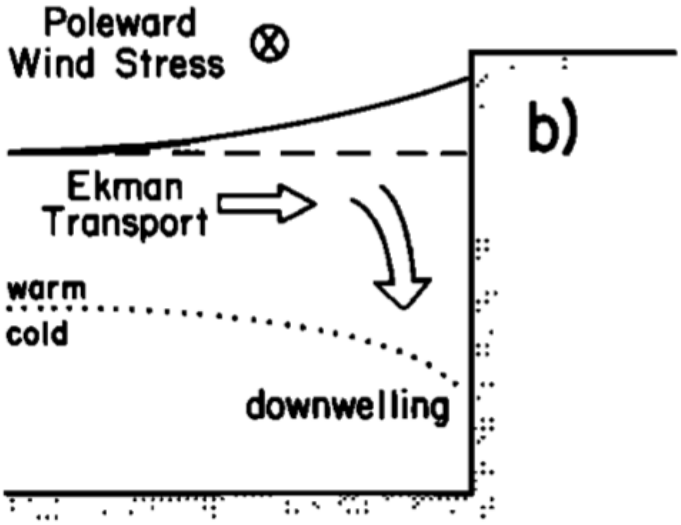

Figure 5: Sketch of the baroclinic response of the ocean, and the consequent sea-level rise, due to a wind field directed along the coast and pointing into the page. Image from Chelton and Enfield (1986).

Ocean currents affect regional sea level by redistributing the sea water throughout the ocean. Currents can modify both the steric component of sea level, through advection of temperature and salinity, and the manometric of sea level, through convergence of divergence of water masses. As an example, variations of the Atlantic Meridional Overturning Circulation (AMOC) and of the gyre circulation have resulted in a warming of the subpolar North Atlantic between 1995 and 2007 circa (Chafik et al., 2019). This, in turn, has led to the positive thermosteric sea level between Greenland and the UK shown in Fig. 6. Another interesting example involves the Pacific Ocean:

as the trade winds in the tropical Pacific have intensified since the 1990s, steric sea level has experienced a positive trend to the east of the Maritime continent between 1992 and 2010 (Meyssignac and Cazenave, 2012).

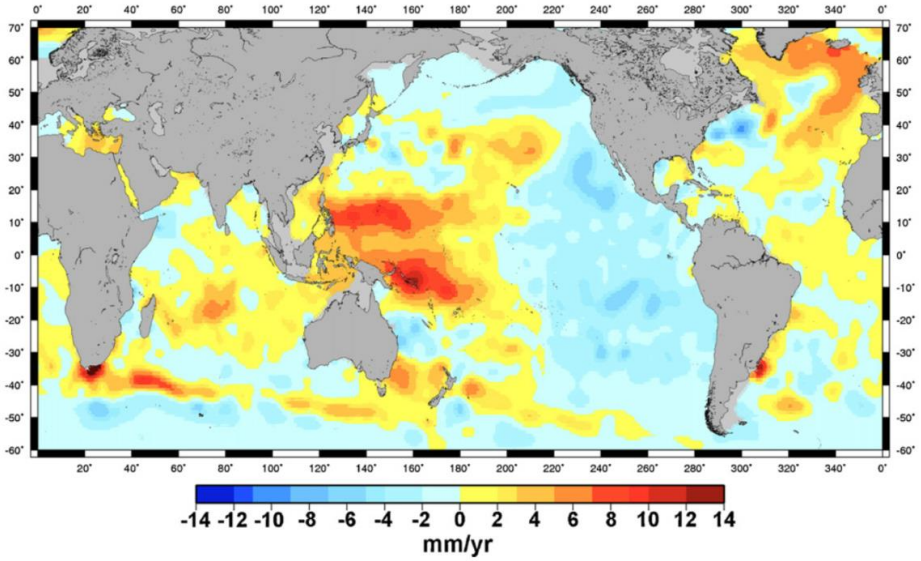

Figure 6: Thermosteric sea level rise over the period from 1992 to 2010 computed using hydrographic measurements from ships and from Argo profiling floats. Image from Meyssignac and Cazenave, 2012) *who used data from* (Levitus et al. 2009).

Despite its importance, oceanic and atmospheric processes do not fully explain regional variations in sea level. Other forcing factors need to be considered to understand the remaining part of the regional sea-level variability. Among these, we recall the role of river runoff, which is associated with a freshwater flux into the ocean. River runoff contributes to the regional sea-level variability over a range of timescales (Durand et al., 2019). At a few days timescales, the contribution is mostly manometric in nature whereas, at longer timescales, it is mostly steric. The continental freshwater runoff becomes more and more important with the size of the river. For example, the river Ganges induces a seasonal sea-level variation of 1 m in the Bay of Bengal (Pugh and Woodworth, 2014), or evidence of the river Amazon appears in the Atlantic ocean at a distance of even 1000 km from its mouth (Korosov et al., 2015).

Land-based ice melting also induces a non-uniform sea-level rise over the ocean. To a great extent, this results from ice sheets and glaciers exerting a weaker gravitational pull on seawater as they lose mass (Mitrovica et al., 2001). Indeed, as the gravitation pool weakens, sea level drops in proximity to the melting ice sheets and glaciers whereas it progressively increases with distance from them. The importance of this phenomenon is evident in Fig. 7, where other contributions of the melting of both ice sheets and glaciers (namely, the elastic response of the Earth, changes in the Earth's rotation and variations in the geometry of the coastal ocean) have also been taken into account. For example, it shows why the melting of the Greenland ice sheets is expected to little affect the northern European coast and to be primarily felt in the southern hemisphere and the tropical Pacific ocean (Fig. 7b).

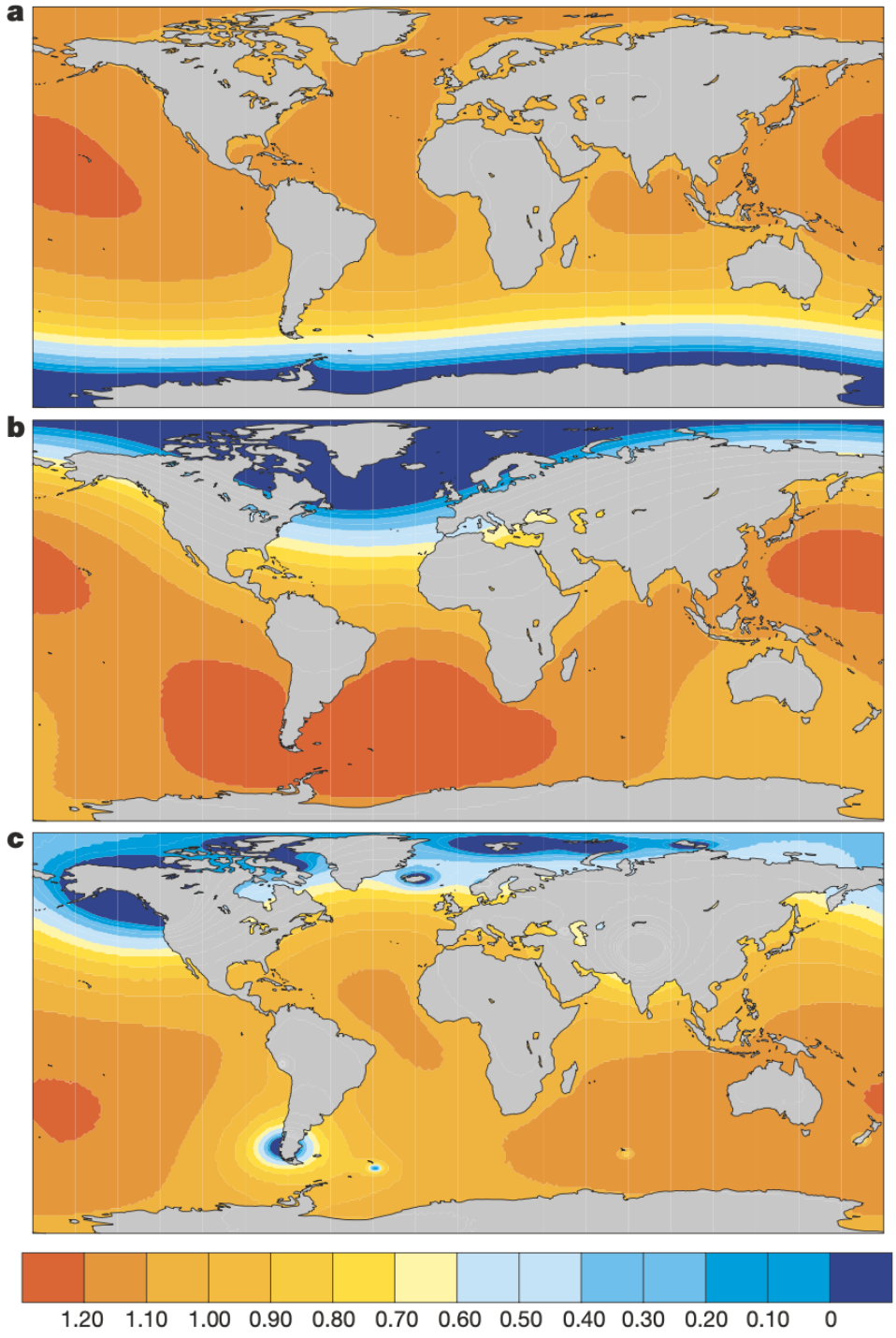
a
b
c
1.20 1.10 1.00 0.90 0.80 0.70 0.60 0.50 0.40 0.30 0.20 0.10 0

Figure 7: Spatial dependence of sea-level rise due to the present-day melting of the Antarctic ice sheets (a), the Greenland ice sheets (b), and glaciers (c). Values have been normalized with respect to the GMSL change that they induce so that it shows the departure from the pattern that would occur if the sea level due to the melting were distributed uniformly over the global ocean. Units are mm/year. Image from Mitrovica et al. (2001).

Vertical land movements (VLMs) of the Earth can significantly affect sea level when measured relative to land. VLMs occur over different temporal scales and with different processes, such as glacial isostatic adjustment (GIA), tectonic movements, subsidence, and sedimentation. Because of its relevance for Norway, we will now briefly discuss the GIA contribution to VLM.

GIA occurs over time scales ranging from centuries to millennia and results from slow and continuous processes such as lithospheric and mantle deformation which follow from the melting of ice sheets. It modifies sea level by altering the Earth's gravitational field and the elevation of the Earth's crust. The latter contribution only affects the sea surface height when it is measured with respect to land because it changes the reference surface to which sea level is measured.

Accounting for sea-level change due to VLMs is important to properly interpret the observed trends in sea-level. This is particularly true in some regions of the World, such as Fennoscandia. Indeed, the Earth's crust in Scandinavia is still adjusting to the melting of the Fennoscandian ice-sheet at the end of the last glaciation period, approximately ten thousands years ago (Stroeven et al., 2016). The case for Nedre Gävle, in Sweden, clearly shows the importance of VLM in the region: because of vertical movements of the Earth's crust, the local tide gauge measures a negative sea-level trend of approximately -6 mm/year (Fig. 3), whereas the GMSL trend ranges between 1 and 1.5 mm/year over the XX century.

To conclude, we would like to note that human activities can also play a role. For example, in some regions of the World, such as California or south-east Asia, the sea level relative to land is rising due to subsidence because of human usage of

groundwater storage (Nicholls et al., 2021). Indeed, land sinks in response to ground water extracted to support agriculture or the growing population living in cities.

Chapter 2 – Methods to estimate the sea-level variability and its components

2.1 Satellite altimetry

Since 1992, with the start of the TOPEX/Poseidon mission, satellite altimetry has revolutionized the field of oceanography (Wunsch and Stammer, 1998). With its continuous sea-level measurements over large parts of the ocean, in areas previously little accessible and unexplored (Cazenave et al., 2018b), satellite altimetry has provided insight into sea-level variations at a global and a regional scale (e.g., Chafik et al., 2017; Nerem et al., 2018) and has led to a better understanding of the ocean circulation and the climate system (Chafik et al., 2015).

There exist a range of satellite altimetry datasets (Cazenave and Moreira, 2022). Among these, we note the sea-level products reprocessed and distributed by the Copernicus Marine Environment Monitoring Service (CMEMS) and the Copernicus Climate Change Service (C3S). The sea-level dataset provided by CMEMS is recommended to analyze the ocean circulation and evaluate ocean models. Indeed, the gridded sea-level product from CMEMS is produced by merging all the available satellite altimetry missions with the intent, at each time step, to provide the most accurate sea-level estimate. Instead, the sea-level dataset provided by the C3S is designed to monitor long-term change in sea-level. Therefore, only two satellite missions are merged at each time: one is used as a reference (in turn, Topex/Poseidon, Jason-1, Jason-2 and Jason-3), whereas the other to improve accuracy and provide data in the high latitudes. C3S have opted for the two-satellite merging because it provides a steady constellation and, therefore, a more stable sea-level product.

Other global and regional sea-level data from satellite altimetry, which have undergone different reprocessings, are provided by research centres and universities around the World, such as the University of Colorado (http://sealevel.colorado.edu), by NASA Goddard Space Flight Center (https://sealevel.jpl.nasa.gov), by NOAA

(https://www.star.nesdis.noaa.gov/socd/lsa/SeaLevelRise/LSA_SLR_products.php), and by the Commonwealth Scienfic and Industrial Research Organization (CSIRO; www.cmar.csiro.au/sealevel/sl_data_cmar.html).

A number of satellite altimetry products have been produced to study sea-level variations in coastal areas. Among these, we note the X-TRACK dataset produced by LEGOS (Birol et al., 2017) and the ALES-retracked coastal satellite altimetry dataset (Passaro et al., 2014) provided by the Technische Universität München. Because of the relevance for this thesis, here we will briefly describe the ALES-reprocessed satellite altimetry dataset. However, it is convenient to first review the basics of the satellite altimetry.

The basic principle of satellite altimetry is relatively simple. A nadir-pointing antenna, in orbit around the Earth at altitudes between 780 and 1330 km circa (depending on the satellite mission), generates short electromagnetic pulses (spherical wavefronts) and measures the echoes that result from their interaction with the surface of the ocean. The power of each echo is recorded as a time series, known as waveform. The waveform helps determine some properties of the ocean, namely the sea surface height, the significant wave height (SWH), and the wind speed at sea level. In the next paragraph, we provide a brief summary of how altimetry works. However, for a thorough description of how satellite altimetry works, the reader is referred to Chelton et al. (2001).

To illustrate the idea behind satellite altimetry, we consider the simplified case of a pulse of duration 2τ that interacts with a specular surface. The waveform that results from the interaction can be divided into three parts (Fig. 8a). The first part corresponds to the time preceding the arrival of the echo, when the radar only records the background thermal noise of the instruments (Fig. 8b). The second part, known as the leading edge, starts when the pulse returns to the antenna. As illustrated in Fig. 8a, in the leading edge section of the waveform, the power of the echo increases linearly with time, being proportional to the area illuminated by the pulse (also known as footprint).

After a time 2τ, when the trailing edge of the pulse intersects the ocean's surface, the size of the footprint and, therefore, the power of the returned signal reach their maximum. Afterward, the footprint turns into an annulus, and the power of the returned signal slightly decreases with time. This last section of the waveform is known as the trailing edge.

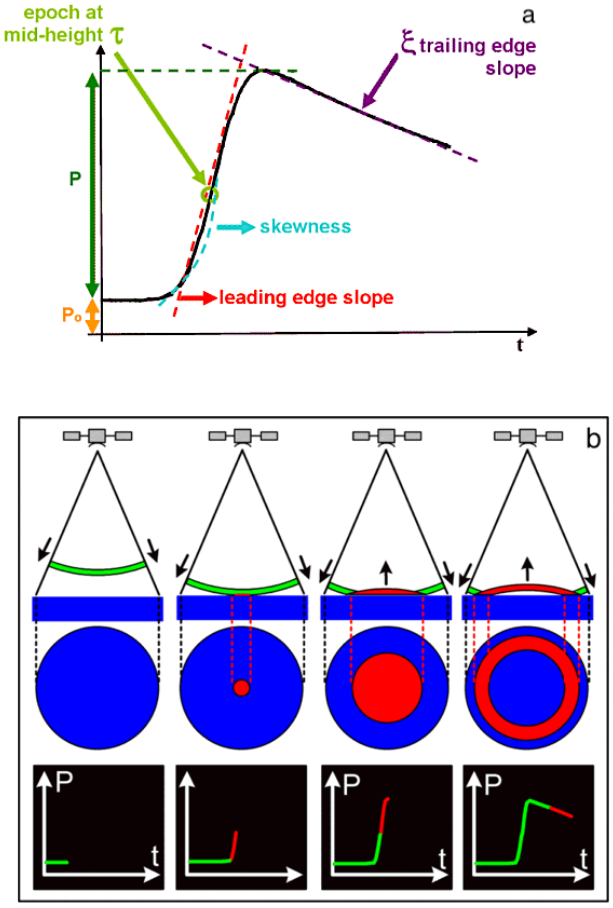

Figure 8: (a) Sketch of a waveform associated with a specular surface. (b) Five sketches showing how the waveform originates from the interaction between the satellite altimetry pulse and a specular surface. Images from Rosmorduc et al. (2011).

If the satellite's location with respect to a reference surface (the reference ellipsoid) is known, one can determine the sea surface height by measuring the distance between the satellite and the ocean's surface, also known as range. Satellite altimeters determine the range by estimating the two-way travel time of the mid-point of the pulse that they generate. The two-way travel time corresponds to the time needed by the mid-point of the leading edge to return to the satellite and, over the open ocean, is usually determined by fitting the waveform with the Brown functional form (Brown, 1977). Once the two-way travel time is known, one can determine the range from the speed of electromagnetic radiation in the atmosphere. However, the speed of light depends on the atmospheric composition and, more precisely, on the concentration of water vapor, dry gases, and free-charged particles encountered by the pulse. Therefore, the range, which is first computed using the speed of electromagnetic radiation in the vacuum, has to be corrected. These modifications go under the name of dry tropospheric, wet tropospheric, and ionospheric corrections and are performed using atmospheric models (Chelton et al., 2001).

The accuracy of radar altimetry, approximately 2 cm over the open ocean (Chelton et al., 2001), deteriorates along the coast (e.g., Gommenginger et al., 2011). Indeed, the Brown functional form does not fit well to the waveform in coastal regions, where the shape of the waveform can differ from the one typical for the open ocean (Xu et al. 2019). Such a difference occurs because the pulse generated by radar altimeters does not interact only with the ocean's surface but also with land. Moreover, rough coastlines can generate patches of calm waters and, therefore, cause variable sea surface conditions within the radar's footprint, therefore altering the backscatter.

Alternative approaches are needed to retrieve the range of satellite altimeters in coastal areas where coastal effects partially corrupt the waveform. An important approach involves using different retrackers to extrapolate geophysical information from the waveform. Because of the variety of shapes that coastal waveforms can have in coastal regions, multiple retracking methods exist (Gommenginger et al., 2011; Passaro et al., 2014). Of all the possible solutions, here we list only a few. A set of solutions classify

the waveforms based on their shapes (e.g., Andersen et al., 2010). Others add peaks to the Brown functional form to include coastal perturbations in the fit to the waveform (e.g., Halimi et al., 2013) Others retrack only the part of the waveform that is not modified by the coast (e.g., Yang et al., 2012).

The Adaptive Leading Edge Subwaveform (ALES) retracker (Passaro et al., 2014), which we will now present, given its role in the thesis, falls in this last category. The ALES retracker follows a two-step procedure. At first, it determines the slope of the leading edge to provide a first estimate of SWH. Then, it uses this estimate to select the portion of the waveform that has not been perturbed and fit it with the Brown functional form. This procedure assures reliable sea-level estimates up to 3 km to the coast, compared to the approximately 20 km of conventional approaches. At the same time, ALES returns estimates with an accuracy similar to conventional altimetry in the open ocean.

Two important geophysical corrections applied to the ALES-retracked satellite altimetry dataset are briefly described: the tidal and dynamic atmospheric corrections. They are relevant in this study since Paper II evaluates the sea-level estimates from satellite altimetry against the Norwegian set of tide gauges. Therefore, we need to apply the corrections used for satellite altimetry to the sea-level estimates from the tide gauge to compare the two datasets properly (see next section). The tidal correction is computed using the EOT11a tidal model. Instead, the dynamic atmospheric correction is performed using the Mog2D-G High Resolution barotropic model (Carrère and Lyard, 2003). This last correction serves two purposes. At first, it removes the atmospheric contribution to the sea-level variability up to a timescale of 20 days. Due to the coarse temporal resolution, this high-frequency variability would otherwise be aliased into the satellite altimetry signal. Secondly, it removes the contribution of pressure to the sea-level variations since it does not contribute to the ocean circulation at timescales of a few days or longer.

2.2 Tide gauges

Tide gauges are instruments designed to measure the sea surface height along the coast. They measure the sea level with respect to a reference value, known as chart datum. Given its importance in the history of sea-level study, the first automatic recording tide gauge, known as stilling-well gauges, is now briefly described (Fig. 9). It became operative during the first half of the XIX century and remained in use until the 1970s. Stilling wells are located along the coast and consist of a vertical, hollow cylinder partially immersed into the water. The cylinder has a few holes for water to partially fill it and contains a float that moves up and down with the sea level. The float is connected to a recording drum which automatically measures and records the sea-level fluctuations on a chart. Notably, close to the seafloor, the cylinder contains a conical structure with a small orifice: this prevents water from filling the cylinder too rapidly and, therefore, filters out the contribution of swells, which would otherwise make the sea level measurements too noisy.

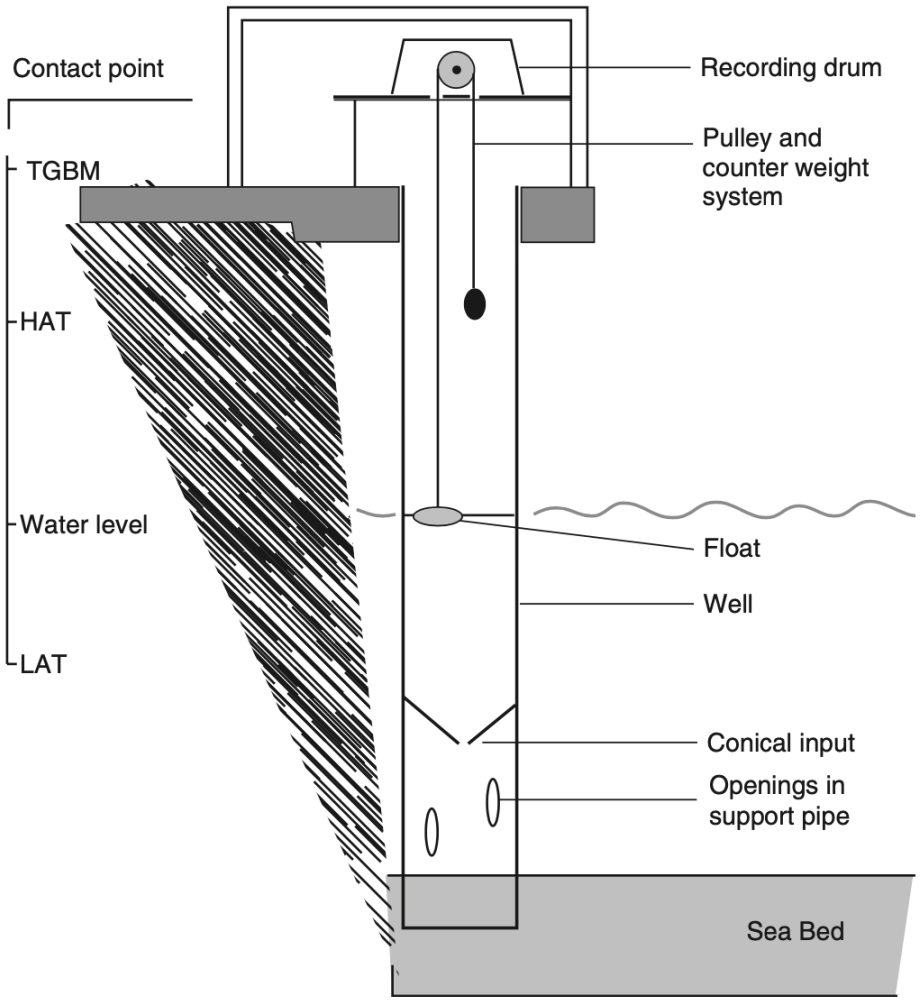

Figure 9: Sketch of stilling-well used by the National Ocean Service of the United States. Image from Pugh and Woodworth, 2014).

Tide gauges have several advantages and disadvantages over satellite altimetry. First, they are cheaper and easier to maintain. Secondly, they can return sea-level measurements with high accuracy and high frequency, whereas sea level variations with periods up to 20 days is removed from the satellite altimetry observations due to aliasing issues. Still, while their number has enormously increased since the 1950s, tide gauges do not cover large portions of the coastal ocean, such as a significant fraction

of the African coast. Moreover, they do not measure sea-level variations over the open ocean unless located on islands or platforms. Furthermore, very local processes, such as the runoff of a local river, can affect their measurements.

In this thesis, twenty-two Norwegian tide gauges are used to evaluate the ALES-retracked coastal satellite altimetry dataset along the coast of Norway. At first, the corrections used on the satellite altimetry data are applied to the tide gauge observations to compare the two datasets. More precisely, the dynamic atmospheric correction and low-frequency tides are removed from the sea level measured by the tide gauges. Then, the tide-gauge observations are corrected for VLMs. VLMs cannot be ignored along the coast of Norway because of their prominent influence on the tide-gauge measurements in the region (Richter et al., 2012). Indeed, contrary to satellite altimetry, tide gauges measure sea level with respect to the solid Earth and, therefore, interpret VLMs as sea-level variations.

2.3 GRACE

The Gravity Recovery and Climate Experiment (GRACE) was a satellite mission, operative between 2002 and 2017, designed to measure spatial and temporal variations of the Earth's gravitational field (Tapley et al., 2004). It consisted of two co-orbiting satellites flying over the Earth at an average distance of 220 km from each other, at an altitude of 450 km circa, and with a repeat cycle of approximately 30 days. Because of its duration and temporal sampling, GRACE mainly measured variations in the gravity field which occurred due variations in the amount of water over the surface of the Earth or within it. Therefore, the GRACE mission can provide insight into the water movements over the Earth and, notably for the present thesis, into the manometric component of the sea-level variability (Chambers and Schröter, 2011).

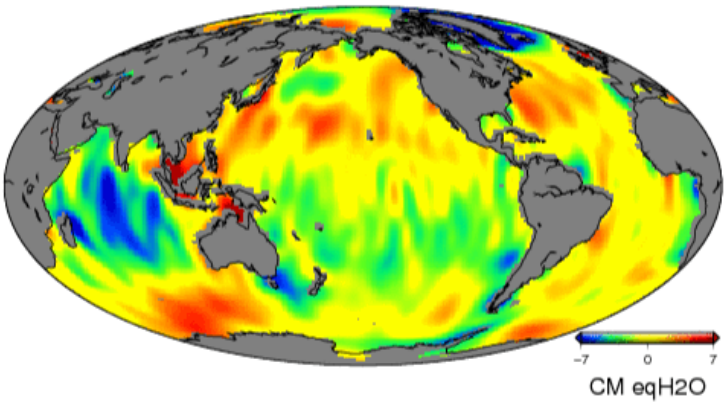

Figure 10: Example of the monthly averaged manometric component of the sea level measured by GRACE over the global ocean. The map shows the result for the month of November 2012. Values are expressed in equivalent water height. Units are cm. Image from https://grace.jpl.nasa.gov/data/monthly-mass-grids/ (accessed on 20/01/2022).

The idea of two co-orbiting satellites to measure the Earth's gravitational field was first proposed by Wolff (1969). It is based on the observation that the leading satellite feels along-track variations in the Earth's gravity field sooner than the trailing satellite because the former is closer to the source of gravitational anomaly. It follows that along-track variations in the Earth's gravity field modify the distance and the relative velocity between the two satellites (Fig. 11). Therefore, by measuring these two quantities, one can determine along-track variations in gravity and, consequently, the changes in mass on the Earth. Because GRACE had a repeat cycle of 30 days circa, it did not only record the spatial but also the temporal variations in the Earth's gravitational field, with a resolution of approximately one month.

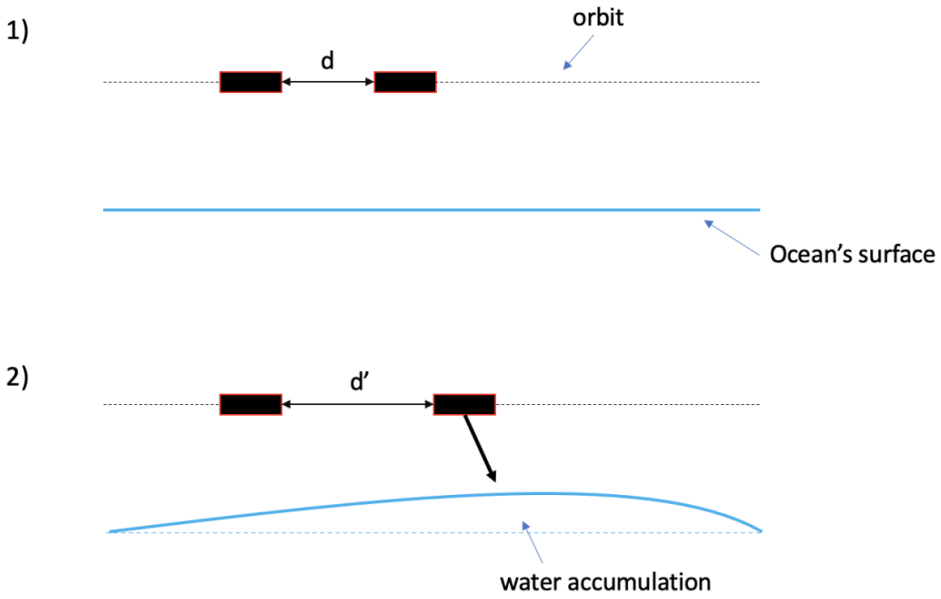

Figure 11: Concept of the GRACE satellite mission. The distance between the twin satellites, originally equal to d (sketch 1), increases to d' as their orbit intersects a region where water has accumulated (sketch 2).

To reconstruct the Earth's gravity field, some research centres, such as NASA Jet Propulsion Laboratory (JPL), the Centre for Space Research (CSR), and GeoForschungsZentrum (GFZ; the German research centre for geosciences), reprocess GRACE observations using spherical harmonics. This approach has the advantage of being computationally efficient, but presents one main drawback in coastal areas. Indeed, because of GRACE's coarse spatial and temporal resolution, the spherical harmonics expansion is commonly truncated at degree and order 60 (Luthcke et al., 2015) since higher degrees and orders contain mostly noise (Wouters and Schrama, 2007). The truncation leads to signal leakage, which is particularly evident in coastal regions, where the water content variability over land has usually larger amplitudes than over the nearby ocean (Johnson and Chambers, 2013).

The mass concentration (mascon) technique has been proposed to overcome this limitation. At first, this approach involves the pixelization of the Earth's surface into cells, with each cell characterized by its own uniform mass and its own associated

gravitational signal. Then, it takes advantage of a-priori information to reconstruct the gravitational field of the Earth preventing the signal leakage problem. Different mascon solutions are provided by a number of research centers. The most important ones are NASA JPL and NASA Goddard Space Flight Center (GSFC) and CSR.

Because of their relevance in the thesis, we briefly describe the mascon solutions provided by NASA JPL and NASA GSFC. The JPL's mascon solution is produced using 4551 3° spherical-cap mascons (Watkins et al., 2015) . Because of their large size, some of the JPL's mascons include both land and ocean.To reconstruct the manometric sea-level variability over these mascons, a coastline resolution improvement (CRI) filter is applied. In other words, manometric sea-level variations in coastal areas are reconstructed using only GRACE observations over the ocean and disregarding those over land.

The GSFC's mascon solution has been solved using 41168 1° spheric-cap mascons (Luthcke et al., 2013; 2015). Spatio-temporal constraints are applied to the mascons. These constraints distinguish between different geographical location, such as land and ocean, and the time of observations. If two mascons belong to the same region, the spatio-temporal constraint is a negative exponential function of the distance and the time between them. Otherwise, it is set to zero.

2.4 Hydrographic stations

This thesis also exploits the temperature and salinity profiles measured by eight fixed hydrographic stations located along the coast of Norway (Albretsen et al., 2012). These have been installed over the Norwegian continental shelf by Jens Eggvin between 1935 and 1947 while working at the Institute for Marine Research (IMR). Temperature and salinity data are usually collected at several depths once or twice a month by local fishermen trained by IMR (Richter et al., 2012).

2.5 EN4 and Argo profiling floats

This thesis has used the EN4 analysis dataset of the Met Office (Good et al., 2013) to compute the steric component of the sea level over the North Atlantic and statistically relate it to the manometric component of the sea level over the Norwegian shelf. The thesis has used the EN4 analysis dataset because it provides temperature and salinity values over the entire global ocean, with a spatial resolution of 1° x 1°, a temporal resolution of 1 month, and over 42 vertical layers. The EN4 dataset is produced by combining direct observations of temperature and salinity, a climatology, and an objective analysis scheme. The observations used are the Argo profiling fleets, the Arctic Synoptic Basin-wide Oceanography (ASBO), the Global Temperature and Salinity Profile Program (GTSPP), and the World Ocean Database (WOD13). Because of the relevance of the Argo profiling fleets for EN4 and, more generally, the study of the ocean, the Argo program will not be briefly described.

Argo is an international program aiming at providing continuous measurements of temperature, salinity, currents, and biogeochemical properties of the ocean at locations far from the coast. The Argo profiling floats have a significant advantage over previous attempts to sample the properties of the ocean: they operate year-round, independently of the weather conditions and with no human supervision. The program was launched in 2000 and now consists of approximately 4000 autonomous drifting floats.
Most Argo profiling floats follow the cycle depicted in Fig. 12. The Argo profiling floats are carried by ocean currents at a depth of approximately 1000 m and rise to the surface once every ten days to send the data they collect to the satellites. A few hours before ascending to the surface, most Argo profiling floats descend to an approximately 2000 m depth to measure the hydrographic properties over a larger fraction of the ocean depth.

While invaluable, the present Argo profiling floats only cover approximately half of the ocean volume. To partially fill this gap, Argo profiling floats that can descend up to 6000 m are currently under design (https://argo.ucsd.edu/expansion/deep-argo-

mission/) and effort has been made to build CTDs able to measure the temperature and salinity values at these depths. At the moment, a number of pilot arrays cover small areas of the global ocean. Norway, for example, contributes with a number of deep Argo profiling floats in the Nordic Seas (see https://norargo.hi.no/ for more information on the Norwegian Argo Infrastructure). When operative at a global scale, the deep Argo profiling floats would provide temperature and salinity measurements over parts of the ocean depth that are still little known due to the lack of continuous observations. These new measurements would help provide a more accurate picture of the Earth's energy balance and better estimate the sea-level budget (e.g., von Schuckmann et al., 2018; Horwath et al., 2022).

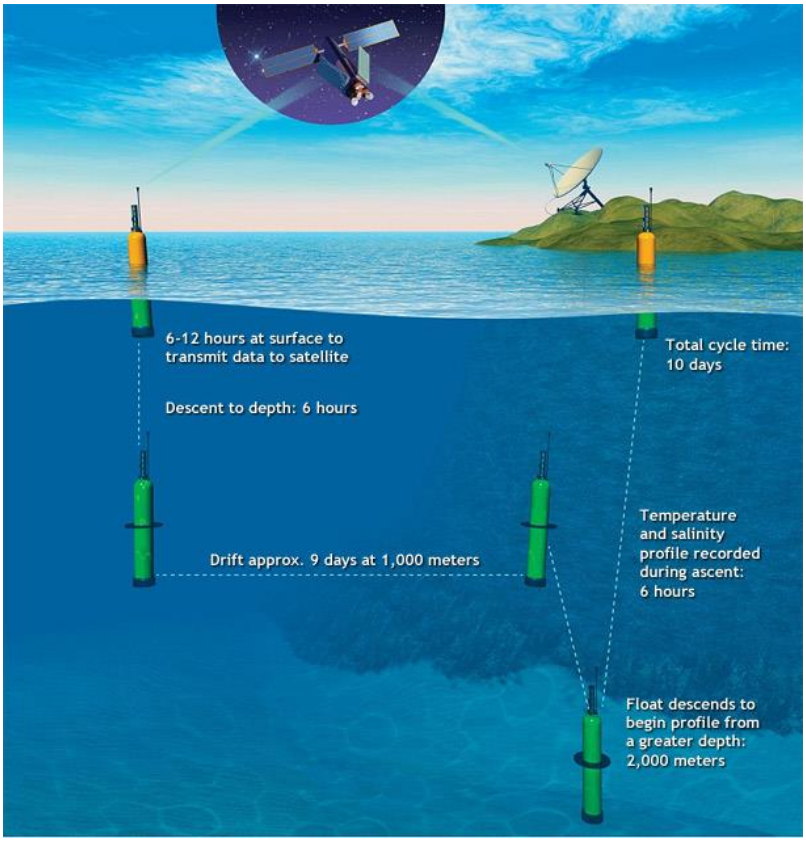

Figure 12: Sketch showing how most Argo profiling floats work. Image downloaded from https://www.climate.gov/news-features/features/argo-revolution.

2.6 GPS stations, levelling and Earth model

In this thesis, GPS measurements and levelling have been used to correct for VLM the sea-level measured by tide gauges along the coast of Norway. This correction was needed for the sea-level from tide gauges to be comparable with that from satellite altimetry. To correct the tide-guage observations, we have applied the same estimates of VLM as in Breili et al. (2017), who implemented a least-squares colocation to combine observations from both GPS and levelling.

The first GPS stations in Norway date back to to the early 1990s. Their number has increased over time and has reached 160 units in 2015 (Simpson et al., 2015). Because GPS stations covering at least a three-year period are needed to provide reliable vertical velocity trends (Kierulf et al., 2012), only 92 of the 160 GPS stations could be used to estimate VLM in Norway (Simpson et al., 2015). Still, because of their good spatial coverage, GPS stations are an invaluable source of information on the vertical movements of the Earth's crust in the region. Indeed, the average minimum distance between GPS stations is approximately 60 km.

Levelling data cover a longer period when compared to the GPS stations (levelling campaigns have been performed in Norway starting from 1916), but they do not provide continuous observations of VLM in Norway. Still, levelling data help cover the areas in between adjacent GPS stations and help constrain VLM estimates (Simpson et al., 2015).

Breili et al. (2017) do not only use levelling and GPS observations to estimate VLM, but also the Earth model by Kierulf et al. (2014) to simulate the GIA-induced impact on the geoid. The model is used to describe the rebound of the Earth's crust and flows within the mantle which result from the disappearance of the Fennoscandian ice sheet. These movements affect sea level trend due to the associated changes in the gravitation field of the Earth.

Breili et al. (2017) correct the Norwegian tide gauge data for this contribution because it can reach up to 0.5 mm/year along the Norwegian coast (Simpson et al., 2015). However, in this study, sea level variations from tide gauges have not been corrected for the geoid changes induced by GIA. Indeed, this contribution is equally measured by both tide gauges and satellite altimetry.

Chapter 3 – Motivations and objectives

A better understanding and quantification of the impact that different drivers have on global and regional sea-level variability, together with more measurements, can help advance sea-level studies. For example, knowledge of the physical processes behind the sea level variability at a particular location can help choose the right predictors when building statistical models (Ponte et al. 2019). Instead, more observations would help reduce the uncertainties of sea-level reconstructions by filling the enormous temporal and spatial gaps. Indeed, for the period preceding the 1950s, sea-level reconstructions are based on a limited number of tide gauges, especially at high latitudes or in the southern Atlantic ocean (Frederikse et al. 2021). While, since the 1950s, tide gauges have increased in number (e.g., Ponte et al., 2019), they still leave uncovered a significant portion of the coastal ocean. Satellite altimetry partly resolves the problem of the spatial coverage of the ocean since it measures the sea level over large portions of the global ocean. However, it has a number of shortcomings in coastal regions due to imprecise geophysical corrections and land contamination.

The work in this thesis considers the northern European continental shelf and:

1. proposes a novel description of the wind contribution to the sea level variability in the region (Paper I)
2. evaluates a coastal altimetry dataset, reprocessed using the ALES-retracker, and a gravimetry mission, GRACE, along the coast of Norway (Papers II and III respectively)
3. exploits these two datasets, together with the Norwegian set of hydrographic stations, to assess the steric and the manometric components of the sea level along the Norwegian coast over a range of timescales (Papers II and III respectively)

In other words, the aim is to advance the state of sea level research in northern Europe by providing a new understanding of the contribution of winds to the sea level variability in the region, and by assessing the quality of two new sets of observations.

This thesis focuses on the northern European continental shelf for two main reasons. At first, northern Europe, and the Norwegian coast in particular, are good locations to evaluate remote sensing data due to the relatively large amounts of in-situ data (for the purpose of this study, tide gauges, and hydrographic stations). Secondly, northern Europe is particularly exposed to sea level variations because of its mostly low-lying and densely populated coasts (Lamb and Frydendahl 1991; Wahl et al. 2013; Kulikov and Medvedev 2017). Even Norway, which at first sight appears little vulnerable to sea level variations due to its mountainous and rocky coast, is relevant from a sea level perspective. Indeed, the most populated and economically relevant Norwegian cities are close to sea level (Simpson et al. 2015).

While only focusing on the Norwegian coast, Paper II and III have a wider breadth. Indeed, the assessment of coastal altimetry (ALES) and satellite gravimetry (GRACE) measurements along the Norwegian coast can give confidence that both datasets can be used to analyze the sea level variability and its manometric contribution in other parts of the coastal ocean.

Chapter 4 – Summary of papers

Paper I

F. Mangini, L. Chafik, E. Madonna, C. Li, L. Bertino, J.E.Ø. Nilsen. The relationship between the eddy-driven jet stream and northern European sea level variability. *Tellus A*, 73, 1-15 (2021). https://doi.org/10.1080/16000870.2021.1886419.

The paper analyzes the contribution of local winds to the winter-time sea-level variability over the northern European continental shelf. Using daily gridded sea-level anomaly from altimetry, it explores the wind contribution by adopting the jet cluster perspective of the atmospheric circulation over the North Atlantic. The jet clusters represent persistent and recurrent states of the atmospheric variability; they are four in number and capture different configurations of the eddy-driven jet stream. Therefore, compared to previous papers on the topic, the paper assesses how the sea level responds to the physical patterns of the atmospheric circulation over the North Atlantic.

Previous studies used the empirical orthogonal functions (EOFs) of the atmospheric variability over the North Atlantic (e.g., Wakelin et al., 2003; Yan et al., 2004; Chafik et al., 2017) or an ad-hoc climate index (Dangendorf et al. 2014b) to explore the statistical relationship between local winds and northern European sea level. However, while the former might not represent physical patterns of the atmosphere, the latter only works at a prescribed location and does not account for anomalous sea-level values to result from more than a single atmospheric pattern.

Through composite analysis, we find that each jet cluster is associated with a different configuration of the sea level over the northern European continental shelf (Fig. 13), whose amplitudes are analogous to those of the typical sea-level variability. We also find that, at some locations, such as the Baltic Sea, anomalously high or low sea-level values are associated with a single jet cluster, whereas at other locations, such as the

interior and the northern parts of the North Sea, sea level responds to two or more jet clusters.

We also note that we cannot easily reconstruct the sea-level pattern associated with each jet cluster starting from the corresponding wind field. However, simple Ekman theory can help understand the sea-level patterns associated with the Central and the Mixed jet clusters.

We conclude the paper with a multiple linear regression model, where the monthly frequency of occurrence of the jet clusters is used to reconstruct the northern European sea level. We find that the jet clusters can explain up to 50% of the sea-level variance and that, in the interior and the western parts of the North Sea, sea level varies more in response to changes in wind direction than in wind speed.

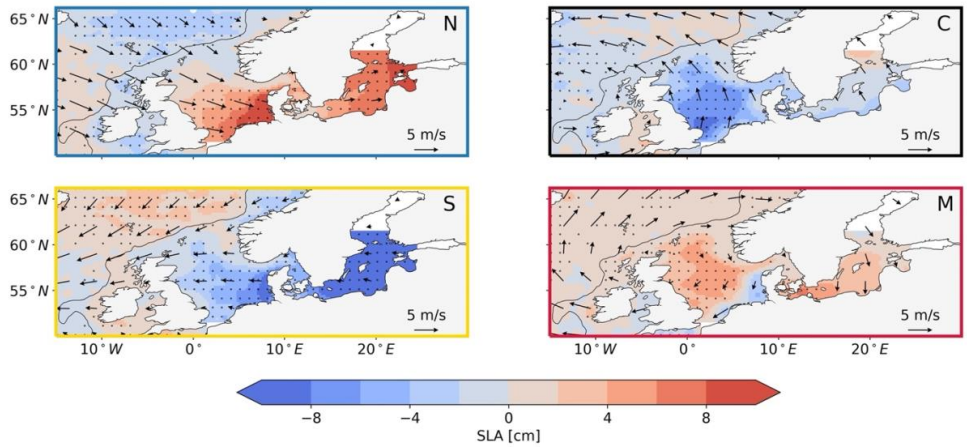

Figure 13: Composite maps of daily sea-level anomaly (shading, in cm) and 10m wind anomaly (arrows, in m/s) for each jet cluster: (N) Northern jet cluster, (C) Central jet cluster, (S) Southern jet cluster, (M) Mixed jet cluster. The black dots denote regions where the sea-level anomaly composite is significantly different from zero at a 0.05 significance level. The grey line shows the location of the continental slope, depicted by the 500m isobath.

Paper II

F. Mangini, L. Chafik, A. Bonaduce, L. Bertino, J.E.Ø. Nilsen. Sea-level variability and change along the Norwegian coast between 2003 and 2018 from satellite altimetry, tide gauges and hydrography. *Ocean Science*, 18, 331-359, 2022. https://doi.org/10.5194/os-18-331-2022.

Satellite altimetry measurements, complemented by in-situ records, have made a fundamental contribution to the understanding of global sea-level variability for almost thirty years. However, due to land contamination and imperfect geophysical corrections, satellite altimetry has historically performed better over the open ocean than in coastal areas. Recently, there has been a significant effort to improve the quality of satellite altimetry products in coastal regions with the aim of complementing the existing tide gauge network which, despite its relevance, does not cover the entire coast.

In the second paper of the PhD, we first evaluate a new coastal altimetry dataset, reprocessed with the ALES-retracker, along the coast of Norway. The Norwegian coast is relatively well covered by tide gauges and, therefore, suitable to evaluate a coastal altimetry dataset. The results show a good agreement between in-situ and remote sensing sea-level signals in terms of linear trend, seasonal cycle, and residual sea level variations. For example, the linear correlation coefficient between the residual sea-level variability from altimetry and tide gauges exceeds 0.8. Likewise, the root mean square difference between the two is less than 2.5 cm at most tide gauge locations (Fig. 14).

The paper also shows that conventional altimetry and ALES overall return comparable results. However, we find that, at some locations in northern Norway, the sea level trend provided by ALES shows a 6% reduction in trend difference with the tide gauges. This conclusion is corroborated by the results in Breili et al. (2017), who used conventional altimetry and tide gauge data to evaluate sea-level trends.

The paper then uses the ALES-reprocessed satellite altimetry dataset to assess the steric contribution to the sea-level variability along the coast of Norway. It uses satellite altimetry data because the Norwegian hydrographic stations and tide gauges are not colocated in space, but they can be as far as 100 km apart. Therefore, the sea level measured by the tide gauges might not be representative of the sea level at the hydrographic stations. While longer time series are needed to assess the steric contribution to the sea-level trends, the paper finds that temperature affects the sea-level annual cycle more than salinity, and that both temperature and salinity give a comparable contribution to the residual sea-level variations along the entire Norwegian coast.

These results go in the direction of obtaining an accurate characterization of coastal sea level at the high latitudes based on coastal satellite altimetry records, which can represent a valuable source of information to reconstruct coastal sea-level signals in areas where in-situ data are missing or inaccurate.

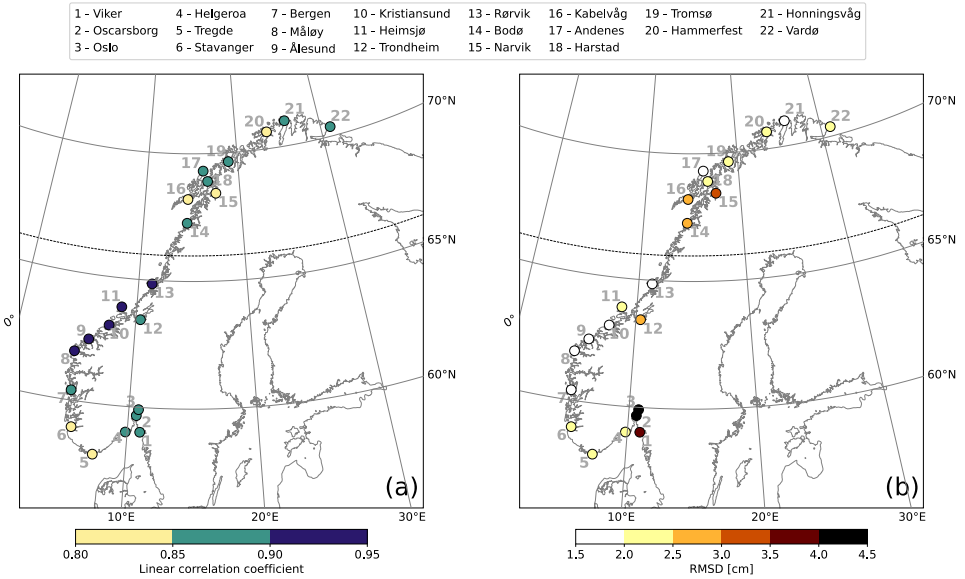

Figure 14: Comparison between coastal sea-level signals from in situ measurements and area-averaged remote-sensing data. At each tide gauge location, linear correlation coefficient (a) and RMSD (b) between the detrended and deseasoned monthly mean SLA from the ALES altimetry dataset and from the tide gauge. The black, dashed line indicates the 66° N parallel.

Paper III

F. Mangini, A. Bonaduce, L. Chafik, R. Raj, L. Bertino. Detection and attribution of manometric sea-level variations along the Norwegian coast using GRACE mascon solutions. *Manuscript in preparation*.

The third paper of the PhD evaluates the quality of the current sea-level observing system along the Norwegian coast. The project is motivated by the importance of reliable observations both for climate studies and society as they help understand the causes behind the observed sea-level variations.

At first, the third paper cross-evaluates the GSFC's and the JPL's GRACE mascon solutions and a combination of satellite altimetry and hydrography to assess their ability to measure the manometric sea-level variability along the Norwegian coast. In particular, it takes advantage of the present understanding of the processes affecting the sea-level variability in the region to provide physical evaluation of the datasets. Then, it exploits GRACE to investigate the ocean contribution to the inter-annual manometric sea-level variability over the Norwegian continental shelf.

The paper finds a qualitative good agreement between the manometric sea-level estimates from the GSFC's and the JPL's mascon solutions and from the combination of satellite altimetry and hydrography, and it explores the similarity between the three datasets further by focusing on the intra-annual and the inter-annual manometric sea-level variability. On intra-annual time scales, both GRACE mascon solutions qualitatively captures the manometric sea-level variability along the Norwegian coast and identify a coherent manometric sea level variation over the entire Norwegian shelf. On inter-annual timescales, we note that the along-slope wind stress, integrated along the eastern boundary of the North Atlantic from the equator up to northern Norway, strongly covaries with the manometric sea level from GSFC's mascon solution averaged along the Norwegian coast (Fig. 15). Moreover, we find that the manometric sea level over the entire Norwegian shelf resembles the leading mode of steric sea-level variability in the North Atlantic. This indicates that GSFC's mascon solution can help assess the role of the open ocean in driving the inter-annual sea-level variability over the Norwegian shelf. Overall, the paper shows that the ability of GRACE to measure the manometric sea-level variability over the Norwegian shelf and that GRACE can help understand the manometric component of the sea-level variability in coastal regions, especially where in-situ measurements are not available.

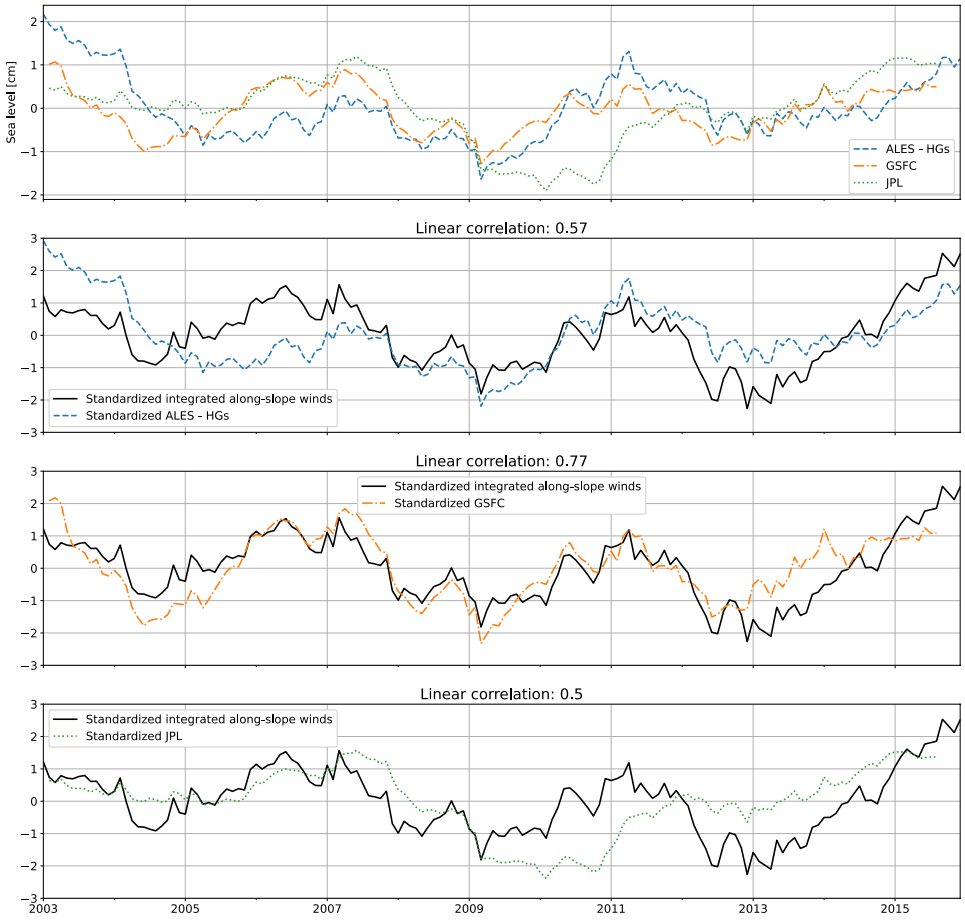

Figure 15: Manometric sea-level variability from ALES and the hydrographic stations (blue, dashed line), the GSFC's mascon solution (orange, dashed dotted line) and the JPL's mascon solution (dotted, green line) on inter-annual timescale (a). Each estimate of the inter-annual manometric sea level is plotted together with the inter-annual integrated along-slope wind stress (black, solid line in b, c, and d). In b, c, and d, each time series has been standardized before plotting.

Chapter 5 – Conclusions and outlook

This thesis examines the sea surface height variability over the northern European continental shelf, with an emphasis on its underlying causes and on the existing sea-level observing system. Paper I adopts the regimes perspective of the winter-time atmospheric variability over the North Atlantic to reassess the wind contribution to the northern European sea-level variation at monthly time scales. Papers II and III evaluate, respectively, a new coastal altimetry product and a gravimetry mission along the coast of Norway. Paper II also uses the satellite altimetry dataset to provide a new estimate of the steric component of sea level for Norway, whereas Paper III investigates the causes of the manometric sea-level variability along the Norwegian coast.

Each paper can be followed up. For example, Paper I finds a good relationship between the atmospheric regimes over the North Atlantic and the northern European mean sea level. However, it neglects the atmospheric contribution to the sea-level extremes and the ocean circulation in northern Europe. Both aspects of the oceanographic variability in the region could be addressed in future works.

The relationship between the jet clusters and the occurrence of storm surges would be of interest due to the risk that sea-level extremes pose to the people living along the low-lying coasts of northern Europe (Lamb and Frydendahl 1991). Similarly to Mastrantonas et al. (2021), who have explored the predictive skills of large-scale atmospheric patterns over the Mediterranean Sea to forecast extreme precipitation events in the region, a future work could investigate the predictability of the jet clusters and assess their ability to forecast severe storm-surge events several weeks in advance. Indeed, the sensitivity of the weather regimes to external forcings, such as the Madden-Julian Oscillation (e.g., Cassou, 2008), indicates that the North Atlantic circulation regimes can be forecasted beyond the limit of two weeks, which is typical of the deterministic predictability of weather (Palmer, 1993). A positive result would be beneficial since a more timely forecasting could help mitigate the negative impact of storm surges along the northern European coasts.

The relationship with the ocean circulation in the North Sea would be also of interest due to the relevance of ocean currents for the local marine ecosystem, the fish industry, and, more generally, for the economy of the region (e.g., Otto et al., 1990; Charnock et al., 1994). A future work could first determine whether the jet clusters induce a set of four persistent and recurrent circulation regimes in the North Sea. Because based on the jet clusters, these circulation regimes would have a clear physical meaning and, therefore, could be used to evaluate the circulation patterns identified in previous papers (Kauker and von Storch 2000; Mathis et al. 2015; Henriksen et al. 2018). Following Henriksen et al. (2018), the circulation regimes based on the jet clusters could also be related to the biology in the North Sea with the objective of forecasting fish recruitment in the region.

Paper II also offers opportunities for further projects. In particular, the good agreement with the Norwegian tide gauges indicates that the ALES-reprocessed satellite altimetry dataset can be used to measure and analyze the sea-level variability in other regions of the coastal ocean poorly covered by in-situ instruments. At the same time, the discrepancy between the sea-level trends along the Norwegian Trench as estimated from the ALES-retracked satellite altimetry dataset and the tide gauges requires more analysis. Indeed, in contrast with satellite altimetry, tide gauges suggest that the sea-level trend in the region increases with latitude, from less than 2 mm/year at Tregde to more than 4 mm/year at Måløy. Therefore, a detailed analysis of the sea-level trend of the four tide gauges located along the Norwegian Trench could help understand whether the difference between the two datasets results from problems in the observations from satellite altimetry or from the tide gauges.

Because GIA plays such a crucial role along the coast of Norway, future work could also follow the methodology proposed by Oelsmann et al. (2021) and use both the ALES-reprocessed coastal altimetry dataset and the Norwegian tide gauges to provide a new estimate of the VLM for Norway. This estimate would evaluate the existing ones based on a GIA model for Norway, GPS, and leveling (Simpson et al. 2015).

Furthermore, by using a coastal altimetry dataset spanning the entire satellite altimetry era, the project could extend the work by (Idžanović et al. 2019), who used seven years of Cryosat-2 and tide gauges observations to assess the VLM along the Norwegian coast.

Paper III focuses on the GRACE mission. It evaluates the GRACE dataset over the Norwegian continental shelf and analyzes the relationship between open ocean steric changes and coastal sea level variations on inter-annual and longer time scales. However, despite its relevance, GRACE covers a relatively short period of time (13 years in total). Therefore, it cannot easily assess the drivers of the inter-annual manometric sea level variability over the Norwegian shelf. Future work could use different datasets (e.g., an ocean reanalysis) to further investigate how temperature and salinity changes in the open ocean affect the sea level along the Norwegian coast.

While still in its draft form, Paper III indicates that GRACE better captures the inter-annual variability of the manometric component of the sea level over the Norwegian continental shelf compared to the combination of satellite altimetry and hydrographic stations. This suggests that the existing hydrographic stations might subsample the steric sea level along the Norwegian coast. Therefore, more hydrographic stations or more frequent observations are needed in the region. The 800m spatial resolution ROMS NorKyst800m regional ocean model provided by the Norwegian Meteorological Institute can be used to determine the spatial variation of temperature and salinity and help position future hydrographic stations. For instance, the number of hydrographic stations in a region could depend on the spatial extent of the temperature and salinity patterns in the area: the larger the pattern, the fewer the hydrographic stations. An observing system simulation experiment (e.g., Halliwell et al., 2017; Bonaduce et al., 2018) could then confirm the advantage of the additional hydrographic stations.

Despite their limitation at reproducing the steric component of the sea-level variability for the entire Norwegian coast, the results in Paper II indicate that the thermosteric and the halosteric components of the sea-level variability vary over spatial scales smaller than the average distance between adjacent hydrographic stations (approximately 250 km). This result confirms the need of climate models with a sufficiently fine spatial resolution to properly assess future sea-level variations and their impact on the coast. However, due their coarse spatial resolution, even the CMIP6 global climate models cannot properly reproduce such a small spatial scale variability. Therefore, a downscaling approach would help in this assessment as shown in (Hermans et al. 2020) who dynamically downscaled some of the CMIP5 model outputs to improve and analyze the sea level projections for the North Sea.

References

Albretsen, J., J. Aure, R. Sætre, and D. S. Danielssen, 2012: Climatic variability in the Skagerrak and coastal waters of Norway. *ICES Journal of Marine Science*, **69**, https://doi.org/10.1093/icesjms/fsr187.

Andersen, O. B., P. Knudsen, and P. A. M. Berry, 2010: The DNSC08GRA global marine gravity field from double retracked satellite altimetry. *Journal of Geodesy*, **84**, https://doi.org/10.1007/s00190-009-0355-9.

Birol, F., N. Fuller, F. Lyard, M. Cancet, F. Niño, C. Delebecque, S. Fleury, F. Toublanc, A. Melet, M. Saraceno, and F. Léger, 2017: Coastal applications from nadir altimetry: Example of the X-TRACK regional product. Advances in Space Research, **59**(4), 936-053, https://doi.org/10.1016/j.asr.2016.11.005.

Bonaduce, A., M. Benkiran, E. Remy, P. Yves Le Traon, and G. Garric, 2018: Contribution of future wide-swath altimetry missions to ocean analysis and forecasting. *Ocean Science*, **14**, https://doi.org/10.5194/os-14-1405-2018.

Breili, K., M. J. R. Simpson, and J. E. Ø. Nilsen, 2017: Observed sea-level changes along the Norwegian coast. *Journal of Marine Science and Engineering*, **5**, https://doi.org/10.3390/jmse5030029.

Brown, G. S., 1977: The Average Impulse Response of a Rough Surface and Its Applications. *IEEE Transactions on Antennas and Propagation*, **25**, https://doi.org/10.1109/TAP.1977.1141536.

Carrère, L., and F. Lyard, 2003: Modeling the barotropic response of the global ocean to atmospheric wind and pressure forcing - Comparisons with observations. *Geophysical Research Letters*, **30**, https://doi.org/10.1029/2002GL016473.

Cassou, C., 2008: Intraseasonal interaction between the Madden-Julian Oscillation and the North Atlantic Oscillation. *Nature*, **455**, https://doi.org/10.1038/nature07286.

Cazenave, A., and Coauthors, 2018a: Global sea-level budget 1993-present. *Earth System Science Data*, **10**, 1551–1590, https://doi.org/10.5194/essd-10-1551-2018.

——, H. Palanisamy, and M. Ablain, 2018b: Contemporary sea level changes from satellite altimetry: What have we learned? What are the new challenges? *Advances in Space Research*, **62**, https://doi.org/10.1016/j.asr.2018.07.017.

——, and Moreira, 2022: Contemporary sea-level changes from global to local scales: a review. *Proceedings of the Royal Society A: Mathematical, Physical and Engineering Sciences,* **478**, https://doi.org/10.1098/rspa.2022.0049.

Chafik, L., J. Nilsson, Skagseth, and P. Lundberg, 2015: On the flow of Atlantic water and temperature anomalies in the Nordic Seas toward the Arctic Ocean. *Journal of Geophysical Research: Oceans*, **120**, https://doi.org/10.1002/2015JC011012.

Chafik, L., J. E. Ø. Nilsen, and S. Dangendorf, 2017: Impact of North Atlantic teleconnection patterns on northern European sea level. *Journal of Marine Science and Engineering*, **5**, https://doi.org/10.3390/jmse5030043.

——, ——, ——, G. Reverdin, and T. Frederikse, 2019: North Atlantic Ocean Circulation and Decadal Sea Level Change During the Altimetry Era. *Scientific Reports*, **9**, https://doi.org/10.1038/s41598-018-37603-6.

Chambers, D. P., and J. Schröter, 2011: Measuring ocean mass variability from satellite gravimetry. *Journal of Geodynamics*, **52**, https://doi.org/10.1016/j.jog.2011.04.004.

Charnock, H., K. R. Dyer, J. M. Huthnance, P. S. Liss, J. H. Simpson, and P. B. Tett, 1994: Understanding the North Sea system. *Understanding the North Sea system*, https://doi.org/10.1016/0025-3227(94)90151-1.

Chelton, D. B., and D. B. Enfield, 1986: Ocean signals in tide gauge records. *Journal of Geophysical Research*, **91**, https://doi.org/10.1029/jb091ib09p09081.

——, J. C. Ries, B. J. Haines, L. L. Fu, and P. S. Callahan, 2001: Chapter 1 Satellite Altimetry. *International Geophysics*, **69**, https://doi.org/10.1016/S0074-6142(01)80146-7.

Church, J. A., and N. J. White, 2011: Sea-Level Rise from the Late 19th to the Early 21st Century. *Surveys in Geophysics*, **32**, https://doi.org/10.1007/s10712-011-9119-1.

——, and Coauthors, 2011: Revisiting the Earth's sea-level and energy budgets from 1961 to 2008. *Geophysical Research Letters*, **38**, https://doi.org/10.1029/2011GL048794.

Dangendorf, S., F. M. Calafat, A. Arns, T. Wahl, I. D. Haigh, and J. Jensen, 2014a: Mean sea level variability in the North Sea: Processes and implications. *Journal of Geophysical Research: Oceans*, **119**, https://doi.org/10.1002/2014JC009901.

——, T. Wahl, E. Nilson, B. Klein, and J. Jensen, 2014b: A new atmospheric proxy for sea level variability in the southeastern North Sea: Observations and future ensemble projections. *Climate Dynamics*, **43**, 447–467, https://doi.org/10.1007/s00382-013-1932-4.

——, M. Marcos, G. Wöppelmann, C. P. Conrad, T. Frederikse, and R. Riva, 2017: Reassessment of 20th century global mean sea level rise. *Proceedings of the National Academy of Sciences of the United States of America*, **114**, https://doi.org/10.1073/pnas.1616007114.

——, C. Hay, F. M. Calafat, M. Marcos, C. G. Piecuch, K. Berk, and J. Jensen, 2019: Persistent acceleration in global sea-level rise since the 1960s. *Nature Climate Change*, **9**, https://doi.org/10.1038/s41558-019-0531-8.

Douglas, B. C., 2001: Chapter 1 An introduction to sea level. *International Geophysics*, **75**, https://doi.org/10.1016/S0074-6142(01)80004-8.

Durand, F., C. G. Piecuch, M. Becker, F. Papa, S. v. Raju, J. U. Khan, and R. M. Ponte, 2019: Impact of Continental Freshwater Runoff on Coastal Sea Level. *Surveys in Geophysics*, **40**, https://doi.org/10.1007/s10712-019-09536-w.

Frederikse, T., S. Jevrejeva, R. E. M. Riva, and S. Dangendorf, 2018: A consistent sea-level reconstruction and its budget on basin and global scales over 1958-2014. *Journal of Climate*, **31**, https://doi.org/10.1175/JCLI-D-17-0502.1.

——, and Coauthors, 2020: The causes of sea-level rise since 1900. *Nature*, **584**, https://doi.org/10.1038/s41586-020-2591-3.

——, and Coauthors, 2021: Constraining 20th-Century Sea-Level Rise in the South Atlantic Ocean. *Journal of Geophysical Research: Oceans*, **126**, https://doi.org/10.1029/2020JC016970.

Gommenginger, C., P. Thibaut, L. Fenoglio-Marc, G. Quartly, X. Deng, J. Gómez-Enri, P. Challenor, and Y. Gao, 2011: Retracking Altimeter Waveforms Near the Coasts. *Coastal Altimetry*.

Good, S. A., M. J. Martin, and N. A. Rayner, 2013: EN4: Quality controlled ocean temperature and salinity profiles and monthly objective analyses with uncertainty estimates. *Journal of Geophysical Research: Oceans*, **118**, https://doi.org/10.1002/2013JC009067.

Gregory, J. M., and Coauthors, 2013: Twentieth-century global-mean sea level rise: Is the whole greater than the sum of the parts? *Journal of Climate*, **26**, https://doi.org/10.1175/JCLI-D-12-00319.1.

Gregory, J. M., and Coauthors, 2019: Concepts and Terminology for Sea Level: Mean, Variability and Change, Both Local and Global. *Surveys in Geophysics*, **40**, https://doi.org/10.1007/s10712-019-09525-z.

Halimi, A., C. Mailhes, J. Y. Tourneret, P. Thibaut, and F. Boy, 2013: Parameter estimation for peaky altimetric waveforms. *IEEE Transactions on Geoscience and Remote Sensing*, **51**, https://doi.org/10.1109/TGRS.2012.2205697.

Halliwell, G. R., M. F. Mehari, M. le Hénaff, V. H. Kourafalou, I. S. Androulidakis, H. S. Kang, and R. Atlas, 2017: North Atlantic Ocean OSSE system: Evaluation of operational ocean observing system components and supplemental seasonal observations for potentially improving tropical cyclone prediction in coupled systems. *Journal of Operational Oceanography*, **10**, https://doi.org/10.1080/1755876X.2017.1322770.

Hamlington, B. D., and Coauthors, 2020: Understanding of Contemporary Regional Sea-Level Change and the Implications for the Future. *Reviews of Geophysics*, **58**, https://doi.org/10.1029/2019RG000672.

Hay, C. C., E. Morrow, R. E. Kopp, and J. X. Mitrovica, 2015: Probabilistic reanalysis of twentieth-century sea-level rise. *Nature*, **517**, https://doi.org/10.1038/nature14093.

Henriksen, O., A. Christensen, S. Jónasdóttir, B. R. MacKenzie, K. E. Nielsen, H. Mosegård, and M. van Deurs, 2018: Oceanographic flow regime and fish recruitment: Reversed circulation in the North Sea coincides with unusually strong sandeel recruitment. *Marine Ecology Progress Series*, **607**, https://doi.org/10.3354/meps12786.

Hermans, T. H. J., J. Tinker, M. D. Palmer, C. A. Katsman, B. L. A. Vermeersen, and A. B. A. Slangen, 2020: Improving sea-level projections on the Northwestern European shelf using dynamical downscaling. *Climate Dynamics*, **54**, https://doi.org/10.1007/s00382-019-05104-5.

——, J. M. Gregory, M. D. Palmer, M. A. Ringer, C. A. Katsman, and A. B. A. Slangen, 2021: Projecting Global Mean Sea-Level Change Using CMIP6 Models. *Geophysical Research Letters*, **48**, https://doi.org/10.1029/2020GL092064.

Horwath, M., and Coauthors, 2022: Global sea-level budget and ocean-mass budget, with a focus on advanced data products and uncertainty characterisation. *Earth System Science Data*, **14**, 411–447, https://doi.org/10.5194/essd-14-411-2022.

Hu, A., and S. C. Bates, 2018: Internal climate variability and projected future regional steric and dynamic sea level rise /704/106/829/2737 /639/766 /139 article. *Nature Communications*, **9**, https://doi.org/10.1038/s41467-018-03474-8.

Idžanović, M., C. Gerlach, K. Breili, and O. B. Andersen, 2019: An attempt to observe vertical land motion along the norwegian coast by CryoSat-2 and tide gauges. *Remote Sensing*, **11**, https://doi.org/10.3390/rs11070744.

Jevrejeva, S., J. C. Moore, A. Grinsted, A. P. Matthews, and G. Spada, 2014: Trends and acceleration in global and regional sea levels since 1807. *Global and Planetary Change*, **113**, https://doi.org/10.1016/j.gloplacha.2013.12.004.

Johnson, G. C., and D. P. Chambers, 2013: Ocean bottom pressure seasonal cycles and decadal trends from GRACE Release-05: Ocean circulation implications. *Journal of Geophysical Research: Oceans*, **118**, https://doi.org/10.1002/jgrc.20307.

Kauker, F., and H. von Storch, 2000: Statistics of "Synoptic Circulation Weather" in the North Sea as derived from a multiannual OGCM simulation. *Journal of Physical Oceanography*, **30**, 3039–3049, https://doi.org/10.1175/1520-0485(2000)030<3039:SOSCWI>2.0.CO;2.

Kierulf, H. P., M. Ouassou, M. J. R. Simpson, and O. Vestøl, 2012: A continuous velocity field for Norway, Journal of Geodesy, **87**, 337–349, doi:10.1007/s00190-012-0603-2.

Kierulf, H. P., H. Steffen, M. J. R. Simpson, M. Lidberg, P. Wu, and H. Wang, 2014: A GPS velocity field for Fennoscandia and a consistent comparison to glacial isostatic adjustment models, Journal of Geophysical Research: Solid Earth, **119**, doi:10.1002/2013JB010889.

Korosov, A., F. Counillon, and J. A. Johannessen, 2015: Monitoring the spreading of the Amazon freshwater plume by MODIS, SMOS, Aquarius, and TOPAZ. *Journal of Geophysical Research: Oceans*, **120**, https://doi.org/10.1002/2014JC010155.

Kulikov, E. A., and I. P. Medvedev, 2017: Extreme Statistics of Storm Surges in the Baltic Sea. *Oceanology*, **57**, https://doi.org/10.1134/S0001437017060078.

Lamb, H. H., and K. Frydendahl, 1991: *Historic Storms of the North Sea, British Isles and Northwest Europe*. Cambridge University Press, 228 pp.

Levitus, S., J. I. Antonov, T. P. Boyer, R. A. Locarnini, H. E. Garcia, and A. v. Mishonov, 2009: Global ocean heat content 1955-2008 in light of recently revealed instrumentation problems. *Geophysical Research Letters*, **36**, https://doi.org/10.1029/2008GL037155.

Luthcke, S. B., T. J. Sabaka, B. D. Loomis, A. A. Arendt, J. J. McCarthy, and J. Camp, 2013: Antarctica, Greenland and Gulf of Alaska land-ice evolution from an iterated GRACE global mascon solution. *Journal of Glaciology*, **59**, https://doi.org/10.3189/2013JoG12J147.

——, D. D. Rowlands, T. J. Sabaka, B. D. Loomis, M. Horwath, and A. A. Arendt, 2014: Gravimetry measurements from space. *Remote Sensing of the Cryosphere*.

MacIntosh, C. R., C. J. Merchant, and K. von Schuckmann, 2017: Uncertainties in Steric Sea Level Change Estimation During the Satellite Altimeter Era: Concepts and Practices. *Surveys in Geophysics*, **38**, https://doi.org/10.1007/s10712-016-9387-x.

Mastrantonas, N., L. Magnusson, F. Pappenberger, and J. Matschullat, 2021: What do large-scale patterns teach us about extreme precipitation over the Mediterranean at medium- and extended-range forecasts? *Quarterly Journal of the Royal Meteorological Society*, https://doi.org/10.1002/qj.4236.

Mathis, M., A. Elizalde, U. Mikolajewicz, and T. Pohlmann, 2015: Variability patterns of the general circulation and sea water temperature in the North Sea. *Progress in Oceanography*, **135**, https://doi.org/10.1016/j.pocean.2015.04.009.

Meyssignac, B., and A. Cazenave, 2012: Sea level: A review of present-day and recent-past changes and variability. *Journal of Geodynamics*, **58**, https://doi.org/10.1016/j.jog.2012.03.005.

Mitrovica, J. X., M. E. Tamisiea, J. L. Davis, and G. A. Milne, 2001: Recent mass balance of polar ice sheets inferred from patterns of global sea-level change. *Nature*, **409**, https://doi.org/10.1038/35059054.

Munk, W., 2002: Twentieth century sea level: An enigma. *Proceedings of the National Academy of Sciences of the United States of America*, **99**, https://doi.org/10.1073/pnas.092704599.

Nerem, R. S., B. D. Beckley, J. T. Fasullo, B. D. Hamlington, D. Masters, and G. T. Mitchum, 2018: Climate-change–driven accelerated sea-level rise detected in the altimeter era. *Proceedings of the National Academy of Sciences of the United States of America*, **115**, https://doi.org/10.1073/pnas.1717312115.

Nicholls, R. J., 2011: Planning for the Impacts of Sea Level Rise . *Oceanography*, **24**, 144–157.

——, and Coauthors, 2021: A global analysis of subsidence, relative sea-level change and coastal flood exposure. *Nature Climate Change*, **11**, https://doi.org/10.1038/s41558-021-00993-z.

Oelsmann, J., M. Passaro, D. Dettmering, C. Schwatke, L. Sanchez, and F. Seitz, 2021: The Zone of Influence: Matching sea level variability from coastal altimetry and tide gauges for vertical land motion estimation. *Ocean Science*, https://doi.org/10.5194/os-2020-29.

Otto, L., J. T. F. Zimmerman, G. K. Furnes, M. Mork, R. Saetre, and G. Becker, 1990: Review of the physical oceanography of the North Sea. *Netherlands Journal of Sea Research*, **26**, https://doi.org/10.1016/0077-7579(90)90091-T.

Palmer, T. N., 1993: Extended-range atmospheric prediction and the Lorenz model. *Bulletin - American Meteorological Society*, **74**, https://doi.org/10.1175/1520-0477(1993)074<0049:ERAPAT>2.0.CO;2.

Passaro, M., P. Cipollini, S. Vignudelli, G. D. Quartly, and H. M. Snaith, 2014: ALES: A multi-mission adaptive subwaveform retracker for coastal and open ocean altimetry. *Remote Sensing of Environment*, **145**, https://doi.org/10.1016/j.rse.2014.02.008.

Ponte, R. M., and Coauthors, 2019: Towards comprehensive observing and modeling systems for monitoring and predicting regional to coastal sea level. *Frontiers in Marine Science*, **6**, https://doi.org/10.3389/fmars.2019.00437.

Pugh, D., and P. Woodworth, 2014: *Sea-level science: Understanding tides, surges, tsunamis and mean sea-level changes*.

Richter, K., J. E. Ø. Nilsen, and H. Drange, 2012: Contributions to sea level variability along the Norwegian coast for 1960-2010. *Journal of Geophysical Research: Oceans*, **117**, https://doi.org/10.1029/2011JC007826.

Rosmorduc, V., J. Benveniste, E. Bronner, S. Dinardo,O. Lauret, C. Maheu, M. Milagro, N. Picot, Radar Altimetry Tutorial, J. Benveniste and N. Picot Ed., http://www.altimetry.info, 2011: Basic Radar Altimetry Toolbox and radar Altimetry Tutorial: A New Set of Tools for All Altimetry Users. Available from: https://www.researchgate.net/publication/259323994_Basic_Radar_Altimetry_Toolbox_and_radar_Altimetry_Tutorial_A_New_Set_of_Tools_for_All_Altimetry_Users [accessed Feb 21 2022].

von Schuckmann, K., and Coauthors, 2018: Copernicus Marine Service Ocean State Report. *Journal of Operational Oceanography*, **11**, https://doi.org/10.1080/1755876X.2018.1489208.

Simpson, M. J. R., and Coauthors, 2015: *Sea Level Change for Norway Past and Present Observations and Projections to 2100*. 1–156 pp. www.miljodirektoratet.no/20803.

Slangen, A. B. A., J. A. Church, C. Agosta, X. Fettweis, B. Marzeion, and K. Richter, 2016: Anthropogenic forcing dominates global mean sea-level rise since 1970. *Nature Climate Change*, **6**, https://doi.org/10.1038/nclimate2991.

Stammer, D., A. Cazenave, R. M. Ponte, and M. E. Tamisiea, 2013: Causes for contemporary regional sea level changes. *Annual Review of Marine Science*, **5**, https://doi.org/10.1146/annurev-marine-121211-172406.

Stroeven, A. P., and Coauthors, 2016: Deglaciation of Fennoscandia. *Quaternary Science Reviews*, **147**, https://doi.org/10.1016/j.quascirev.2015.09.016.

Tapley, B. D., S. Bettadpur, M. Watkins, and C. Reigber, 2004: The gravity recovery and climate experiment: Mission overview and early results. *Geophysical Research Letters*, **31**, https://doi.org/10.1029/2004GL019920.

Wahl, T., and Coauthors, 2013: Observed mean sea level changes around the North Sea coastline from 1800 to present. *Earth-Science Reviews*, **124**, 51–67, https://doi.org/10.1016/j.earscirev.2013.05.003.

Wakelin, S. L., P. L. Woodworth, R. A. Flather, and J. A. Williams, 2003: Sea-level dependence on the NAO over the NW European continental shelf. *Geophysical Research Letters*, **30**, 56–1–56–4, https://doi.org/10.1029/2003GL017041.

Watkins, M. M., D. N. Wiese, D. N. Yuan, C. Boening, and F. W. Landerer, 2015: Improved methods for observing Earth's time variable mass distribution with GRACE using spherical cap mascons. *Journal of Geophysical Research: Solid Earth*, **120**, https://doi.org/10.1002/2014JB011547.

Wolff M, 1969: Direct Measurements of the Earth's Gravitational Potential Using a Satellite Pair. *J Geophys Res*, **74**, https://doi.org/10.1029/jb074i022p05295.

Woodworth, P. L., D. T. Pugh, and R. M. Bingley, 2010: Long-term and recent changes in sea level in the Falkland Islands. *Journal of Geophysical Research: Oceans*, **115**, https://doi.org/10.1029/2010JC006113.

Wouters, B., and E. J. O. Schrama, 2007: Improved accuracy of GRACE gravity solutions through empirical orthogonal function filtering of spherical harmonics. *Geophysical Research Letters*, **34**, https://doi.org/10.1029/2007GL032098.

Wunsch, C., and D. Stammer, 1998: Satellite altimetry, the marine geoid, and the oceanic general circulation. *Annual Review of Earth and Planetary Sciences*, **26**, https://doi.org/10.1146/annurev.earth.26.1.219.

Xu, X.-Y., K. Xu, Y. Xu, and L.-W. Shi, 2019: Coastal Altimetry: A Promising Technology for the Coastal Oceanography Community. *Estuaries and Coastal Zones - Dynamics and Response to Environmental Changes*, 1–19.

Yan, Z., M. N. Tsimplis, and D. Woolf, 2004: Analysis of the relationship between the North Atlantic oscillation and sea-level changes in northwest Europe. *International Journal of Climatology*, **24**, 743–758, https://doi.org/10.1002/joc.1035.

Yang, L., M. Lin, Q. Liu, and D. Pan, 2012: A coastal altimetry retracking strategy based on waveform classification and sub-waveform extraction. *International Journal of Remote Sensing*, **33**, https://doi.org/10.1080/01431161.2012.701350.

Tellus
SERIES A
DYANAMIC
METEOROLOGY
AND OCEANOGRAPHY
PUBLISHED BY THE INTERNATIONAL METEOROLOGICAL INSTITUTE IN STOCKHOLM

The relationship between the eddy-driven jet stream and northern European sea level variability

By FABIO MANGINI[1]*, LÉON CHAFIK[2], ERICA MADONNA[3], CAMILLE LI[3], LAURENT BERTINO[1], and JAN EVEN ØIE NILSEN[1,4], [1]*Nansen Environmental and Remote Sensing Center and Bjerknes Centre for Climate Research, Bergen, Norway;* [2]*Department of Meteorology and Bolin Centre for Climate Research, Stockholm University, Stockholm, Sweden;* [3]*Geophysical Institute and Bjerknes Centre for Climate Research, University of Bergen, Bergen, Norway;* [4]*Institute of Marine Research, Bergen, Norway*

(Manuscript Received 14 July 2020; in final form 22 January 2021)

ABSTRACT

Wintertime sea level variability over the northern European continental shelf is largely wind-driven. Using daily gridded sea level anomaly from altimetry, we examine both the spatial and the temporal relationship between northern European sea level variability and large-scale atmospheric circulation patterns as represented by the jet cluster paradigm. The jet clusters represent different configurations of the eddy-driven jet stream and, therefore, provide a physical description of the atmospheric variability in the North Atlantic. We find that each of the four jet clusters is associated with a distinct northern European sea level anomaly pattern whose magnitudes are comparable to those of typical sea level variations on the shelf. In certain locations, such as the German Bight and the east coast of England, sea level anomalies are mainly associated with one single jet cluster. In other locations, such as the interior and the northern part of the North Sea, sea level anomalies are found to be sensitive to at least two jet configurations. Based on these regional sea level variations, we map out the locations on the shelf where each jet cluster or combination of clusters is most active before discussing the role of Ekman transport in inducing the resulting patterns. Through a multiple linear regression model, we also find that the jet clusters reconstruct up to 50% of the monthly mean sea level anomaly variance over the northern European continental shelf. The model best performs in the interior and the western part of the North Sea, suggesting that wind direction rather than wind speed plays a more prominent role over these regions. We conclude that the jet cluster approach gives valuable new insights compared to linear regression techniques for characterising wind-driven sea level variability over the northern European continental shelf.

Keywords: northern European sea level, jet clusters, wind forcing, eddy-driven jet stream, satellite altimetry

1. Introduction

Local winds contribute to sea level variability over the northern European continental shelf from hourly up to interannual timescales. At timescales shorter than a few days, local winds can generate storm surges that severely affect the coastal regions of northern Europe, most of which are low-lying and densely populated (e.g. Wahl et al., 2013; Gill, 1982; Lamb and Frydendahl, 1991). At longer timescales, they modify the height and frequency of storm surges and partly explain the departure of northern European sea level rise from the global average (e.g. Dangendorf et al., 2012). An in-depth knowledge of sea level variations at different timescales would thus benefit both climate scientists in understanding the processes involved and coastal planners in decision making.

Previous studies showed a relationship between northern European sea level and the North Atlantic Oscillation (NAO), the leading mode of atmospheric variability over the North Atlantic (e.g. Wakelin et al., 2003; Yan et al., 2004; Jevrejeva et al., 2005; Richter et al., 2012). The NAO is a simple index that allows for a compact description of North Atlantic atmospheric conditions (e.g. Hurrell, 1995) and, as such, has been widely used in the past to investigate the variability of the climate system. It has been found that the positive and the negative phases of the NAO are, respectively, associated with high and low sea level over the entire northern European continental shelf (e.g. Wakelin et al., 2003; Richter et al., 2012;

*Corresponding author. e-mail: fabio.mangini@nersc.no

Citation: Tellus A: 2021, **73**, 1886419, https://doi.org/10.1080/16000870.2021.1886419

Chafik et al., 2017). Moreover, the sea level variability connected to the NAO has been found to be strongest at annual and interannual timescales (e.g. Yan et al., 2004) and in specific locations such as the southern North Sea (e.g. Wakelin et al., 2003).

There remains, however, a substantial portion of North Atlantic atmospheric variability that is unrelated to the NAO, and this has been found to contribute to the spatial and the temporal sea level variability over the northern European continental shelf. For example, Chafik et al. (2017) showed that additional patterns of atmospheric variability, defined via empirical orthogonal function (EOF) analysis, contribute significantly to regional sea level variations across the North Sea and the Norwegian shelf. Dangendorf et al. (2014) focused on one region, the German Bight, and built a bespoke atmospheric index to reproduce the contribution of both wind and pressure to the sea level. Their index explains ~80% of the sea level variance at this specific location, compared to 30–35% from a standard NAO index. In summary, sea level variability may be better explained by accounting for atmospheric variability beyond the NAO.

While these approaches give insight into wind-driven sea level variability, there is some uncertainty as to whether the wind patterns they identify correspond to real (observed) large-scale atmospheric conditions. EOFs must satisfy symmetry and orthogonality constraints and, therefore, do not necessarily describe patterns that occur in nature. Moreover, the method proposed by Dangendorf et al. (2014) yields only one atmospheric pattern associated with either high or low sea level values at one selected location. Therefore, their approach is not designed to identify the atmospheric conditions responsible for coherent sea level patterns over a large area like the northern European continental shelf.

Here, we study how northern European sea level variability relates to wind patterns using the jet cluster paradigm (Madonna et al., 2017), an approach that provides a physical description of large-scale atmospheric variability and has so far not been used in sea level research. The jet clusters represent observed configurations of the eddy-driven jet stream which are associated with a set of well-known weather regimes that characterise Euro-Atlantic climate. We start with a brief description of the datasets used (Section 2). We then describe the sea level patterns associated with the jet clusters and explore where the jet clusters account for a substantial portion of the interannual sea level variability (Section 3). We discuss the balance of forces on the shelf and the role of Ekman transport as a mechanism for creating the observed sea level patterns (Section 4). We then examine how the jet clusters and the northern European sea level co-vary at daily and monthly time scale (Section 5) and conclude with some final remarks (Section 6).

2. Data

2.1. Time-mean barotropic circulation on the shelf

We use the barotropic streamfunction (ψ) from the TOPAZ4 ocean reanalysis (Xie et al., 2017) to derive the barotropic currents over the northern European continental shelf and parts of the Nordic Seas. The dataset is provided daily from 01 January 1991 and covers the North Atlantic and the Arctic oceans on a Cartesian grid of 0.25° × 0.25°. The ocean model data is only used for illustration of the current patterns.

To calculate the time-mean barotropic circulation, we first select the period between 01 January 1993 and 31 December 2014, common to the time series of the sea level anomaly and of the jet clusters (see Sections 2.2 and 2.4). Then, we remove the linear trend and the seasonal cycle (daily climatology) from the barotropic streamfunction, and we average the result over the period under consideration. Finally, we compute the time-mean barotropic current using the formula:

$$u = -\frac{1}{H}\frac{\partial \psi}{\partial y}; \quad v = \frac{1}{H}\frac{\partial \psi}{\partial x} \tag{1}$$

where u and v are the zonal and meridional components of the currents, and H is the ocean depth.

In Fig. 1A, we recognise the main features of the time-mean barotropic circulation over the northern European continental shelf and the Nordic Seas. Along the northern European continental slope, we identify the slope current which flows northward at a speed of a few cm s^{-1}. In the North Sea, we recognise the Dooley current, which follows the 100 m isobath, and the coastal current, which flows along the southern coast of the North Sea. Both cross the North Sea from west to east and converge into the Skagerrak. From the Skagerrak, the flow continues northward in the Norwegian Trench along the Norwegian coast as the Norwegian Coastal Current. This description of the main ocean currents on the shelf will be helpful in the discussion later in the study.

2.2. Sea level

We use the absolute dynamic topography (ADT), which is the sea surface height relative to the geoid, of the DUACS reprocessed multi-mission altimetry products DT2014 version (Pujol et al., 2016). The ADT is provided daily from 01 January 1993 and globally on a Cartesian grid of 0.25° × 0.25°. A number of geophysical corrections have been

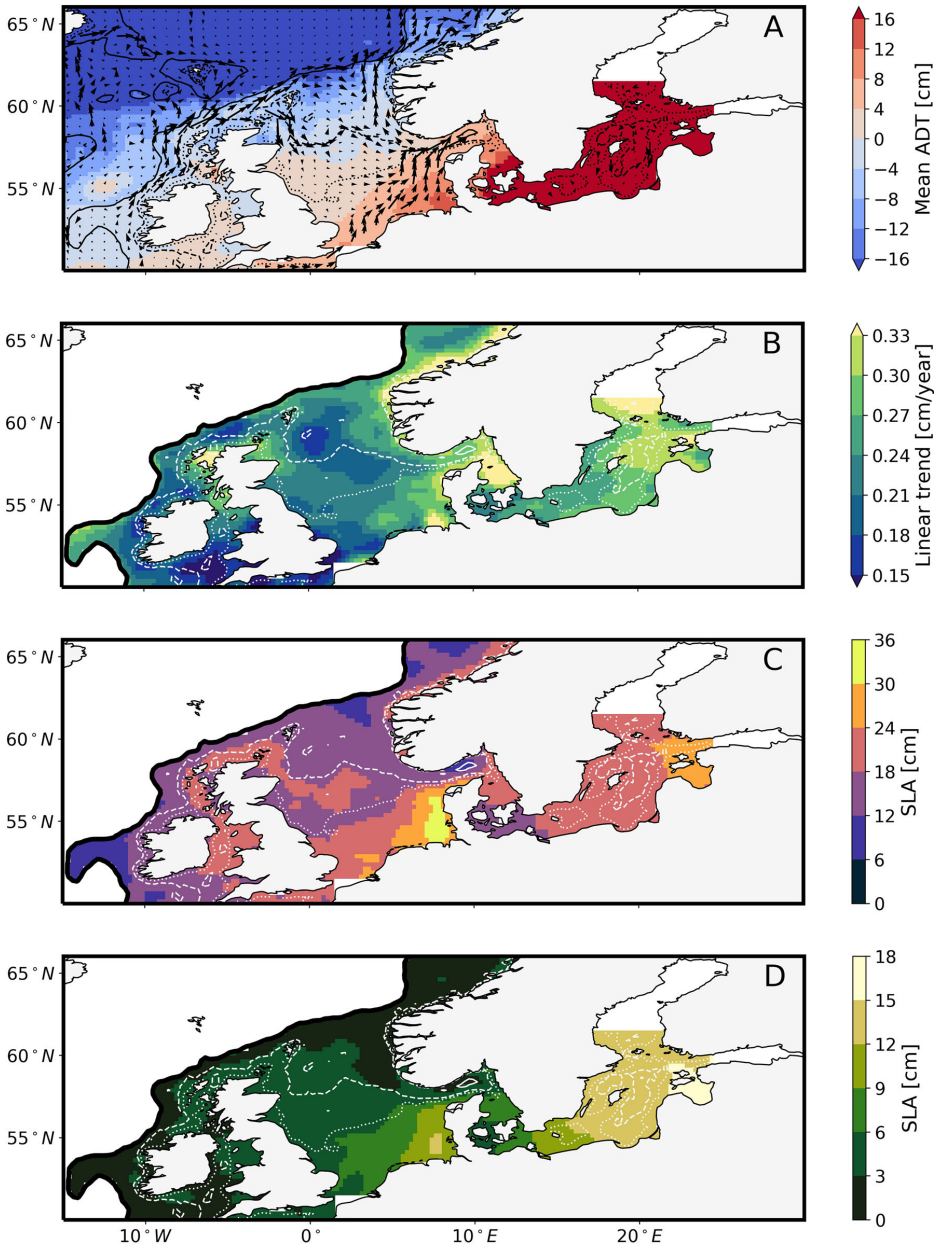

Fig. 1. Spatial sea level statistics from satellite altimetry: (A) annual mean absolute dynamic topography (shading, in cm) over the 1993–2014 period, (B) linear trend (cm/year), (C) range of the seasonal cycle of the sea level anomaly (cm), and (D) standard deviation of the winter-mean sea level anomaly, after removing the linear trend and the seasonal cycle (cm). Mean depth-averaged current from the TOPAZ4 reanalysis (arrows, in m s^{-1}) over the 1993–2014 period (A). The solid/dashed/dotted black/white lines indicate the 500 m/100 m/50 m isobaths, respectively. In B, C and D, the grid points over the open ocean are masked and the continental shelf is delimited by the thick black line.

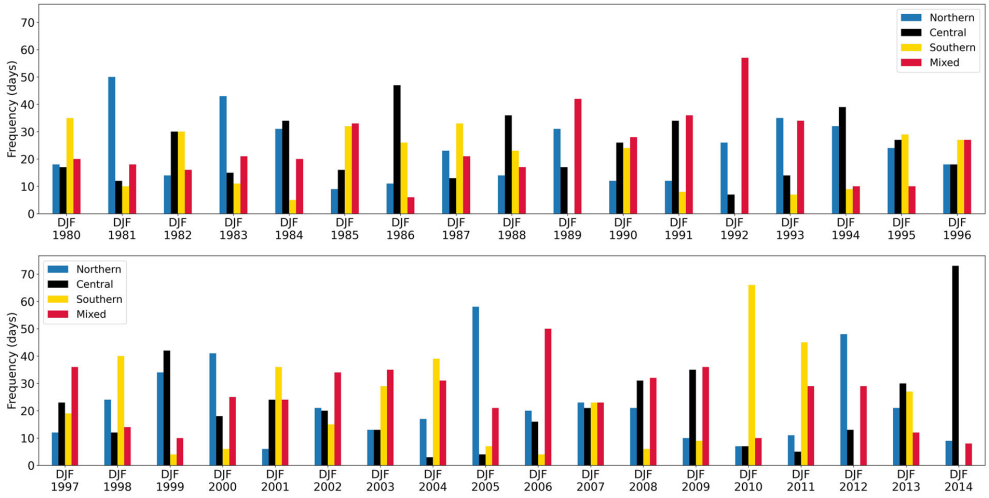

Fig. 2. Frequency (in days) of the jet clusters for each winter between December 1979 and February 2014.

applied to the altimetry data, such as the removal of astronomical tides and the inverse barometer effect, which is the pressure contribution to sea level. Sea level variability with periods shorter than 20 days has been removed as it may lead to aliasing of the satellite data.

We use the ADT to calculate the sea level anomaly (SLA), which is the sea surface height relative to the time-mean (1993–2014) sea level. We focus on the period between January 1993 and December 2014 for the ADT time series to overlap with that used for the calculation of the jet clusters (see Section 2.4). The domain of interest is 15°W–30°E and 50°N–66°N (Fig. 1), which includes the northern European continental shelf and parts of the Nordic Seas (the region located north of the northern European continental slope). To calculate the SLA, we remove the average of the daily ADT over the 21-year period between January 1993 and December 2014 at each grid point within the domain (Fig. 1A). We exclude all grid points whose time series of the ADT have gaps, most of which are concentrated in the northern part of the Baltic Sea and the Gulf of Finland, and appear in white in the figures below. Next, we remove the linear trend (Fig. 1B) and seasonal cycle (daily climatology; Fig. 1C). As a measure of the interannual variability of the winter SLA, which is the season of interest in this study, we also show the standard deviation of the winter-mean (December to February) SLA, after removing both the linear trend and the seasonal cycle (Fig. 1D).

Briefly, we note that the mean ADT (Fig. 1A) shows a meridional gradient in the North Sea (with values of −12 cm near the northern boundary and values of 4 cm in the south) and a zonal gradient in the southern part of the North Sea (with values ranging from approximately 4 cm in the southwest to 16 cm in the German Bight). Trends in sea level (Fig. 1B) are on the order of 1.5 to 3.3 mm year^{-1}, with the highest values being comparable to global mean sea level trends (Cazenave et al., 2018). The range of the seasonal cycle in ADT (Fig. 1C) depends strongly on the considered region, with smaller variations (∼15 cm) close to the continental slope and larger variations (∼20–30 cm) over the rest of the continental shelf. Finally, the standard deviation of the winter-mean SLA (Fig. 1D) ranges from 0 to 18 cm and has its minimum in the Norwegian Trench and the Norwegian shelf, and its maximum in the German Bight and the Baltic Sea.

2.3. Atmospheric data

We use the daily 10 m wind and mean sea level pressure (MSLP) fields from the ERA-Interim reanalysis dataset (Dee et al., 2011) of the European Centre for Medium-Range Weather Forecast (ECMWF) with a spatial resolution of 0.75° × 0.75°. We focus on the North Atlantic-European sector and December–January–February (DJF) winter seasons between 1993 and 2014 (21 winters in total) to overlap with the time period over which the jet clusters are calculated (see Section 2.4). Anomalies are calculated for all fields by removing the linear trend and the seasonal cycle (daily climatology).

We also use surface wind stress from satellite scatterometers merged with the ERA-Interim 6-hourly reanalysis dataset (Bentamy et al., 2017). Data are provided at a spatial resolution of 0.25° × 0.25° from January 1992

onwards. This dataset provides more reliable wind stress values over the northern European continental shelf compared to ERA-Interim, which tends to underestimate wind speeds associated with winter storms (A. Bentamy, personal communication). Similar to the 10 m wind and MSLP fields, we remove the linear trend and seasonal cycle (daily climatology) from the wind stress, and we consider only the winter seasons between December 1993 and February 2014.

The surface wind stress dataset contains gaps over the ocean west of the prime meridian. At any grid point, the gaps jointly comprise less than 20% of the days between January 1993 and December 2014, and mainly occur between 1996 and 2001. The presence of the gaps is a source of error for Fig. 6 (see Section 4) since it creates a band of anomalously high/low rate of change of the sea level along the prime meridian. Therefore, to produce Fig. 6, we identify and exclude all the days when the number of gaps over the ocean was anomalously high.

2.4. Jet clusters

We classify the winter-time large-scale variability of the atmosphere according to four North Atlantic jet clusters (Madonna et al., 2017). The jet clusters represent different configurations of the eddy-driven jet stream: northern (N), central (C), southern (S), and 'mixed' (split or strongly tilted; M). They are defined from the daily low-pass filtered zonal wind field between 900 and 700 hPa over the North Atlantic (60°W–0°, 15°N–75°N) using a k-mean clustering algorithm (see details in Madonna et al., 2017) and correspond directly to the four classical Euro-Atlantic weather regimes (e.g. Vautard, 1990; Michelangeli et al., 1995).

The relationship between the jet clusters and the weather regimes gives confidence that the jet clusters represent physical states of the atmosphere. Previous studies (e.g. Michelangeli et al., 1995; Cassou et al., 2011; Barrier et al., 2013, 2014) confirmed that the same North Atlantic regimes emerge robustly when the analysis is repeated with different variables (e.g. MSLP, 500 hPa geopotential height), different methods (e.g. k-mean clustering, hierarchical clustering), and different reanalysis products covering different periods. A sufficiently long record is needed, however, to properly sample the large internal variability of the atmosphere, especially in the largely eddy-driven North Atlantic sector (Li and Wettstein, 2012). Therefore, to calculate the jet clusters, we use 35 winters from 01 December 1979 to 28 February 2014 (as in Madonna et al., 2017), even if for sea level analysis we only consider the period starting from December 1993. Even though the frequency of occurrence exhibits a large interannual variability (Fig. 2), we expect not to under-represent any jet cluster by selecting this period of time. Indeed, the jet clusters occur with similar frequency over the periods 1993–2014, 1979–1993 and 1979–2014 (Table 1), in agreement with Madonna et al. (2019) (their Fig. 6). When compared to the NAO, Madonna et al. (2017) showed that the negative phase of the NAO resembles the Southern jet cluster, whereas the positive phase of the NAO does not clearly relate to any jet cluster and, therefore, corresponds to different jet configurations.

Figure 3 shows composites of the daily 10 m wind and MSLP anomalies for each jet cluster. The Northern jet cluster (Fig. 3N, blue frame) is characterised by a zonal eddy-driven jet stream directed towards Scandinavia (contours at ~55°N) and a MSLP dipole with positive values over the subpolar gyre and negative values over the Nordic Seas. During Central jet cluster events (Fig. 3C, black frame), the eddy-driven jet stream is located at ~45°N, directed towards France and the UK, with a low MSLP anomaly over the North East Atlantic and the North Sea. The Southern jet cluster (Fig. 3S, yellow frame) has a zonally oriented eddy-driven jet stream located at approximately 35°N over the mid-latitude North Atlantic and is characterised by an atmospheric high pressure anomaly over Greenland. The Mixed jet cluster (Fig. 3M, red frame) is characterised by a split or strongly tilted jet stream. Its main features are strong westerly winds over the Nordic Seas and a high pressure anomaly over northern and central Europe that is linked to Scandinavian blocking (Madonna et al., 2017).

3. Spatial relationship between the northern European sea level and the jet clusters

3.1. Sea level patterns and jet clusters

Each jet cluster is associated with a distinct sea level pattern over the northern European continental shelf (Fig. 4). We identify each pattern through composite analysis, by averaging the SLA over all the days of occurrence of each jet cluster. This approach does not account for the time needed for the sea level to adjust to variations in the wind field and, therefore, does not consider that the sea level pattern over the northern European continental shelf might not be representative of the dominant jet cluster during its first few days of occurrence. To check whether this might affect the results in Fig. 4, we repeat the composite maps, this time selecting only those cases when the jet clusters persist for four days or longer (Fig. S1). We find that the results in Fig. 4 are robust. In fact, Fig. S1 shows the same patterns as in Fig. 4, but the former are slightly more pronounced than the latter (by 1 to 2 cm).

Table 1. Frequency of occurrence of each jet cluster over the entire period considered (December 1979–February 2014), between December 1979 and February 1993 and over the period covered in the paper (December 1993 and February 2014).

	December 1979–February 2014	December 1979–February 1993	December 1993–February 2014
Northern jet cluster	~25%	~26%	~25%
Central jet cluster	~25%	~25%	~25%
Southern jet cluster	~22%	~19%	~23%
Mixed jet cluster	~28%	~29%	~27%

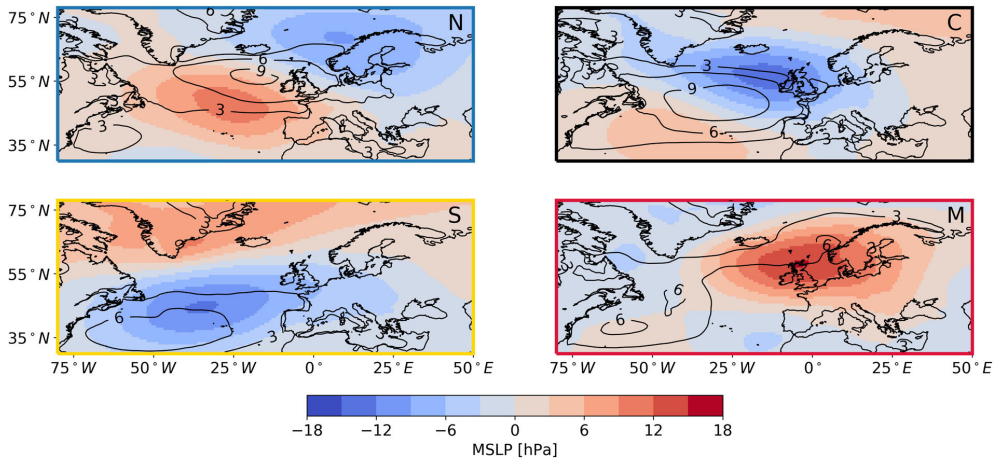

Fig. 3. Composite maps of daily mean sea level pressure anomaly (shading, in hPa) and 10 m zonal winds (black contours, 3 m s^{-1} intervals from 3 m s^{-1}) for each jet cluster: (N) Northern jet cluster, (C) Central jet cluster, (S) Southern jet cluster, (M) Mixed jet cluster.

The sea level patterns associated with the jet clusters are particularly strong in the North Sea and the Baltic Sea. In the German Bight and the Baltic Sea, extremely low SLA values (less than −8 cm) are associated with the Southern jet cluster, whereas, along the east coast of England, they are associated with the Central jet cluster. Extremely high SLA values (exceeding 8 cm) are also found in the German Bight and the Baltic Sea, but are associated with the Northern jet cluster. Over the rest of the North Sea, anomalous sea level values are not related to one single jet cluster: negative SLA values are associated with both the Southern and the Central jet clusters, whereas positive SLA values are associated with both the Northern and the Mixed jet clusters. We note that the lowest (−6 cm circa) and the highest (6 cm circa) SLA values in the middle and the northern part of the North Sea are associated with the Central and Mixed jet cluster, respectively.

Sea level anomalies over the Norwegian shelf are generally small compared to the rest of the study area. This is to be expected to some extent, as the Norwegian shelf also exhibits a weaker seasonal cycle (Fig. 1C) and weak overall sea level variability (Fig. 1D, see also Section 3.2). In fact, SLA is statistically different from zero (at a 0.05 significance level) only for the Southern jet cluster. Despite it being relatively small, the SLA pattern associated with the Southern jet cluster is still of interest since it is comparable in magnitude to the interannual SLA variability over the Norwegian shelf (Fig. 1D), meaning that the Southern jet cluster contributes meaningfully to the interannual SLA variability in the region.

The amplitude of the SLA patterns associated with each jet cluster is smaller but not negligible relative to the amplitude of the seasonal cycle, which is one of the most pronounced features of sea level variability (Fig. 1C). In fact, the magnitude of the SLA associated with the Northern and the Southern jet clusters is approximately one fourth the amplitude of the seasonal cycle in the southern North Sea and approximately one third in the Baltic Sea. Similarly, in the southwest part of the North Sea, the SLA associated with the Central jet cluster is up to one third the amplitude of the seasonal cycle. Therefore, the wind-driven sea level variability associated

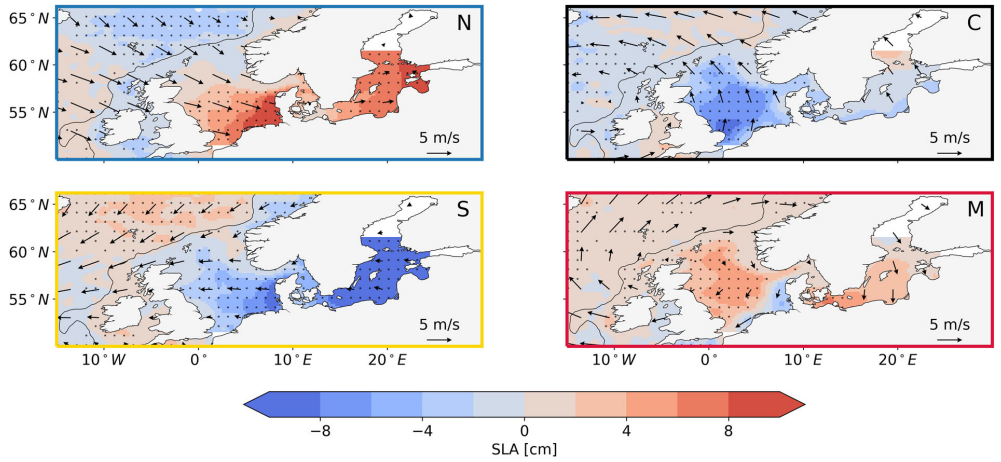

Fig. 4. Composite maps of daily sea level anomaly (shading, in cm) and 10 m wind anomaly (arrows, in m s^{-1}) for each jet cluster: (N) Northern jet cluster, (C) Central jet cluster, (S) Southern jet cluster, (M) Mixed jet cluster. The black dots denote regions where the sea level anomaly composite is significantly different from zero at a 0.05 significance level. The grey line shows the location of the continental slope, depicted by the 500 m isobath.

with the jet clusters accounts for interannual variability of the seasonal cycle in sea level over a large portion of the northern European shelf, which, in turn, can affect both the height and frequency of occurrence of storm surges in the region (Dangendorf et al., 2012).

Finally, a longer term perspective shows that the SLA patterns associated with the jet clusters are of the same order of magnitude as the sea level rise from 1993 to 2014. Indeed, over the period considered, northern European sea level has risen from approximately 3 cm in the northern North Sea up to 6 cm in the Baltic Sea and the German Bight (Fig. 1B). A comparison between Figs. 1B and 4 can help identify the regions of the shelf where the computed rate of change of sea level is most subject to errors. For example, the error associated with the rate of sea level change is likely to be higher for the southern Baltic Sea and the interior of the North Sea than over the Norwegian shelf. Indeed, compared to the former regions, the latter experiences a similar sea level trend but a weaker atmospheric component of the sea level variability.

3.2. Variability in jet-based sea level anomalies

To better identify the locations of the northern European continental shelf where the SLA variability is most strongly associated with the jet clusters, we compare the composite maps of the SLA (Fig. 4) to a measure of total sea level variability on the shelf. At each grid point, we standardise the composite map of the SLA associated with each jet cluster ($\overline{SLA_{jc}}$) by dividing it by the standard deviation of the daily SLA over the 21-winter record (s_{SLA}):

$$\frac{\overline{SLA_{jc}}}{s_{SLA}} \tag{2}$$

When complemented with Fig. 4, Fig. 5 helps identify smaller scale features in the sea level patterns associated with the Northern, the Central, and the Southern jet clusters. From Fig. 5, we learn that the Northern jet cluster explains a higher fraction of the SLA variability in the German Bight than in the Baltic Sea, despite the corresponding composite values of the SLA exceeding 8 cm in both regions (Fig. 4). In addition, we note that, for the Northern jet cluster, the standardised SLA does not significantly change in the southern North Sea, meaning that the Northern jet cluster describes a similar fraction of the SLA variability in the region, even though the composite of the SLA shows lower values along the coast of England than in the German Bight. From Fig. 4, we also know that the lowest sea level values (< -8 cm) occur along the east coast of England during Central jet cluster events, and in the German Bight and the Baltic Sea during Southern jet clusters events. However, when we compare the corresponding standardised values of the SLA, we note that the Central jet cluster describes a larger fraction of the SLA than the Southern jet cluster (the Central jet cluster explains more than 70% of the variability there). In addition, we also note that, opposite to the Northern jet cluster, the Southern jet cluster

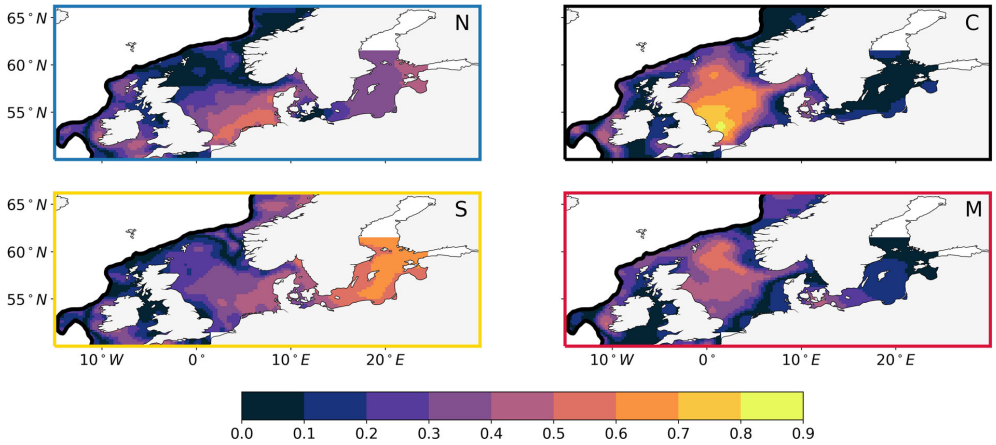

Fig. 5. Standardised maps of the composite of the daily sea level anomaly for each jet cluster: (N) Northern jet cluster, (C) Central jet cluster, (S) Southern jet cluster, (M) Mixed jet cluster. To standardise the maps in Fig. 4, we divide them by the standard deviation of the daily sea level anomaly over the 21-winter record. The grid points over the open ocean are masked and the continental shelf is delimited by the thick black line (the 500 m isobath).

describes a higher fraction of the SLA variability in the Baltic Sea than in the German Bight.

Additionally, one interesting message emerges for the Norwegian shelf. For the southern jet cluster, Fig. 5S shows similar values over the Norwegian shelf and in the German Bight. Therefore, even though the actual SLA over the Norwegian shelf is much smaller than in the German Bight (Fig. 4S), the southern jet cluster gives a similar contribution to sea level variability in the two regions.

3.3. Attribution of sea level variability

We now summarise the results in the previous sections by showing, into two maps, the jet clusters that are mostly associated with anomalously high and anomalously low SLA values across the northern European continental shelf. At each grid point, we compute the frequency of occurrence of the jet clusters during the days when the SLA is particularly high and during the days when it is particularly low. Then, at each grid point, we count the frequency of occurrence of the jet clusters on days when the SLA departs from the mean by more than -1.5 and by more than 1.5 standard deviations. In the end, we colour each grid point according to the frequency of occurrence of the jet clusters, to highlight the jet clusters that are most strongly associated with anomalous sea level values at that location (Fig. 6). If one of the jet clusters occurs at least 50% of time the SLA is anomalously high or low, the point is assigned to this jet cluster. If no single jet cluster satisfies this condition, we consider all possible combinations of two jet clusters amounting to at least 50% frequency and assign the point to the combination with the highest frequency (see the caption of Fig. 6 for more information on the corresponding colours). If the frequency of occurrence associated with each combination is lower than 0.5, we colour the grid point grey.

The results in Fig. 6 mostly agree with those in Fig. 4, even though the former are partly contaminated by the SLA variability within each jet cluster. Both figures show that the Northern and Mixed jet clusters are important for anomalously high SLA values in the North Sea (Fig. 6A), and that the Central jet cluster is important for anomalously low SLA values in the North Sea (Fig. 6B). At the same time, however, anomalously low SLA values in the German Bight correspond both to the Central and the Southern jet clusters, despite the composite of the SLA for the Central jet cluster showing values close to zero in the region (Fig. 4). This suggests that, in the German Bight, over individual Central jet cluster events, the SLA can significantly depart from the composite value of the SLA associated with the Central jet cluster. We reach a similar conclusion for the Baltic Sea. In fact, Fig. 6 relates anomalously high SLA values to the Northern and the Mixed jet clusters, and anomalously low SLA values to the Southern and the Central jet clusters, even though Fig. 4 only associates the Northern and the Southern jet clusters with particularly high and low SLA values in the region. Over the Norwegian shelf, we only focus on the negative SLA values since Fig. 4 has already shown that positive values are not

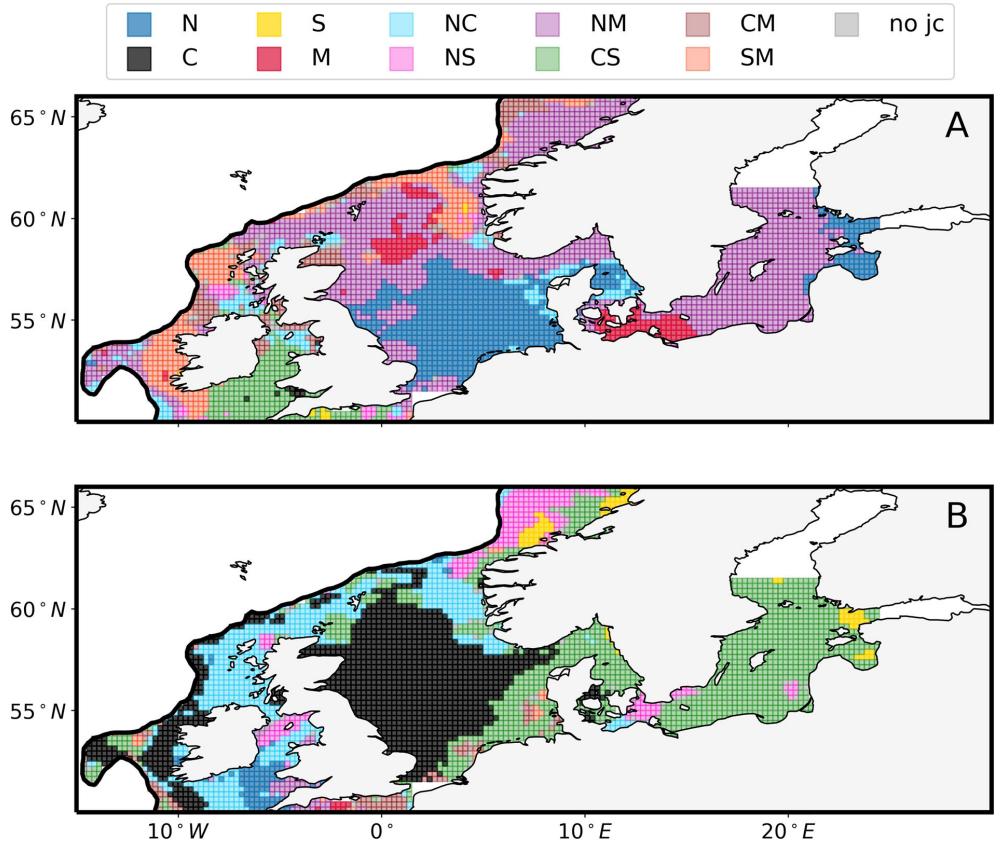

Fig. 6. Maps of jet clusters most strongly associated with anomalously high (A) and with anomalously low (B) sea level anomaly. Colours correspond to: Northern jet cluster (blue), Central jet cluster (black), Southern jet cluster (yellow), Mixed jet cluster (red), Northern and Central jet clusters (light blue), Northern and Southern jet clusters (lilla), Northern and Mixed jet clusters (purple), Central and Southern jet clusters (green), Central and Mixed jet clusters (brown), Southern and Mixed jet clusters (orange), otherwise ('no jc', grey). The grid points over the open ocean are masked and the continental shelf is delimited by the thick black line (i.e. the 500 m isobath).

clearly associated with any jet cluster. We note that Fig. 6 only partly agrees with Fig. 4. In fact, Fig. 6 shows that particularly low SLA values in the region correspond to the Northern, the Central, and the Southern jet clusters, even though we note that only the Southern jet cluster is associated with anomalously low SLA values over the entire Norwegian shelf.

4. Dynamic considerations

In this paper, we have adopted the jet cluster perspective of the winter-time atmospheric circulation in the North Atlantic to document the contribution of local winds to the sea level variability over the northern European continental shelf. As a result, we have identified four patterns of SLA, each corresponding to a different configuration of the eddy-driven jet stream over the North Atlantic. In this section, we briefly discuss the dynamics of the ocean over the northern European continental shelf to investigate the role of local winds in driving the sea level patterns associated with each jet cluster. We start the discussion by identifying the main forces operating on the shelf. We conclude it by discussing the ability of the simple Ekman theory to explain the sea level patterns associated with each jet cluster.

Table 2. Magnitude of the depth-averaged Coriolis force, of the depth-averaged pressure gradient force and, of the depth-averaged force exerted by the winds, all averaged over the entire northern European continental shelf (more precisely, over the region of the shelf delimited by the coordinates 3°W–30°E and 51°N–66°N). Units are m s^{-2}.

	Coriolis force	Pressure gradient force	Force exerted by the winds
Northern jet cluster	1.7×10^{-6}	1.3×10^{-6}	2.0×10^{-6}
Central jet cluster	2.0×10^{-6}	1.5×10^{-6}	1.7×10^{-6}
Southern jet cluster	1.8×10^{-6}	1.7×10^{-6}	1.3×10^{-6}
Mixed jet cluster	1.7×10^{-6}	1.5×10^{-6}	1.4×10^{-6}

To describe the barotropic response of the ocean over the northern European continental shelf to each jet cluster, we use the depth-averaged momentum equation which, based on considerations found in previous studies, reduces to the balance of only three forces: the depth-averaged Coriolis force, the depth-averaged pressure gradient force and the depth-averaged force exerted by the winds. The ocean in the North Sea needs approximately two days to adjust to changes in the winds (e.g. Weenink, 1956; Pingree and Griffiths, 1980): since the jet clusters persist on average five days (Madonna et al., 2017), we expect the sea level pattern associated with each jet cluster (Fig. 4) to be approximately in steady state and, consequently, the term $d\boldsymbol{u}/dt$ in the depth-averaged momentum equation to be negligible. Through scaling considerations, Pingree and Griffiths (1980) showed that the vertically averaged advection and bottom friction can also be neglected. Therefore, the depth-averaged momentum equation becomes:

$$f\hat{k} \times \boldsymbol{u} = -g\nabla(SLA) + \frac{1}{\rho_w \cdot H}\boldsymbol{\tau_w} \tag{3}$$

where the term on the left-hand side of Eq. (3) is the depth-averaged Coriolis force, the first term on the right-hand side is the depth-averaged pressure gradient force, and the second term is the depth-averaged force exerted by the wind stress; $f = 2\Omega \sin(\phi)$ is the Coriolis parameter, $\hat{k}$ is the vertical unit vector, $\boldsymbol{u}$ is the depth-averaged current, $g = 9.8\,\mathrm{m\ s^{-2}}$ is the gravitational acceleration, ρ_w is the density of seawater, H is the water depth, and $\boldsymbol{\tau}_w$ is the wind stress.

It is not possible to simplify Eq. (3) further, as all three forces have similar magnitudes over the northern European continental shelf (Table 2). Table 2 shows, for each jet cluster, the magnitude of the depth-averaged Coriolis force, of the depth-averaged pressure gradient force, and of the depth-averaged force exerted by the winds, all averaged over the northern European continental shelf (more precisely, over the region of the shelf delimited by the coordinates 3°W–30°E and 51°N–66°N). We note that the three forces are comparable in magnitude on the shelf. This result is robust since we reach a very similar conclusion when we compare the magnitude of the three forces at each grid point on the shelf (not shown).

Since both the wind stress term and the Coriolis force are important, the relationship between local winds and sea-level patterns associated with each jet cluster can be partly explained in terms of Ekman transport. To show its contribution, we compute the Ekman transport associated with each jet cluster and the rate of change of the sea level that it induces (Fig. 7). To calculate the Ekman transport, we use the formula for the volume transport generated by a stable wind blowing over an infinitely deep ocean (e.g. Gill, 1982; Cushman-Roisin and Beckers, 2010):

$$\boldsymbol{U}_{ek} = -\frac{1}{\rho_w f}\hat{k} \times \boldsymbol{\tau} \tag{4}$$

where $\boldsymbol{U}_{ek}$ is the Ekman volume transport, ρ_w is the mean density (chosen equal to $1030\,\mathrm{kg\ m^{-3}}$), f is the Coriolis parameter, $\hat{k}$ is the vertical unit vector, and $\boldsymbol{\tau}$ is the wind stress at 10 m above the sea surface.

We find that Ekman transport explains well the sea level pattern associated with the Mixed jet cluster, it partly explains the sea level patterns associated with the Central and the Southern jet clusters, but it cannot explain the sea level pattern associated with the Northern jet cluster (Fig. 7). During Mixed jet cluster events, the anticyclonic winds over northern Europe cause water to converge into the middle and the northern parts of the North Sea and onto the Norwegian shelf (Fig. 7M). Indeed, the south-westerly winds over the Nordic Seas generate a south-eastward Ekman transport, whereas the easterly winds over the southern North Sea generate a northward Ekman transport. As a result, local winds drive water into the interior and the northern North Sea and, therefore, sustain the positive SLA in the region (Fig. 4M). Through Ekman transport, the winds over the Nordic Sea also push water onto the Norwegian shelf and, therefore, explain the positive SLA in the area. During Central jet cluster events, the southerly winds over the North Sea induce an eastward Ekman transport, which drives water from the UK to the coasts of

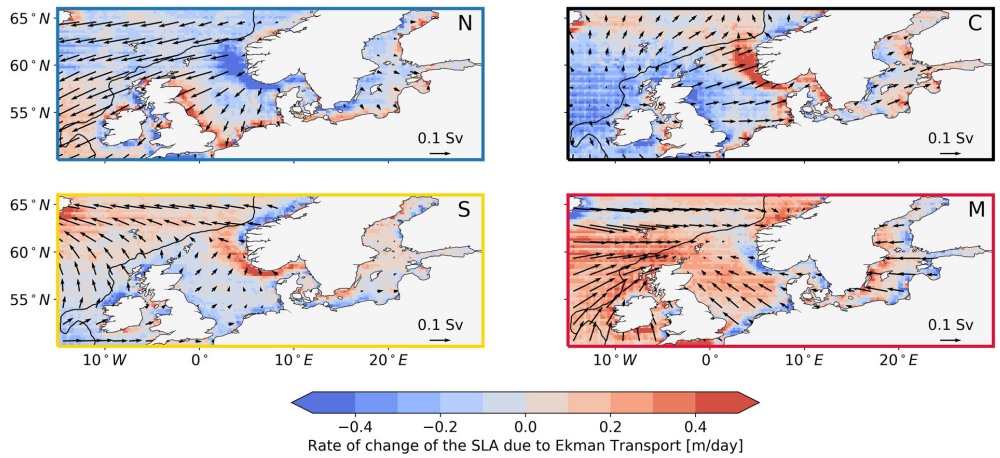

Fig. 7. Ekman transport associated with each jet cluster (arrows, $1\,\mathrm{Sv} = 10^{-6}\ \mathrm{m^3\,s^{-1}}$) and rate of change of the sea level anomaly as a result of Ekman transport (m $\mathrm{day^{-1}}$) for each jet cluster: (N) Northern jet cluster, (C) Central jet cluster, (S) Southern jet cluster, (M) Mixed jet cluster. Positive values indicate regions of convergence, whereas negative values indicate regions of divergence.

Denmark and Norway (Fig. 7C) and, therefore, explain the eastward sea level gradient in the basin (Fig. 4C). Similarly, during Southern jet cluster events, the easterly winds generate a northward Ekman transport, which pushes water into the open ocean and, in turn, decreases the sea level over the entire northern European continental shelf (Fig. 4S). As previously stated, Ekman transport does not explain all the features of the composite maps in Fig. 4 such as the meridional sea level gradient associated with the Northern jet cluster. As a possible explanation, we need to remember that the effects of the winds are highly affected by the bathymetry and the coastline geometry. As an example, Davies and Heaps (1980) showed how the presence of the Norwegian trench modifies the wind driven circulation and, therefore, the sea level pattern in the North Sea.

We would like to conclude this section with a note on the ocean circulation over the northern European continental shelf. By relating the wind stress, the SLA, and the depth-averaged currents, Eq. (3) suggests that the jet clusters might not only relate to sea level patterns, but also to ocean circulation patterns on the shelf (Fig. 1A). Figure 4 suggests this hypothesis: since the SLA gradient associated with each jet cluster is comparable with that of the mean ADT (Fig. 1A), the jet clusters could alter the geostrophic component of the circulation on the shelf. As an example, we note that the meridional SLA gradient associated with the Northern jet cluster is approximately half that of the mean ADT, meaning that the geostrophic component of the circulation in the North Sea might be strengthened by circa 50% during Northern jet cluster events.

5. Temporal relationship between the northern European sea level and the jet clusters

While in the previous sections, we have considered the spatial relationship between the northern European SLA and the jet clusters, we now address their temporal covariability at daily and monthly time scales. At first, we focus on the relationship at a few days' time scale, and we describe the evolution of the northern European SLA as the jet clusters persist for a few consecutive days. Then, we focus on the relationship at monthly time scale, and we assess to what extent the jet clusters reconstruct the monthly mean SLA variation over the northern European continental shelf.

5.1. Daily sea level evolution

The SLA from altimetry contains information on how the northern European sea level approaches equilibrium as the jet clusters persist for a few consecutive days. To analyse the adjustment process, we identify those cases when the jet clusters persist five days or longer and, for each jet cluster, we composite the SLA over the first and the fifth day of persistence, respectively (Fig. 8). We set the threshold at five days because we expect the northern European SLA to reach the equilibrium within this amount of time (e.g. Pingree and Griffiths, 1980; Saetre et al., 1988; Leppäranta and Myrberg, 2009) and also because it ensures a sufficiently large number of cases for a robust composite analysis (see Table 3).

Figure 8 shows a clear evolution of the SLA in relation to the Central and the Mixed jet clusters. If, on its first day

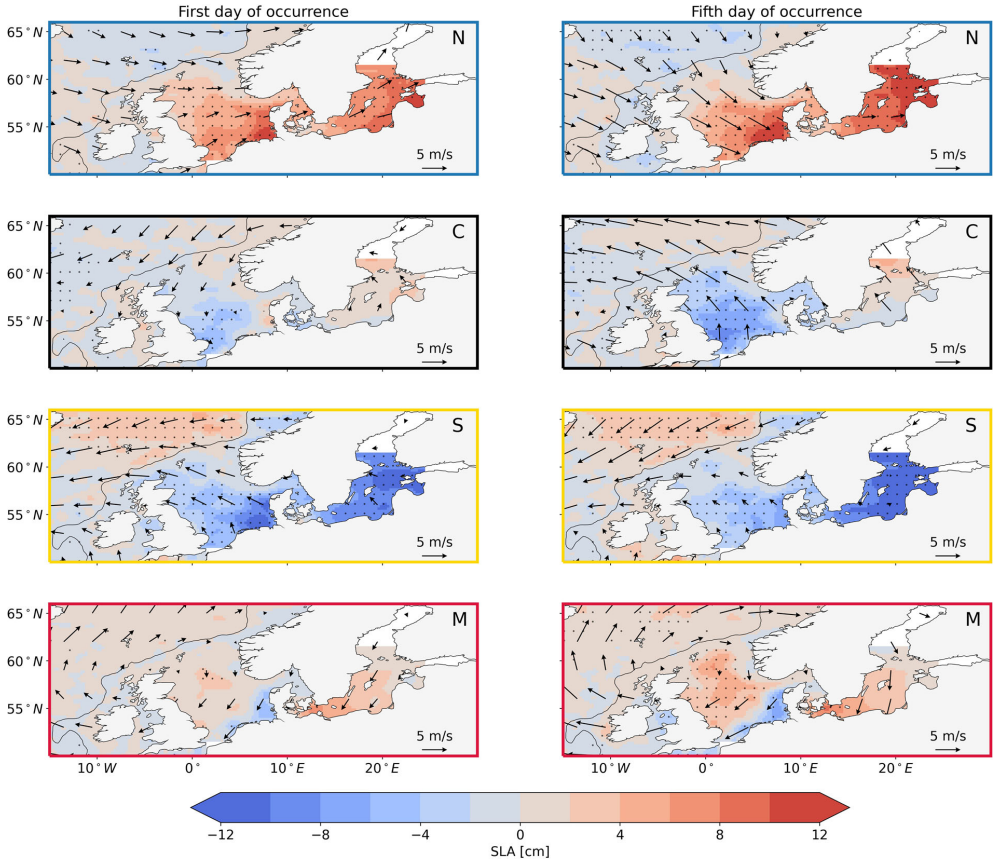

Fig. 8. Composite maps of daily sea level anomaly (shading, in cm) and 10 m wind anomaly (arrows, in m s^{-1}) over the first days (left column) and the fifth days (right columns) of persistence of each jet cluster: (N) Northern jet cluster, (C) Central jet cluster, (S) Southern jet cluster, (M) Mixed jet cluster. The black dots denote regions where the sea level anomaly composite is significantly different from zero at a 0.05 significance level. The grey line shows the location of the continental slope, depicted by the 500 m isobath.

of persistence, the Central jet cluster is associated with weak winds, on its fifth day of persistence, winds are southerly/south-easterly and their intensity exceeds 5 m s^{-1} over most of the continental shelf. Over the same period of time, the SLA drops by a few centimetres both in the western side and in the interior of the North Sea. Likewise, as the Mixed cluster persists for five consecutive days, the anticyclonic wind pattern over northern Europe intensifies, and the SLA rises in the interior of the North Sea.

On the contrary, the evolution of the SLA in relation to the Northern and the Southern jet clusters is less evident. We still see a slight increase of the SLA in the German Bight and the Baltic Sea during Northern jet cluster events and a few centimetres drop in the Baltic Sea during Southern jet cluster events. However, contrary to our expectations, the SLA in the German Bight rises as the Southern jet cluster persists for a few consecutive days. Moreover, on their first day of occurrence, both jet clusters are already associated with well developed SLA patterns.

5.2. *Interannual sea level variability*

The atmospheric circulation over Europe is linked to the configuration of the jet stream over the North Atlantic (e.g. Madonna et al., 2017). Therefore, we expect the frequency of occurrence of different jet configurations to explain part of the monthly mean sea level variability over the northern European continental shelf. To estimate the strength of this relationship, at each grid point of the

Table 3. Number of cases when each jet cluster persists at least five consecutive days.

	Northern jet cluster	Central jet cluster	Southern jet cluster	Mixed jet cluster
Number of cases	38	32	28	43

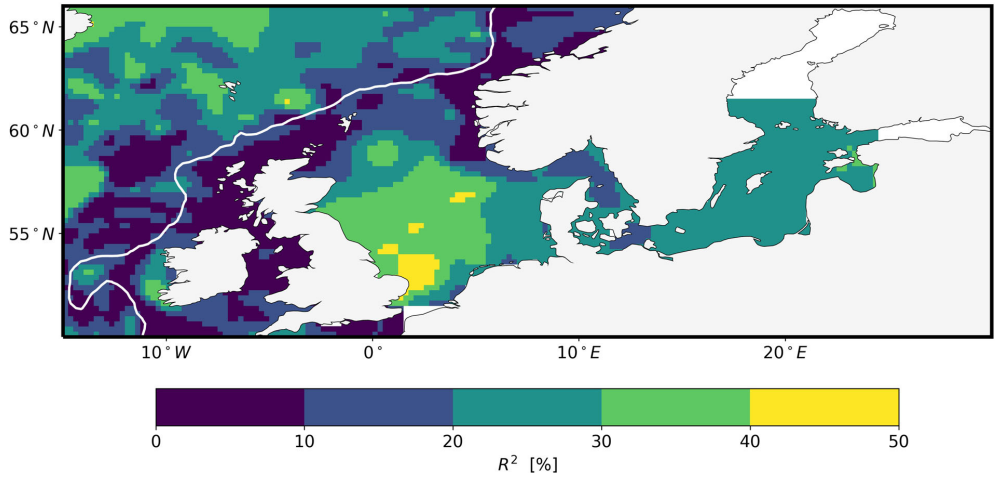

Fig. 9. At each grid point, fraction of the monthly mean sea level anomaly variance in winter that is explained by the multiple linear regression model.

northern European continental shelf, we build the following multiple linear regression model:

$$SLA = a + b \cdot freq_N + c \cdot freq_C + d \cdot freq_S + e \cdot freq_M \quad (5)$$

where SLA is the monthly mean SLA in winter, and $freq_N$, $freq_C$, $freq_S$, $freq_M$ are the monthly frequency of occurrence of the Northern, the Central, the Southern, and the Mixed jet clusters. We expect the regression model based on the jet clusters to explain a lower fraction of the monthly mean SLA variance when compared to a model based on the EOFs since this, by design, would maximise the explained variance of the SLA. However, the model above is still valuable: it can help quantify the contribution of the wind direction to the northern European sea level variability since the jet clusters determine the spatial pattern of the daily wind field over the North Atlantic, rather than its intensity.

Figure 9 shows that the temporal co-variability between the jet clusters and the northern European sea level varies considerably over the northern European continental shelf. We find the strongest covariance in the interior and in the western part of the North Sea, where the model explains between 40 and 50% of the SLA variance. The fraction of the variance explained by the model decreases in the Baltic Sea and the eastern part of the North Sea, where it mostly ranges between 20 and 30%, and reaches its lowest values in the Norwegian Trench, over the Norwegian shelf and along the continental slope, where it does not exceed 20%.

6. Conclusions and outlook

The jet cluster approach helps identify a number of locations (~40% of the northern European continental shelf) where a single jet cluster induces either high or low sea level values and therefore sheds new lights on the atmospheric control on the North European sea level. For example, negative SLA values along the east coast of England are mainly associated with the Central jet cluster, whereas positive SLA values in the German Bight are mainly associated with the Northern jet cluster. The case of the German Bight offers an interesting comparison with Dangendorf et al. (2014), who used both a correlation map and a composite analysis approach to determine the single atmospheric pattern responsible for anomalously high sea level values in the region. Indeed, we note that the approach based on the jet clusters and the one developed by Dangendorf et al. (2014) return partly different results: while the spatial structure of the atmospheric pattern in Dangendorf et al. (2014) resembles the Northern jet cluster, its centres of actions are located

eastward with respect to those of the Northern jet cluster (Fig. 3N). This discrepancy might result from the linear regression approaches mixing different jet clusters since high sea level in the German Bight is not uniquely associated with the Northern jet cluster. An additional study that focuses on the sea level variations in the German Bight could help clarify whether the atmospheric index by Dangendorf et al. (2014) is accurate enough to reconstruct the wind component of the sea level variability in the region.

In other parts of the shelf, the sea level responds to more than one jet cluster. In Fig. 4, we note that positive SLA values along the east coast of England are associated with both the Northern and the Mixed jet clusters. Similarly, in the interior of the North Sea, negative SLA values are associated with both the Southern and the Central jet clusters. In addition, Fig. 6 shows that, in the Baltic Sea, anomalously low sea level values are associated with both the Southern and the Central jet clusters, whereas positive sea level values are associated with both the Northern and the Mixed jet clusters. Therefore, even though a composite analysis would return a single atmospheric pattern associated with either high or low sea level at these locations, this would not correspond to any typical atmospheric condition since it would result from a combination of several jet clusters.

The jet cluster approach can only partly describe the evolution and adjustment of northern European sea level to wind variations over the North Atlantic and northern Europe. In this regard, while the Central and the Mixed jet clusters are associated with an intuitive evolution of the northern European SLA, with the corresponding SLA patterns intensifying with the days of persistence, the Northern and the Southern jet clusters are not. Indeed, the SLA patterns associated with the Northern and the Southern jet clusters already reach the equilibrium on the first day of occurrence.

Considering longer timescales, the jet clusters framework provides new insights on the contribution of the winds to interannual sea level variability over the northern European continental shelf. Applying a multiple linear regression model, we show that the jet clusters can explain up to 50% of the SLA variance. The explained variance varies regionally and suggests that in some regions (e.g. the interior and western side of the North Sea), the large-scale flow (i.e. the wind direction) rather than the strength of the winds (i.e. the wind speed) affects the SLA variability, but further studies are required to investigate this in more details.

Future works might further explore the relationship between the jet clusters and the ocean circulation over the northern European continental shelf. An in-depth investigation of the link between the jet clusters and the two EOFs of surface circulation identified by Kauker and von Storch (2000) would be a follow-up of this study. In addition, the jet cluster perspective suggests that approximately 25% of the winter days are characterised by blocking conditions over northern Europe. We believe that a reference study that describes the ocean response to an anticyclonic wind pattern over northern Europe would be of interest since, to the authors' knowledge, it does not exist. Finally, the jet clusters could also be used to extend the work by Winther and Johannessen (2006), who used the NAO to investigate the atmospheric contribution to the exchange of water between the open-ocean and the North Sea. However, the NAO explains only a fraction of the atmospheric variability in the North Atlantic and might give an incomplete description of the atmospheric contribution to inflow and outflow of the northern European continental shelf. The jet clusters might provide a more complete and more realistic description of the exchange of water between the Nordic Seas and the shelf since they represent physical patterns of the atmosphere.

Acknowledgements

This study has been conducted using E.U. Copernicus Marine Service Information and the ERA-Interim reanalysis dataset provided by the European Centre for Medium-Range Weather Forecasts. The authors would like to thank an anonymous reviewer for the comments and suggestions, which improved the quality of the manuscript.

Disclosure statement

No potential conflict of interest was reported by the authors.

Funding

Fabio Mangini is funded with an institute fellowship of the Research Council of Norway (contract no. 272411/F40). This work was also supported by the Research Council of Norway project jetSTREAM (231716) and by the Climate Hazards and EXtremes (CHEX) project of the Bjerknes Centre from Climate Research. To conclude, Léon Chafik acknowledges support from the Swedish National Space Agency through the FiNNESS project (Dnr: 133/17).

Supplemental data

Supplemental data for this article can be accessed here.

References

Barrier, N., Treguier, A. M., Cassou, C. and Deshayes, J. 2013. Impact of the winter north-atlantic weather regimes on subtropical sea-surface height anomaly. *Clim. Dyn.* **41**, 1159–1171. doi:10.1007/s00382-012-1578-7

Barrier, N., Cassou, C., Deshayes, J. and Treguier, A. M. 2014. Response of North Atlantic circulation to atmospheric weather regimes. *J. Phys. Oceanogr.* **44**, 179–201. doi:10.1175/JPO-D-12-0217.1

Bentamy, A., Grodsky, S. A., Elyouncha, A., Chapron, B. and Desbiolles, F. 2017. Homogenization of scatterometer wind retrievals. *Int. J. Climatol.* **37**, 870–889. doi:10.1002/joc.4746

Cassou, C., Minvielle, M., Terray, L. and Périgaud, C. 2011. A statistical-dynamical scheme for reconstructing ocean forcing in the atlantic. Part I: weather regimes as predictors for ocean surface variables. *Clim. Dyn.* **36**, 19–39. doi:10.1007/s00382-010-0781-7

Cazenave, A., Meyssignac, B., Ablain, M., Balmaseda, M., Bamber, J. and co-authors. 2018. Global sea-level budget 1993-present. *Earth Syst. Sci. Data* **10**, 1551–1590.

Chafik, L., Nilsen, J. E. Ø. and Dangendorf, S. 2017. Impact of North Atlantic teleconnection patterns on northern European sea level. *JMSE.* **5**, 43. doi:10.3390/jmse5030043

Cushman-Roisin, B. and Beckers, J. M. 2010. *Introduction to Geophysical Fluid Dynamics. Physical and Numerical Aspects*. Vol. **101**. Academic Press, Cambridge, Massachusetts.

Dangendorf, S., Wahl, T., Hein, H., Jensen, J., Mai, S. and co-authors. 2012. Mean sea level variability and influence of the North Atlantic oscillation on long-term trends in the German Bight. *Water* **4**, 170–195. doi:10.3390/w4010170

Dangendorf, S., Wahl, T., Nilson, E., Klein, B. and Jensen, J. 2014. A new atmospheric proxy for sea level variability in the southeastern North Sea: observations and future ensemble projections. *Clim. Dyn.* **43**, 447–467. doi:10.1007/s00382-013-1932-4

Davies, A. M. and Heaps, N. S. 1980. Influence of the Norwegian Trench on the wind-driven circulation of the North Sea. *Tellus* **32**, 164–175.

Dee, D. P., Uppala, S. M., Simmons, A. J., Berrisford, P., Poli, P. and co-authors. 2011. The ERA-Interim reanalysis: configuration and performance of the data assimilation system. *QJR Meteorol. Soc.* **137**, 553–597. doi:10.1002/qj.828

Gill, A. 1982. *Atmosphere-Ocean Dynamics*. Elsevier, New York.

Hurrell, J. W. 1995. Decadal trends in the North Atlantic oscillation: Regional temperatures and precipitation. *Science* **269**, 676–679. doi:10.1126/science.269.5224.676

Jevrejeva, S., Moore, J. C., Woodworth, P. L. and Grinsted, A. 2005. Influence of large-scale atmospheric circulation on European sea level: results based on the wavelet transform method. *Tellus A* **57**, 183–193. doi:10.3402/tellusa.v57i2.14609

Kauker, F. and von Storch, H. 2000. Statistics of "Synoptic Circulation Weather" in the North Sea as derived from a multiannual OGCM simulation. *J. Phys. Oceanogr.* **30**, 3039–3049. doi:10.1175/1520-0485(2000)030<3039:SOSCWI>2.0.CO;2

Lamb, H. H. and Frydendahl, K. 1991. *Historic Storms of the North Sea, British Isles and Northwest Europe*. Cambridge University Press, Cambridge.

Leppäranta, M. and Myrberg, K. 2009. *Physical Oceanography of the Baltic Sea*. Springer-Verlag, Berlin-Heidelberg-New York.

Li, C. and Wettstein, J. J. 2012. Thermally driven and eddy-driven jet variability in reanalysis. *J. Clim.* **25**, 1587–1596. doi:10.1175/JCLI-D-11-00145.1

Madonna, E., Li, C. and Wettstein, J. J. 2019. Suppressed eddy driving during southward excursions of the north atlantic jet on synoptic to seasonal time scales. *Atmos. Sci. Lett.* **20**, 1–11. doi:10.1002/asl.937.

Madonna, E., Li, C., Grams, C. M. and Woollings, T. 2017. The link between eddy-driven jet variability and weather regimes in the North Atlantic-European sector. *QJR Meteorol. Soc.* **143**, 2960–2972. doi:10.1002/qj.3155

Michelangeli, P. A., Vautard, R. and Legras, B. 1995. Weather regimes: recurrence and quasi stationarity. *J. Atmos. Sci.* **52**, 1237–1256. > 2.0.CO;2. doi:10.1175/1520-0469(1995)052<1237:WRRAQS>2.0.CO;2

Pingree, R. D. and Griffiths, D. K. 1980. Currents driven by a steady uniform wind stress on the shelf seas around the british-isles. *Oceanol. Acta* **3**, 227–236.

Pujol, M.-I., Faugère, Y., Taburet, G., Dupuy, S., Pelloquin, C. and co-authors. 2016. DUACS DT2014: the new multi-mission altimeter data set reprocessed over 20 years. *Ocean Sci.* **12**, 1067–1090. doi:10.5194/os-12-1067-2016

Richter, K., Nilsen, J. E. Ø. and Drange, H. 2012. Contributions to sea level variability along the Norwegian coast for 1960–2010. *J. Geophys. Res.* **117, 1-12. doi:**10.1029/2011JC007826.

Saetre, R., Aure, J. and Ljøen, R. 1988. Wind effects on the lateral extension of the Norwegian Coastal water. *Cont. Shelf Res.* **8**, 239–253. doi:10.1016/0278-4343(88)90031-3

Vautard, R. 1990. Multiple weather regimes over the North Atlantic: analysis of precursors and successors. *Mon. Wea. Rev.* **118**, 2056–2081. MWROTN⟩2.0.CO;2. doi:10.1175/1520-0493(1990)118<2056:MWROTN>2.0.CO;2

Wahl, T., Haigh, I. D., Woodworth, P. L., Albrecht, F., Dillingh, D. and co-authors. 2013. Observed mean sea level changes around the North Sea coastline from 1800 to present. *Earth Sci. Rev.* **124**, 51–67. doi:10.1016/j.earscirev.2013.05.003

Wakelin, S. L., Woodworth, P. L., Flather, R. A. and Williams, J. A. 2003. Sea-level dependence on the NAO over the NW European continental shelf. *Geophys. Res. Lett.* **30**, 1403.

Weenink, M. P. 1956. The "twin" storm surges during 21st–24th December, 1954. A case of resonance. *Dtsch. Hydrogr. Z.* **9**, 240–249. doi:10.1007/BF02020089

Winther, N. G. and Johannessen, J. A. 2006. North Sea circulation: Atlantic inflow and its destination. *J. Geophys. Res.* **111**, 1–12, doi:10.1029/2005JC003310.

Xie, J., Bertino, L., Counillon, F., Lisaeter, K. A. and Sakov, P. 2017. Quality assessment of the TOPAZ4 reanalysis in the Arctic over the period 1991–2013. *Ocean Sci.* **13**, 123–144. doi:10.5194/os-13-123-2017

Yan, Z., Tsimplis, M. N. and Woolf, D. 2004. Analysis of the relationship between the North Atlantic oscillation and sea-level changes in northwest Europe. *Int. J. Climatol.* **24**, 743–758. doi:10.1002/joc.1035

Ocean Sci., 18, 331–359, 2022
https://doi.org/10.5194/os-18-331-2022

Ocean Science Open Access EGU

Sea-level variability and change along the Norwegian coast between 2003 and 2018 from satellite altimetry, tide gauges, and hydrography

Fabio Mangini[1], Léon Chafik[2,3], Antonio Bonaduce[1], Laurent Bertino[1], and Jan Even Ø. Nilsen[4]

[1]Nansen Environmental and Remote Sensing Center and Bjerknes Centre for Climate Research, Bergen, Norway
[2]Department of Meteorology and Bolin Centre for Climate Research, Stockholm, Sweden
[3]National Oceanography Centre, Southampton, UK
[4]Institute of Marine Research and Bjerknes Centre for Climate Research, Bergen, Norway

Correspondence: Fabio Mangini (fabio.mangini@nersc.no)

Received: 9 June 2021 – Discussion started: 6 July 2021
Revised: 16 January 2022 – Accepted: 7 February 2022 – Published: 18 March 2022

Abstract. Sea-level variations in coastal areas can differ significantly from those in the nearby open ocean. Monitoring coastal sea-level variations is therefore crucial to understand how climate variability can affect the densely populated coastal regions of the globe. In this paper, we study the sea-level variability along the coast of Norway by means of in situ records, satellite altimetry data, and a network of eight hydrographic stations over a period spanning 16 years (from 2003 to 2018). At first, we evaluate the performance of the ALES-reprocessed coastal altimetry dataset (1 Hz posting rate) by comparing it with the sea-level anomaly from tide gauges over a range of timescales, which include the long-term trend, the annual cycle, and the detrended and deseasoned sea-level anomaly. We find that coastal altimetry and conventional altimetry products perform similarly along the Norwegian coast. However, the agreement with tide gauges in terms of trends is on average 6 % better when we use the ALES coastal altimetry data. We later assess the steric contribution to the sea level along the Norwegian coast. While longer time series are necessary to evaluate the steric contribution to the sea-level trends, we find that the sea-level annual cycle is more affected by variations in temperature than in salinity and that both temperature and salinity give a comparable contribution to the detrended and deseasoned sea-level variability along the entire Norwegian coast. A conclusion from our study is that coastal regions poorly covered by tide gauges can benefit from our satellite-based approach to study and monitor sea-level change and variability.

1 Introduction

Global mean sea level (GMSL) has been rising during the XX century and the beginning of the XXI century at a rate of approximately 1.5 mm yr^{-1} (Frederikse et al., 2020). Its rise is projected to continue, and even accelerate, in the future (Hermans et al., 2021), thus posing significant stress on coastal communities (Nicholls, 2011). At a local scale, though, sea-level variations can largely depart from the global average (Stammer et al., 2013). Therefore, accurate estimation and attribution of sea-level rise at regional scale are among the major challenges of climate research (Frederikse et al., 2018), with large societal benefit and impact due to the large human population living in coastal areas (e.g. Lichter et al., 2011). The Norwegian coast is no exception. While it appears less vulnerable to sea-level variations because of its steep topography and rocks resistant to erosion, it has a large number of coastal cities, most of which have undergone significant urban development in recent times (Simpson et al., 2015).

Since August 1992, when NASA and CNES launched the TOPEX/Poseidon mission, satellite altimetry has enormously expanded our knowledge of the ocean and the climate system (e.g. Cazenave et al., 2018). With the help of satellite altimetry, oceanographers and climate scientists could observe sea-level variations over almost the entire ocean (e.g. Nerem et al., 2010; Madsen et al., 2019) and understand their causes (e.g. Richter et al., 2020), detect ocean currents (e.g. Zhang et al., 2007) and monitor their variability (e.g. Chafik et al., 2015), and observe the evolution of climate events (e.g.

Ji et al., 2000) and investigate their origins (e.g. Picaut et al., 2002). Satellite altimetry has made these, and other achievements, possible because it has provided continuous sea-level observations over large parts of the ocean in areas where sea-level measurements were previously only occasional.

While invaluable over the open ocean, satellite altimetry measurements have historically been flagged as unreliable in coastal areas (e.g. Benveniste et al., 2020). Indeed, the accuracy of radar altimetry, which is 2–3 cm over the open ocean (e.g. Volkov and Pujol, 2012), deteriorates in coastal regions because of technical issues (e.g. Xu et al., 2019). Notably, large variations in the backscattering of the area illuminated by the radar altimeters (for example, due to the presence of land or to patches of very calm water in sheltered areas; Gómez-Enri et al., 2010) contaminate the returned echoes of radar altimeters, and the complex topography of continental shelves, together with the irregular shape of most coastlines, makes geophysical corrections in coastal areas less accurate than in the open ocean.

To increase the accuracy of radar altimetry in coastal regions, Passaro et al. (2014) have developed the Adaptive Leading Edge Subwaveform (ALES) retracking algorithm. The ALES retracker addresses the altimeter footprint contamination issue by avoiding echoes from bright targets (e.g. land). Several studies have found a clear improvement of the ALES-reprocessed satellite altimetry observations over conventional altimetry products in different areas of the world (e.g. Passaro et al., 2014, 2015, 2016, 2018, 2021), with the new algorithm providing estimates of the altimetry parameters in coastal areas with levels of accuracy typical of the open ocean for distances to the coast of up to circa 3 km (e.g. Passaro et al., 2014).

In this paper, we investigate how the ALES-reprocessed satellite altimetry dataset resolves sea level along the coast of Norway compared to all the tide-gauge records available over the 16-year period between 2003 and 2018. Indeed, to the best of our knowledge, previous validation studies have not considered the entire Norwegian coast but only parts of it: Passaro et al. (2015) focused on the transition zone between the North Sea and the Baltic Sea, whereas Rose et al. (2019) focused on Honningsvåg in northern Norway. The Norwegian coast also appears particularly interesting for validation purposes because, during the altimetry period, it is well covered by tide gauges and because conventional altimetry products have previously failed to reproduce the sea-level trends in the region (Breili et al., 2017). The present study will thus investigate the performance of ALES in relation to these issues.

We further use the ALES-reprocessed altimetry dataset in combination with a network of hydrographic stations along the coast of Norway to study the steric contribution to the sea-level variability in the region, which is known to be challenging at the regional scale (e.g. Raj et al., 2020; Richter et al., 2012). Richter et al. (2012) have already used tide gauges and hydrographic stations to assess the different contributions to the Norwegian sea-level variability between 1960 and 2010. However, compared to their study, we use the coastal altimetry dataset to reconstruct a monthly mean sea-level time series centred over each hydrographic station. This is an advantage over Richter et al. (2012) since some of the Norwegian tide gauges are located in sheltered areas and might not be representative of the variability captured by the nearest hydrographic station (which can be as far as 100 km apart). Moreover, compared to Richter et al. (2012), we analyse the annual cycle of the sea level in more detail by describing how its properties change along the Norwegian coast. Furthermore, sea-level measurements from satellite altimetry, unlike those from tide gauges, do not need to be corrected for vertical land motion.

This paper is organized as follows. Section 2 describes the data used in the coastal sea-level signal analysis. An analysis of sea-level components retrieved by each observational instrument is provided in Sect. 3. The coastal sea level from tide gauges and satellite altimetry is compared in terms of temporal variability and trends in Sect. 4. Section 5 focuses on the steric contribution to the sea-level estimates from altimetry, tide gauges, and hydrographic data. Section 6 summarizes and concludes.

2 Data

2.1 ALES-reprocessed multi-mission satellite altimetry

To provide more accurate sea-level estimates in coastal regions, the ALES retracker operates in two stages. At first, it fits the leading edge of the waveform to have a rough estimate of the significant wave height (SWH). Then, depending on the SWH, the algorithm selects a portion of the waveform (known as subwaveform) and fits it to estimate the range (the distance between the satellite and the sea surface), the SWH, and the backscatter coefficient.

The dataset is freely available on the Open Altimetry Database website of the Technische Universität München (https://openadb.dgfi.tum.de/en/, last access: 22 July 2020). The European Space Agency (ESA) also provides, through the Sea Level Climate Change Initiative Programme, a coastal satellite altimetry dataset reprocessed with the ALES retracker. However, it only covers the northern latitudes up to 60° N and, therefore, only part of the region of interest in this study (Benveniste et al., 2020).

The dataset includes observations from the following altimetry missions: Envisat (version 3), Jason-1, Jason-1 extended mission, Jason-1 geodetic mission, Jason-2, Jason-2 extended mission, Jason-3, SARAL, and SARAL drifting phase. These are provided at a 1 Hz posting rate (equivalent to an along-track resolution of circa 7 km) and cover the period from June 2002 to April 2020, with the exception of one data gap between November 2010 (end of Envisat) and March 2013 (start of SARAL) to the north of 66° N. Data

from different missions have been cross-calibrated so that there are no inter-mission biases.

Prior to distribution, several corrections have been applied to the satellite altimetry data. Among them, the geophysical corrections are of particular interest for the purpose of this study. Indeed, to validate the ALES-reprocessed altimetry against the Norwegian tide gauges, the same physical signal must be removed from both datasets. The geophysical corrections applied to the ALES-reprocessed altimetry data include the tidal and the dynamic atmospheric corrections (COSTA user manual, http://epic.awi.de/43972/1/User_Manual_COSTA_v1_0.pdf, last access: 22 July 2020). The correction for ocean and pole tides has been performed using the EOT11a tidal model. The solid-Earth-related tides have also been subtracted from the orbital altitude but, as it leaves the altimetry data in sync with the tide gauges (which are based on the solid Earth), this correction has no further interest for this study. The dynamic atmospheric correction (DAC), available at https://www.aviso.altimetry.fr/index.php?id=1278 (last access: 12 April 2021), removes both the wind and the pressure contribution to the sea-level variability at timescales shorter than 20 d and only the pressure contribution to the sea-level variability at longer timescales. The high-frequency component of the DAC is computed using the Mog2D-G high-resolution barotropic model (Carrère and Lyard, 2003), and it is removed because it would otherwise alias the altimetry data. The low-frequency component accounts for the static response of the sea level to changes in pressure, a phenomenon also known as the inverse barometer effect (IBE), according to which a 1 hPa increase or decrease in sea-level pressure corresponds to a 1 cm decrease or increase in sea level. To validate the ALES-reprocessed altimetry against the Norwegian tide gauges, the relevant physical signals at the relevant timescales must be removed from the tide-gauge data (Sect. 2.2).

The producers of ALES flag some of the data as unreliable. More precisely, they recommend excluding observations that fall within a distance of 3 km from the coast and whose sea-level anomaly (SLA), SWH, and standard deviation exceed 2.5, 11, and 0.2 m, respectively. We have followed these recommendations with one exception: we have lowered the threshold on the sea-level anomaly from 2.5 to 1.5 m because this choice leads to better agreement between the tide gauges and the ALES altimetry dataset between Måløy and Rørvik along the west coast of Norway (Fig. 1).

2.2 Tide gauges

The Norwegian Mapping Authority (Kartverket) provides information on observed water levels at 24 permanent tide-gauge stations along the coast of Norway. Data are updated, referenced to a common datum, quality-checked, and freely distributed through a dedicated web API (http://api.sehavniva.no, last access: 28 April 2021).

Even though most tide gauges provide a few decades of sea-level measurements, in this study we only consider the period between January 2003 and December 2018 because it overlaps with the time window spanned by the ALES altimetry dataset. Moreover, we only select 22 of the 24 permanent tide gauges available: we exclude Mausund, since it has no measurements available before November 2010, and Ny-Ålesund because it is outside our region of interest.

Over the period considered, the only tide gauges with missing values are Heimsjø and Hammerfest with a 1-month gap and Oslo with a 2-month gap. We expect the Norwegian set of tide gauges to map the coastal sea level with a spatial resolution of circa 130 km as it corresponds to the mean distance between adjacent tide gauges. This estimate should be treated only as a first-order approximation of the spatial resolution since the distance between adjacent tide gauges varies along the Norwegian coast and ranges from ~ 30 km in southern Norway to ~ 300 km in western Norway (more precisely, between Rørvik and Bodø).

A number of geophysical corrections have been applied to the tide-gauge data for them to be consistent with the sea-level anomaly from altimetry. These include the effects of the glacial isostatic adjustment (GIA), the low-frequency tides, and the DAC.

The GIA results from the adjustment of the Earth to the melting of the Fennoscandian ice sheet since the Last Glacial Maximum, circa 20 000 years ago. The Earth's relaxation substantially affects the sea-level change relative to the Norwegian coast, with values ranging from approximately 1 up to 5 mm yr^{-1} (e.g. Breili et al., 2017). Along the Norwegian coast, the GIA affects the sea-level reading from the tide gauges because it induces vertical land movement (VLM) and, to a lesser extent, the sea level itself because it modifies the Earth's gravity field. The first effect has been corrected using both GNSS observations and levelling, whereas the second has not been corrected since the satellite altimetry data are also influenced by geoid changes (Simpson et al., 2017).

The low-frequency constituents of ocean tide, derived from the EOT11a tidal model, are removed from the tide-gauge data as they are from the ALES-reprocessed altimetry dataset. Hammerfest, Honningsvåg, and Vardø, the three northernmost tide gauges (Fig. 1), are located outside the EOT11a model domain. Therefore, at these three locations, we remove the low-frequency constituents of ocean tide for Tromsø. The constituents in question are the solar semiannual, solar annual, and the nodal tide. For Norway the solar annual astronomical tide is negligible, while the two latter constituents have amplitudes on the order of 1 cm. The nodal tide has a period of approximately 18.61 years and results from the precession of the lunar nodes around the ecliptic (Woodworth, 2012). As our time series are shorter than the nodal cycle, this constituent is not negligible with regards to our trend analysis. None of the solid-Earth-related tides need to be removed from landlocked tide-gauge measurements to

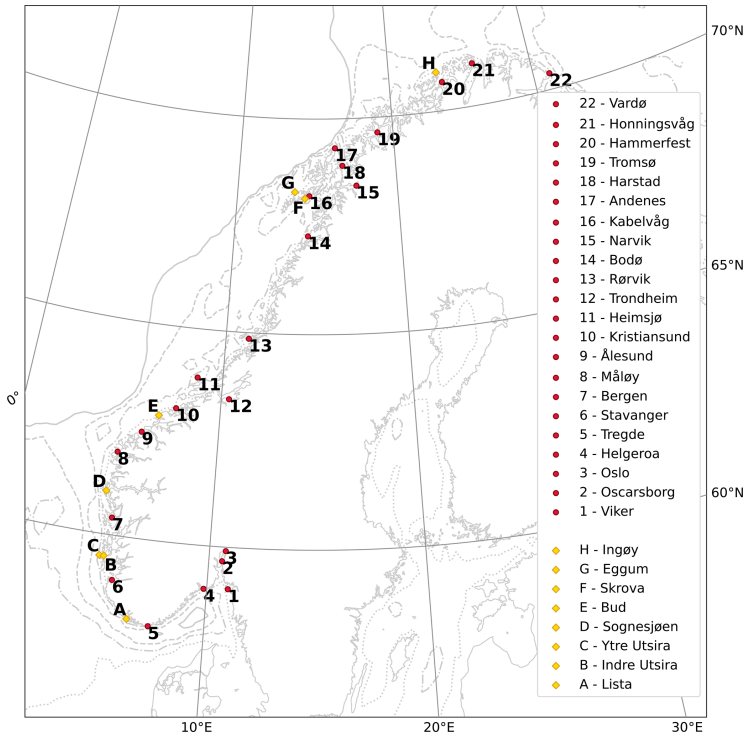

Figure 1. Location of the tide gauges and of the hydrographic stations considered in this study (red circles and yellow diamonds, respectively). The solid, dashed, dash-dotted, and dotted light gray lines indicate the 500, 300, 150, and 50 m isobaths, respectively.

produce sea-level records comparable to altimetric sea surface height. Moreover, the ocean pole tide, not provided by the EOT11a, has not been removed from the tide-gauge data. However, it is negligible in our region.

Since we have provided a description of the DAC in the previous section, here we only briefly describe how we have applied it to the tide-gauge data. At first, we have monthly-averaged the 6-hourly DAC dataset (available at the AVISO+ website, https://www.aviso.altimetry.fr/en/data/products/auxiliary-products/dynamic-atmospheric-correction.html, last access: 12 April 2021). Then, for each tide gauge, we have computed the difference between the monthly mean sea level and DAC at the nearest grid point of the DAC product.

2.3 Coastal hydrographic stations

Over the time window covered by this study, the Institute of Marine Research (IMR) in Bergen, Norway, has maintained eight permanent hydrographic stations over the Norwegian continental shelf at a short distance from the coast (Fig. 1). Data are updated and available at http://www.imr.no/forskning/forskningsdata/stasjoner/index.html (last access: 11 November 2020).

Along the Norwegian coast, the number of hydrographic stations is approximately one-third the number of tide gauges. Therefore, compared to the tide gauges, the hydrographic stations provide a coarser spatial resolution of the physical properties of the ocean. We find that the distance between adjacent hydrographic stations is approximately 250 km on average. This distance is minimum between the twin stations Indre Utsira–Ytre Utsira and Eggum–Skrova, where it does not exceed 30 km, whereas it is maximum in western Norway between Bud and Skrova, where it is approximately 670 km.

We select the temperature and salinity profiles taken between January 2003 and December 2018 for them to overlap with the period covered by the ALES-reprocessed altimetry dataset. The data are irregularly sampled and are mostly collected once every 1 or 2 weeks. To allow a comparison with the satellite altimetry dataset, we have monthly-averaged the temperature and salinity profiles at each hydrographic station. We should note that the monthly averaged time series of temperature and salinity contain missing values (Fig. 2). Bud

has the largest number of missing values with 76 gaps out of 192. It is followed by Indre Utsira and Ytre Utsira with 44 and 41 gaps, respectively. The remaining hydrographic stations have fewer than 16 gaps each.

The hydrographic data were used to obtain estimates of the thermosteric and the halosteric sea-level components over the spatial domain considered in this study.

3 Methods

3.1 Harmonic analysis of sea level

Following an approach similar to the one found in previous papers (e.g. Cipollini et al., 2017; Breili et al., 2017), we use the Levenberg–Marquardt algorithm and fit the following function to sea-level records from remote sensing and in situ data:

$$z(t) = a + b \cdot t + c \cdot \sin(2\pi t + d) + e \cdot \sin(4\pi t + f), \quad (1)$$

where a is the offset, b the linear trend, c and d the amplitude and the phase of the annual cycle, and e and f the amplitude and the phase of the semi-annual cycle. Then, we compare the linear trend, the amplitude, and the phase of the annual cycle and the detrended, deseasoned sea-level signals from remote sensing and in situ data. It is important to note that the use of this formula does not account for inter-annual variations of the seasonal cycle.

In this study, we present estimates of the sea-level trend from both satellite altimetry and tide gauges with corresponding 95 % confidence intervals (see below). Moreover, we assess how strongly the linear trends from altimetry depend on the time period considered and show those trends that are significant at a 0.05 significance level (see below). To compute the confidence intervals and the statistical significance, we account for the serial correlation in the time series. Indeed, successive values in the sea-level time series might be significantly correlated and, therefore, not drawn from a random sample. To account for this non-zero correlation, we compute the semi-variogram of the detrended and deseasoned SLA from satellite altimetry and the tide gauges and then determine the effective number of degrees of freedom, N^*, for each time series (Wackernagel, 2003), as described in Appendix A. To compute the 95 % confidence interval of the linear trends, we then use Eq. (A4) in Appendix A. Together with the semi-variogram, we also estimate the effective number of degrees of freedom using the formula $N^* = N \cdot (1 - r_1)/(1 + r_1)$, where N is the length of the time series and r_1 is its lag-1 autocorrelation (Bartlett, 1935). However, in this paper, we opt for the more stringent approach and only present the confidence interval derived using the semi-variograms. Indeed, we find that the semi-variogram approach returns either the same or fewer effective degrees of freedom (not shown) when compared to the other method. This is not the case for the effective number of degrees of freedom of the detrended and deseasoned SLA difference between ALES and the tide gauges. However, we find that the choice of the approach does not alter our conclusions.

3.2 Colocation of satellite altimetry and tide gauges

To compare the sea level from satellite altimetry and tide gauges, we first need to preprocess the altimetry observations since these are not colocated in space or in time with the tide gauges. The colocation consists of two steps. At first, we select the altimetry observations that are located near each tide gauge. Then, we average these observations both in space and in time to create, for each tide-gauge location, a single time series of monthly mean sea-level anomaly from altimetry.

During the process, we verify that the selected altimetry observations represent the sea-level variability at each tide-gauge location. More precisely, since tide gauges represent the sea-level variability along a stretch of the coast, we monthly-average all the altimetry observations within a certain distance d from the coast and a certain radius r from the tide gauge (Fig. 3). We try different combinations of d and r by allowing the first to range between 5 and 20 km, with steps of 2.5 km, and the second between 20 and 200 km, with steps of 15 km. Then, we pick the combination that maximizes the linear correlation coefficient between the detrended and deseasoned SLA measured by satellite altimetry and by the tide gauge (as, for example, in Cipollini et al., 2017). To set the maximum values of d and r at 20 and 200 km, respectively, we have first performed a sensitivity test and noted that larger values of d and r return slightly higher linear correlation coefficients (especially in northern Norway) but do not alter the main results of this study. At the same time, a maximum distance of 20 km from the coast and of 200 km from the tide gauge ensures that all the selected altimetry points are located over the continental shelf and that we can better capture the spatial-scale variability of the seasonal cycle of the sea level and of the sea-level trend.

We use the process described above to build a time series of monthly mean sea-level anomaly from altimetry at each tide-gauge location. The resulting sea-level time series have no missing values between Viker and Bodø. Instead, to the north of Bodø, they have 29 missing values which result from the lack of altimetry observations between November 2010 and March 2013.

3.3 Colocation of satellite altimetry and hydrographic stations

We preprocess the altimetry observations to examine the steric contribution to the sea-level variability at each hydrographic station since the two datasets are not colocated in space or in time. More precisely, we select all the altimetry observations located within 20 km from the Norwegian coast

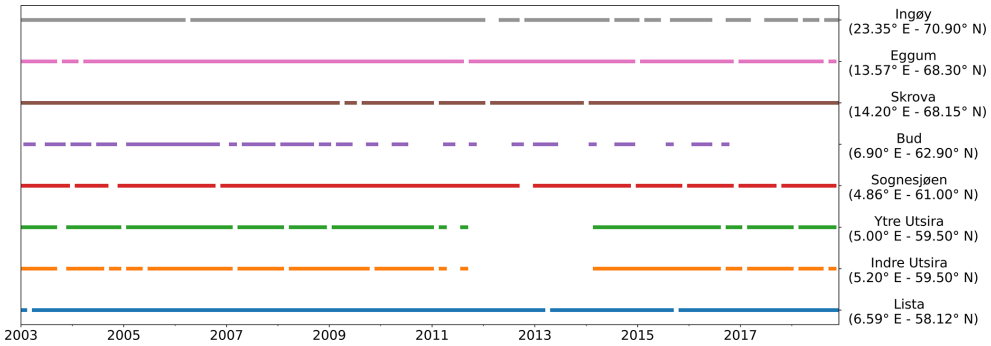

Figure 2. Data available at each hydrographic station between 1 January 2003 and 31 December 2018.

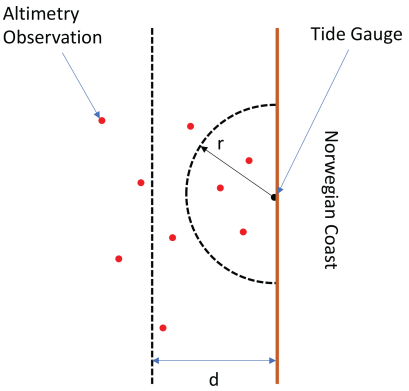

Figure 3. Sketch to illustrate the procedure used to build a monthly averaged SLA time series from the ALES-reprocessed satellite altimetry dataset at each tide-gauge location. The parameter r is the distance from the tide gauge, whereas d is the distance from the coast.

and within 200 km from each hydrographic station. Then, for each station, we monthly-average the altimetry observations to build a sea-level anomaly time series from altimetry. The results in the previous subsection give confidence that the monthly mean sea level computed over such a large area is representative of the sea-level variability at each hydrographic station.

3.4 Monthly mean thermosteric, halosteric, and steric sea-level components

To compute the thermosteric and halosteric components of the sea-level variability at each hydrographic station, we first monthly-average the temperature and salinity profiles. Then, at each hydrographic station, we compute the monthly mean thermosteric and halosteric components of the sea level as in Richter et al. (2012):

$$\eta_t = \int \alpha(T^*, S^*) \cdot (T - T_0)\,dz, \tag{2}$$

$$\eta_s = -\int \beta(T^*, S^*) \cdot (S - S_0)\,dz, \tag{3}$$

where α and β are the coefficients of thermal expansion and haline contraction, both computed at $T^* = (T + T_0)/2$ and $S^* = (S+S_0)/2$. For each hydrographic station, T_0 and S_0 are reference values and represent time-mean temperature and salinity averaged over the entire water column (Siegismund et al., 2007).

The steric component of the sea level at each hydrographic station, η_{st}, is simply the sum of the corresponding thermosteric and halosteric components of the sea level (Gill and Niiler, 1973).

3.5 Steric contribution to the Norwegian sea level

At each hydrographic station, we assess the contribution of temperature and salinity to the linear trend and the seasonal cycle of the SLA, as well as to the detrended and deseasoned SLA.

We do not use the harmonic analysis approach to estimate the linear trend and the seasonal cycle of the SLA and of the thermosteric, halosteric, and steric components of the sea level at each hydrographic station. Instead, we use simple linear regression to estimate the linear trend, and we compute the monthly climatology of each detrended time series to estimate the corresponding seasonal cycle. Indeed, the seasonal cycle of the SLA and of the thermosteric, halosteric, and steric sea level might depart from the linear combination of the annual and semi-annual cycles.

4 Comparison of satellite altimetry and tide-gauge measurements

In this section, we assess the quality of the ALES-reprocessed coastal altimetry dataset against tide-gauge records by comparing the detrended and deseasoned sea-level variability, the sea-level annual cycle, and sea-level trends provided by the remote sensing and in situ data. We also focus on the stability of linear trend estimates obtained from satellite altimetry (Liebmann et al., 2010; Bonaduce et al., 2016).

4.1 Detrended and deseasoned coastal sea level

Before comparing the detrended and deseasoned SLA from altimetry and tide gauges, we briefly describe how the detrended and deseasoned SLA evolves along the Norwegian coast during the period under study. More precisely, we low-pass-filter the detrended and deseasoned SLAs with a 1-year running mean to identify their main features at each tide-gauge location. Figure 4 shows years when the detrended and deseasoned SLA variations are coherent along the whole Norwegian coast and years when the sea-level variability occurs at smaller spatial scales (between 100 and 1000 km). As an example, between mid-2009 and the beginning of 2011, the detrended and deseasoned SLA shows negative values of up to −6 cm along the entire Norwegian coast. On the contrary, between 2003 and mid-2009, we note a dipole pattern, with SLA with opposite sign in the south and in the north of Norway. Indeed, up to the beginning of circa 2006, the Norwegian coast experienced a negative SLA to the south of Hemsjø and a positive SLA to the north of Heimsjø. During the following 3 years, the opposite situation occurred. These results suggest that, although coherent sea-level variability occurs along the Norwegian coast as seen from tide gauges, there are periods when it does not: during these periods, the sea-level variability is likely driven by local changes.

Figure 5 shows very good agreement between the detrended and deseasoned monthly mean SLA from ALES and the tide gauges. The two datasets agree best along the west coast of Norway where, if we exclude Trondheim, the linear correlation coefficients exceed 0.90 and the root mean square differences (RMSDs) range between 1.5 and 2.5 cm. As expected, satellite altimetry performs better between Måløy and Rørvik than in southern and northern Norway because of the convergence of altimeter tracks in the region. We suspect that Trondheim is an exception because it is located in the Trondheim fjord, where satellite altimetry might not adequately capture local sea-level variations: the presence of land and patches of calm water affects the quality of the satellite altimetry measurements (Gómez-Enri et al., 2010; Abulaitijiang et al., 2015), and the complex bathymetry and coastline hamper geophysical corrections (Cipollini et al., 2010). Similar peculiarities of the coastline along the Norwegian Trench, in the Skagerrak, and in the Oslofjord are also likely to affect the agreement, causing the linear correlation coefficients to fall between 0.80 and 0.90 and the highest RMSDs to range between 2.5 and 4.5 cm. Instead, in northern Norway, where we find linear correlation coefficients between 0.80 and 0.90 (statistically significant at a 0.05 significance level) and RMSDs between 1.5 and 3 cm, the problem might result from the smaller number of altimetry observations in the region. Indeed, only the tracks of Envisat, SARAL, and SARAL drifting phase cover the Norwegian coast north of 66° N.

Figure 6 supports our previous conclusions on the relationship between satellite altimetry and the tide gauges at Trondheim, Oslo, and Oscarborg. In Fig. 6, we show, for each tide gauge, the standard deviation of the linear correlation coefficient and of the RMSDs over all the possible combinations of the distance from the coast and from the tide gauge to measure the geometrical uncertainty of the SLA estimates from satellite altimetry. We find that, at Trondheim, both the linear correlation coefficient and the RMSD depend more on the size of the selection window when compared to other regions of the Norwegian coast. Similarly, at Oslo and Oscarborg, we note an anomalously high standard deviation of the linear correlation coefficient. We expect anomalously high values of the standard deviation of the linear correlation coefficients and RMSDs because these three tide gauges are in sheltered areas (Trondheim is in the Trondheim fjord, whereas Oslo and Oscarborg are in the Oslofjord), which can favour the formation of patches of calm water and negatively affect the quality of the satellite altimetry observations.

4.2 Annual cycle of coastal sea level

Figures 7 and 8 show good agreement between the annual cycle estimated using the ALES altimetry dataset and the tide gauges. The difference between the amplitudes of the annual cycle from ALES and the tide gauges ranges between −1.2 and 1.8 cm. However, at most tide-gauge locations (15 out of 22), the differences are much smaller at between −1 and 1 cm, which is less than 10 % of the amplitude of the corresponding annual cycle (Fig. 7a). We note that the differences between the amplitudes are mostly negative along the southern and western coast of Norway and that, to the north of Rørvik, they become smaller and even change sign at some locations (Fig. 7b).

The difference between the phases of the annual cycle estimated using the ALES altimetry dataset and the tide gauges ranges between −10 and +10 d (Fig. 8b). Such a great similarity indicates that both radar altimetry and the tide gauges capture the phase lag of approximately 2 months between the annual cycle in the north and in the south of Norway. The annual cycle peaks during the second half of September in the Skagerrak and in the Oslofjord region, in October along the Norwegian Trench and in southwestern Norway, and mainly during the first week of November north of Kristiansund.

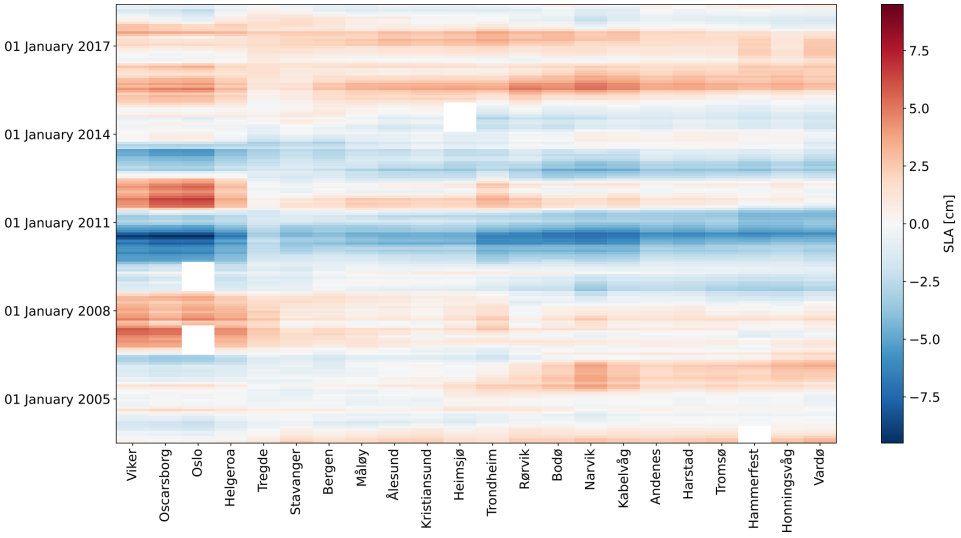

Figure 4. Hovmöller diagram of the detrended and deseasoned monthly mean SLA from tide gauges. The SLA at each tide gauge has been low-pass-filtered with a 1-year running mean. The tide gauges are displayed on the x axis. Time is displayed on the y axis and increases from bottom to top.

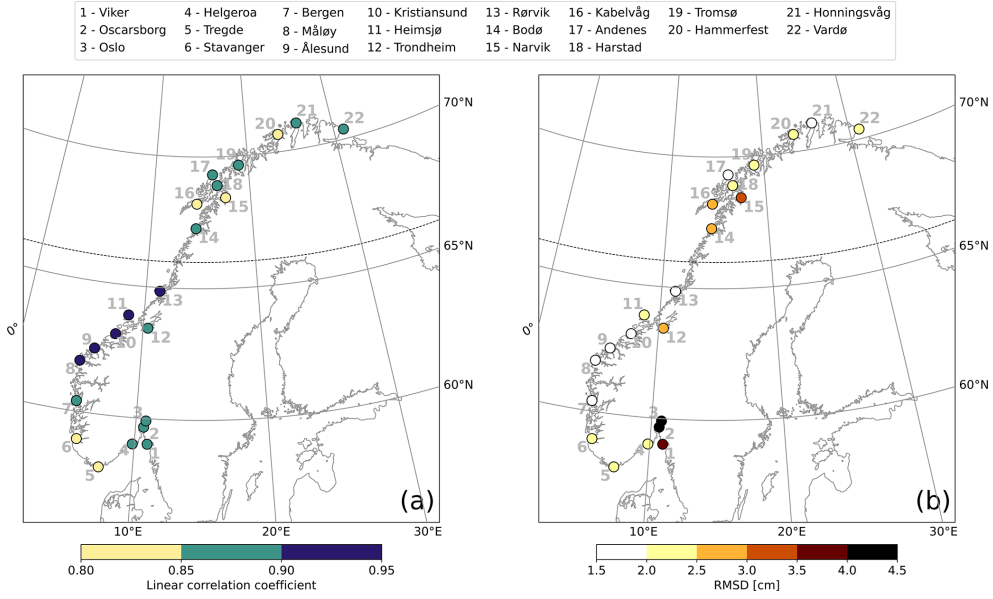

Figure 5. Comparison between coastal sea-level signals from in situ measurements and area-averaged remote sensing data. At each tide-gauge location, the linear correlation coefficient **(a)** and RMSD **(b)** between the detrended and deseasoned monthly mean SLA from the ALES altimetry dataset and from the tide gauge. The black dashed line indicates the 66° N parallel.

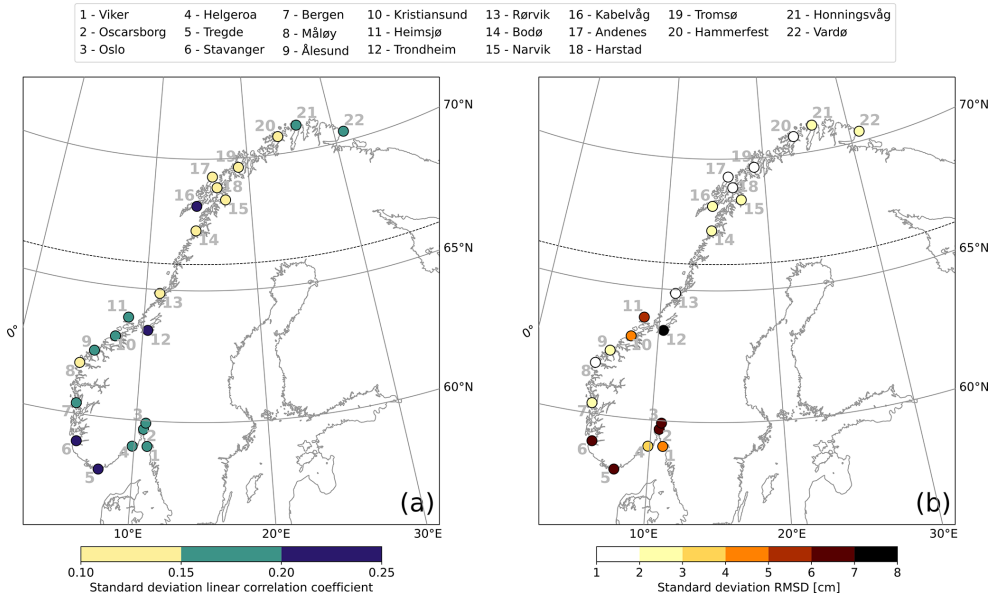

Figure 6. Comparison between coastal sea-level signals from in situ measurements and area-averaged remote sensing data. At each tide-gauge location, the standard deviation of the linear correlation coefficients **(a)** and of the RMSDs **(b)** is computed over each possible combination of the distance from the coast and of the distance from the tide gauge. The black dashed line indicates the 66° N parallel.

4.3 Linear trend of coastal sea level

The differences between sea-level trend estimates obtained from the in situ and remotely sensed signals range between -0.85 and $1.15\,\mathrm{mm\,yr^{-1}}$ along the Norwegian coast (Fig. 9). Both datasets return a similar spatial dependence of the sea-level trend along the Norwegian coast, with the lowest values found in the Skagerrak and the Oslofjord (between 2 and $3\,\mathrm{mm\,yr^{-1}}$) and the highest to the north of Heimsjø (around $4\,\mathrm{mm\,yr^{-1}}$). Moreover, the two datasets return a similar uncertainty of the sea-level trend at each tide-gauge location.

Despite their similarities, we still find that the difference between the sea-level trend from altimetry and tide gauges is significantly different from zero at a 0.05 significance level at 3 out of 22 tide gauges. Following Benveniste et al. (2020), we assess the significance in terms of fractional differences (FDs). Fractional differences are defined as $\mathrm{FD} = |\tau|/(t_{0.05/2} \cdot \mathrm{SE} \cdot N/N^*)$, where $|\tau|$ is the absolute value of the linear trend of the SLA difference between altimetry and each tide gauge, $t_{0.05/2}$ is the critical value of the Student's t test distribution for a 95 % confidence level with $N^* - 2$ degrees of freedom, SE is the standard error, and N/N^* is the ratio between the total number of observations and the effective number of degrees of freedom. When $\mathrm{FD} > 1$, the difference between the two trends is statistically significant at a 0.05 significance level, a condition that occurs at Tregde, Måløy, and Bergen. Interestingly, none of these tide gauges are located north of 66° N despite only some of the altimetry missions considered in this study having an inclination exceeding 66° N (namely, Envisat, SARAL, SARAL drifting phase). Therefore, the fewer altimetry observations to the north of 66° N seem not to deteriorate the agreement between the ALES-reprocessed altimetry and the tide gauges.

Following Liebmann et al. (2010), we use the satellite altimetry data to assess how strongly the sea-level trend depends on the time length of the period considered. Each point in Fig. 10 shows the sea-level trend computed over the number of years on the y axis up to the year specified on the x axis. Between 2003 and circa 2013, we do not find a significant sea-level trend along the Norwegian coast. Indeed, with very few exceptions, the trends are not statistically different from zero at a 0.05 significance level. The exceptions consist of a small number of cases, each characterized by a sea-level trend lower than $-4\,\mathrm{mm\,yr^{-1}}$.

On the contrary, with the exception of the three southernmost tide-gauge locations, we note a significant positive sea-level trend along the entire coast of Norway when the period considered for the calculation ends in 2015 or later. The linear trends decrease as the length of the period selected increases. When sea-level rates are computed over periods of a few years only, they even exceed $6\,\mathrm{mm\,yr^{-1}}$. Instead, over longer periods of time (e.g. more than 10 years), they mainly

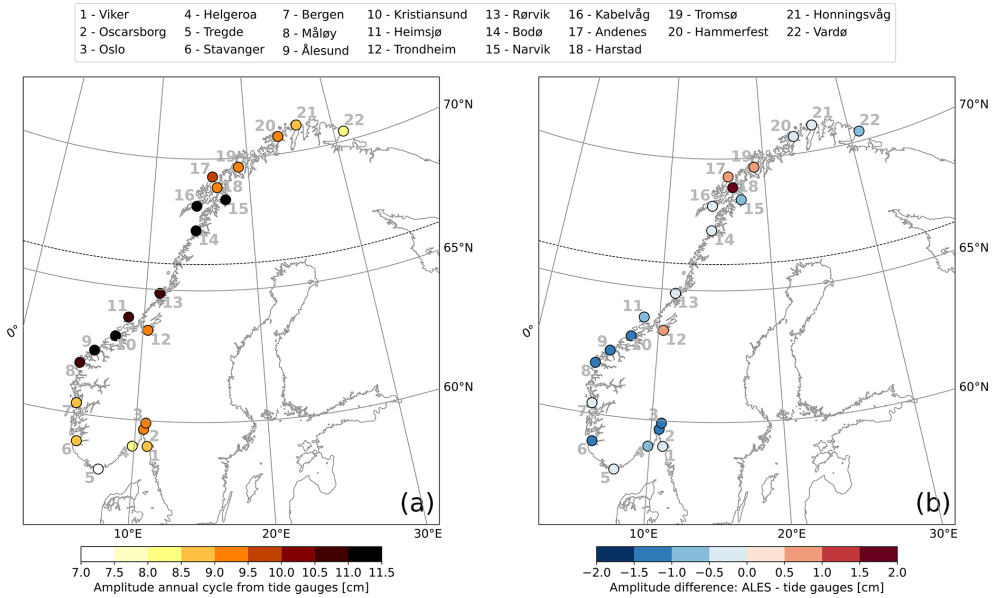

Figure 7. Comparison between the amplitude of coastal sea-level annual cycle from in situ measurements and area-averaged remote sensing data. At each tide-gauge location, the amplitude of the annual cycle from the tide gauges **(a)** and difference between the amplitude of the annual cycle from the ALES-reprocessed altimetry dataset and the tide gauges **(b)**. The black dashed line indicates the 66° N parallel.

range between 3 and 5 mm yr^{-1}. A visual inspection of the time series confirms that the sea level has increased since 2014.

5 Steric contribution to the sea-level variability

In this section, we use the Norwegian set of hydrographic stations to assess how temperature and salinity affect the sea-level trend, the seasonal cycle of sea level, and the detrended, deseasoned sea-level variability at different locations along the Norwegian coast.

5.1 Variability of the thermosteric and the halosteric sea-level components

The variability of the thermosteric and halosteric sea-level components along the Norwegian coast mainly occurs over two different spatial and temporal scales (Fig. 11). Notably, the seasonal cycle dominates the thermosteric sea-level variability at each hydrographic station and is responsible for the thermosteric sea level varying approximately uniformly along the coast of Norway. On the contrary, the halosteric component shows a variability at shorter spatial and temporal scales, possibly due to the contributions from local rivers. The main exceptions are, due to their proximity, the two sets of twin hydrographic stations, Indre Utsira–Ytre Utsira and Eggum–Skrova (Fig. 1).

Despite these differences, both the thermosteric and halosteric components of the sea level give a comparable contribution to the sea-level variability along the Norwegian coast (Fig. 11). This ranges approximately between −10 and 10 cm at each hydrographic station.

In the following sections, we investigate the spatial variability of these two components along the Norwegian coast, focusing on the linear trend, the seasonal cycle, and the residuals, as well as on their contribution to the sea-level variability in the region.

5.2 Steric contribution to the sea-level trend

In this section, we perform a fit-for-purpose assessment of the Norwegian hydrographic station network to obtain estimates of the steric sea-level trends from satellite altimetry and in situ data.

Over the period 2003–2018, we find that the linear trends of the thermosteric, halosteric, and steric components of the sea level approximately range between −1.0 and 2.5 mm yr^{-1}. The steric contributions to coastal sea-level trends experience large spatial variability that is even negative at Sognesjøen and reaches a peak of approximately 55 % of the sea-level trend estimated from satellite altime-

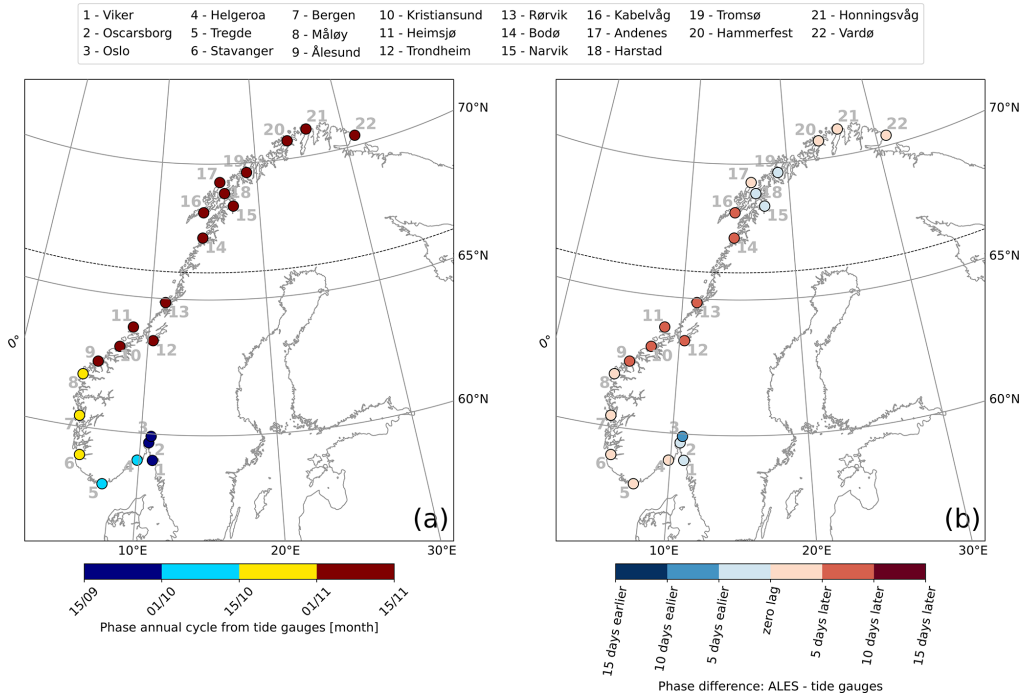

Figure 8. Comparison between the phase of coastal sea-level annual cycle from in situ measurements and area-averaged remote sensing data. At each tide-gauge location, the phase of the annual cycle from the tide gauges **(a)** and phase difference of the annual cycle from the ALES-reprocessed altimetry dataset and from the tide gauges **(b)**. The black dashed line indicates the 66° N parallel.

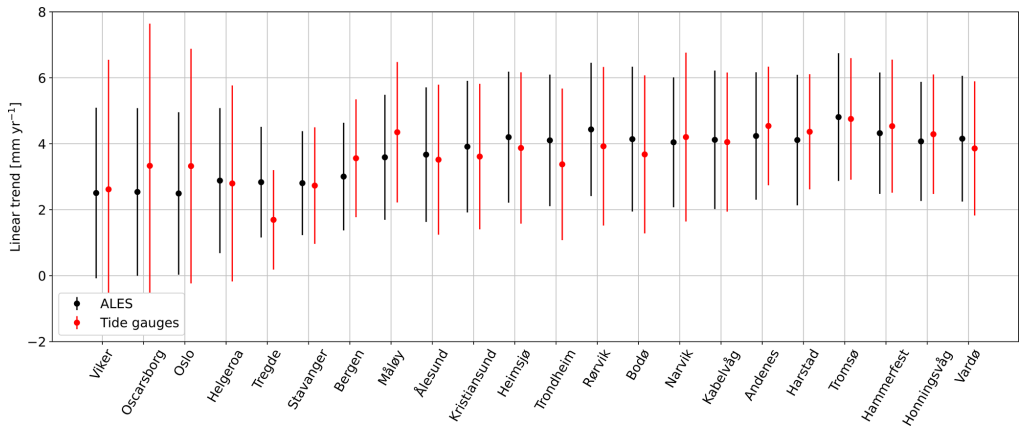

Figure 9. At each tide-gauge location, the linear trend of the SLA from the ALES-reprocessed altimetry dataset (black dots) and from tide gauges (red dots). The error bars show the 95th confidence intervals of the sea-level trend at each tide-gauge location.

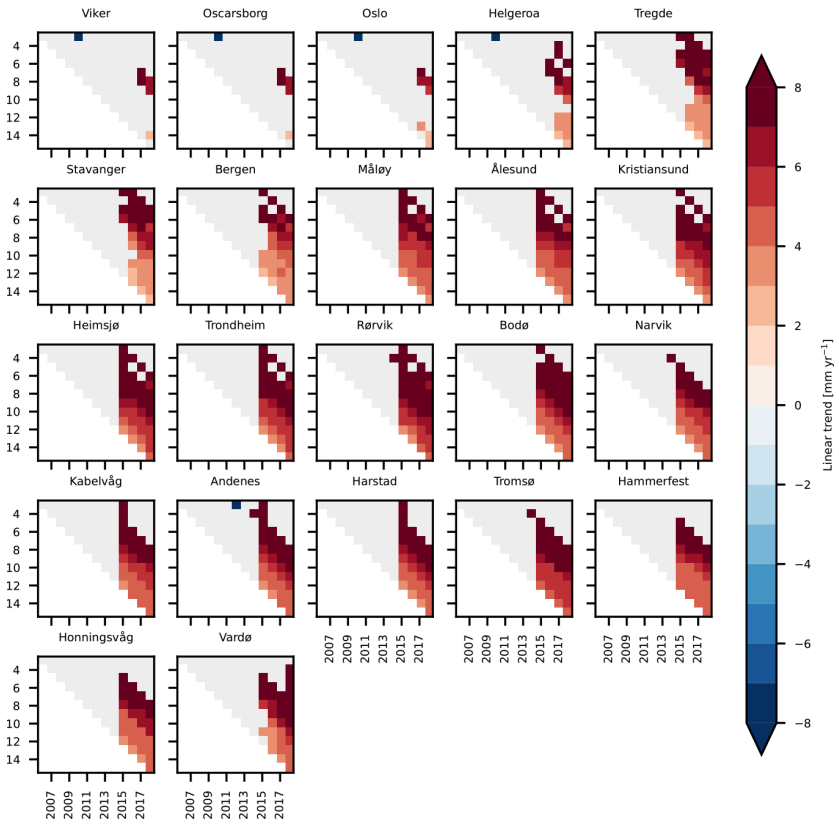

Figure 10. Stability of the sea-level trend along the Norwegian coast. At each tide-gauge location, the linear trend of the SLA from ALES as a function of the period considered. Each panel refers to a tide-gauge location and shows all the possible trends computed up to the year shown on the x axis, considering the number of years displayed on the y axis. For example, the point ($x = 2014$, $y = 5$) in each panel shows the linear trend of the SLA computed over the 5-year period between 1 January 2009 and 31 December 2014. Light gray is used to mask values that are not significantly different from zero at the 0.05 significance level.

try at Lista and Ingøy. Moreover, when we compare the thermosteric and halosteric signals at these locations, we note that the latter contributes more than the former to the coastal sea-level trends (up to 50 % of the sea-level trend from altimetry). The width of the confidence intervals of the thermosteric, halosteric, and steric contributions ranges between 4.0 and circa 12.0 mm yr^{-1}, with northern Norway exhibiting larger uncertainties (Fig. 12). This is a result of the high interannual variability of the thermosteric and halosteric components in the region (Figs. B1 and B2), which leads to fewer effective degrees of freedom and, therefore, to less accurate estimates of the linear trend.

We also test if using tide gauges, instead of satellite altimetry, could alter our estimates of the relative contribution of these components (thermosteric, halosteric, and steric) to the sea-level trend along the coast of Norway. Such alteration may indeed occur because the sea-level variations measured by the Norwegian tide gauges might not properly represent those occurring in proximity to the hydrographic stations since the two sets of instruments are not colocated in space (Fig. 1).

With the exception of Lista, the choice of the dataset has a minimal influence on the estimates of the thermosteric, halosteric, and steric relative contributions to the sea-level trend along the coast of Norway. We reach this conclusion by visual inspection, but we also provide a more quantitative analysis based on the ratio between the linear trend of the SLA and of the thermosteric, halosteric, and steric components of the sea level. We find that, apart from Lista, the choice of the dataset modifies such a ratio by less than 13 %. At Lista, the change amounts to 59 % and results from the ALES-retracked satellite altimetry dataset returning a sea-

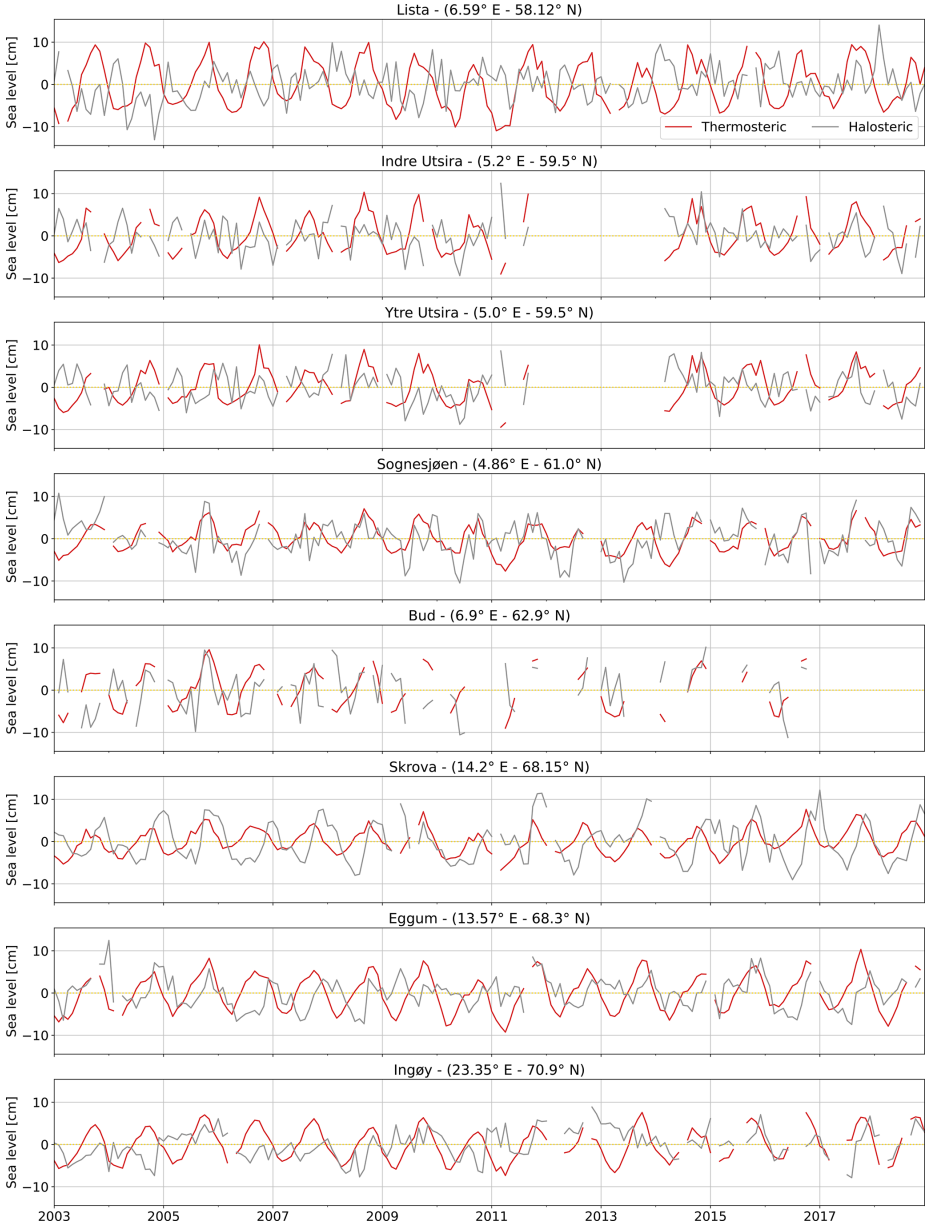

Figure 11. Thermosteric (red) and halosteric (gray) components of the sea-level anomaly at each hydrographic station along the Norwegian coast.

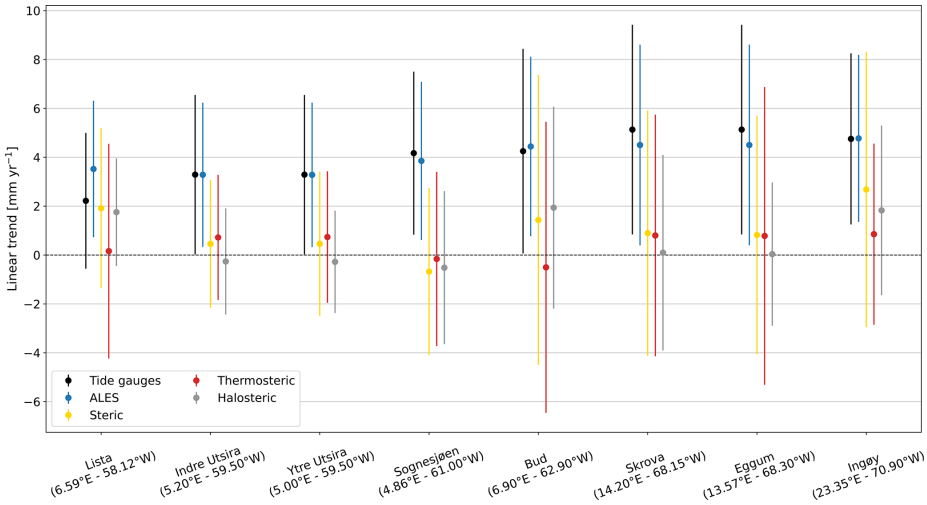

Figure 12. At each hydrographic station, the linear trend of the sea level from tide gauges and from ALES (black and blue dots, respectively), as well as of the steric, thermosteric, and halosteric components of the sea level (yellow, red, and gray dots, respectively). The bars indicate the 95 % confidence intervals.

level trend approximately 1.6 times larger than that provided by the tide gauge at Tregde (this is the tide gauge we use to compute the thermohaline contribution at Lista). Such a large variation is expected since, as we have already noticed, the sea-level rates obtained considering tide-gauge and satellite data at Tregde show less accurate agreement (Figs. 9 and C5).

5.3 Steric contribution to the seasonal cycle of sea level

In this section, we build on the results by Richter et al. (2012) and assess the thermosteric, halosteric, and steric contributions to the seasonal cycle of the sea level at each hydrographic station along the Norwegian coast.

We find that using the tide-gauge data, instead of satellite altimetry measurements, only minimally affects the estimate of the thermosteric, halosteric, and steric contributions to the seasonal cycle of SLA (Fig. 13), even though the tide gauges are not colocated in space with the hydrographic stations. Indeed, the seasonal cycle returned by satellite altimetry at each hydrographic station strongly resembles that returned by the nearby tide gauge (Fig. 13, fourth column). At the same time, the RMSD between the seasonal cycle of the SLA and steric sea level, scaled by the range (maximum minus minimum) of the seasonal cycle of SLA, minimally depends on the dataset used (Table 1, first and second columns).

We also note that density changes substantially contribute to the seasonal cycle of SLA along the Norwegian coast, as shown by Fig. 13 and Table 1. The seasonal cycle of SLA and steric sea level are 1 month out of phase along the southern and western coast of Norway up to Yndre Utsira and in phase over the remaining part of the Norwegian coast. Moreover, the ratio between the range of seasonal cycles of steric sea level and of SLA varies between 0.6 at Ytre Utsira and 0.9 at Bud (Table 1, third column).

Along the Norwegian coast, the seasonal cycle of steric sea level is more affected by variations in temperature than in salinity. We note that, with the exception of Bud and Skrova, the seasonal cycle of the steric component mostly resembles that of the thermosteric component in terms of both amplitude and phase. At the same time, we note a clear discrepancy between the seasonal cycle of the halosteric and steric components in both southern Norway, where they are in anti-phase, and at Bud, where the seasonal cycle of the halosteric sea level is dominated by the semi-annual cycle. A more quantitative analysis returns comparable results; the RMSD between the steric and halosteric seasonal cycles exceeds by a factor of 1.4 the RMSD between the steric and thermosteric seasonal cycles along the entire coast of Norway (with the exception of Skrova, where the ratio between the two RMSDs is 0.7).

5.4 Detrended and deseasoned coastal sea level and its components

The detrended and deseasoned thermosteric sea level along the Norwegian coast shows larger spatial variability compared to the detrended and deseasoned halosteric component (Fig. 14). The correlation matrix of the thermosteric sea level (Fig. 14a) shows larger values compared to the one obtained

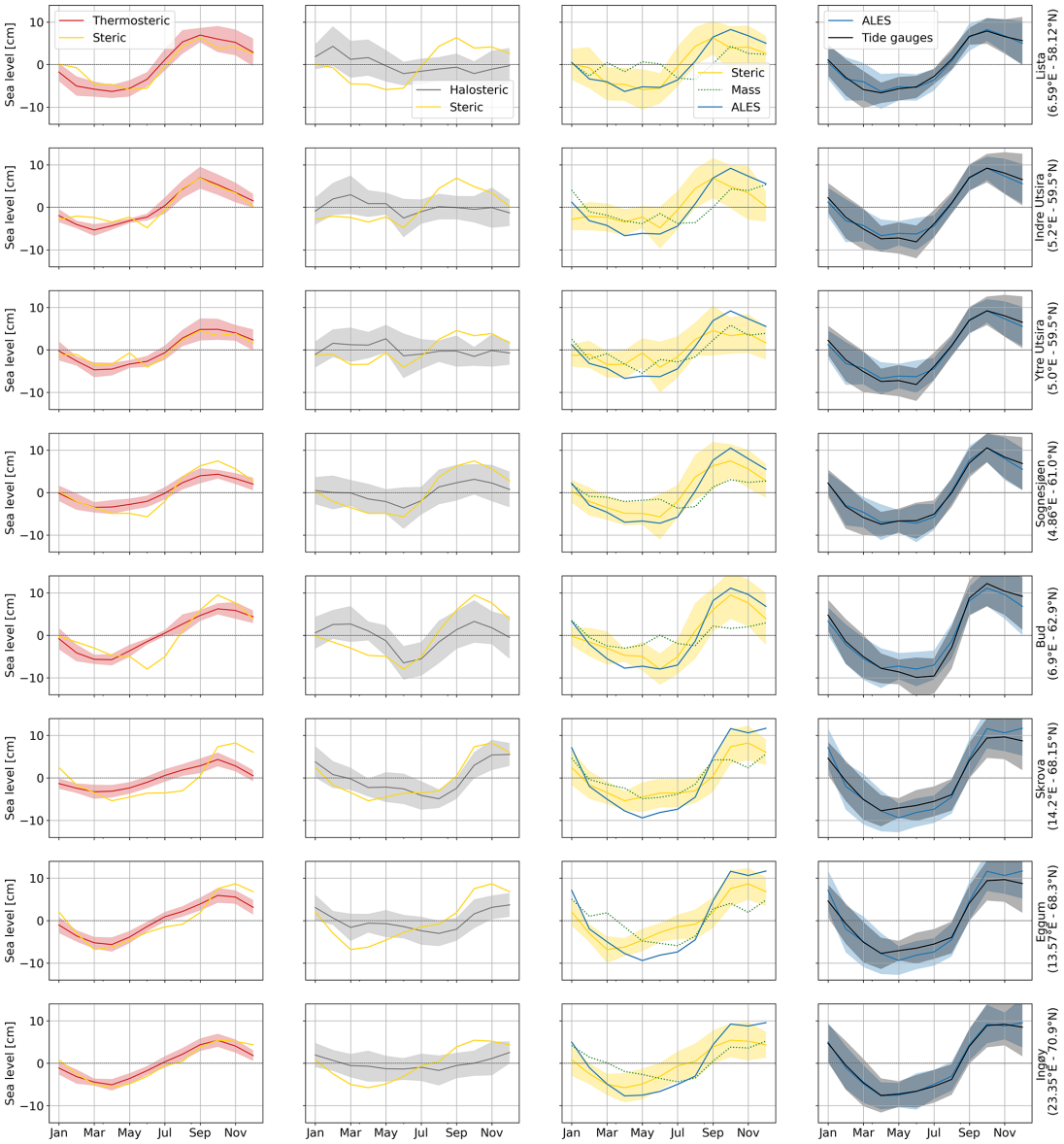

Figure 13. Monthly climatology of the sea-level signals at the hydrographic station positions. The panels show the steric (yellow lines), thermosteric (red lines), halosteric (gray lines), and mass (green lines) components of the sea level. The monthly climatology obtained from altimetry (blue lines) and tide-gauge (black lines) measurements is also shown. The shading enveloping the monthly climatologies shows the region departing from each line by 1 climatological standard deviation.

Table 1. Comparison between the seasonal cycle of SLA from ALES, of SLA from the tide gauges, and of steric sea level at each hydrographic station position. The first and the second columns show, for ALES and the tide gauges, the RMSD between the seasonal cycle of SLA and the steric sea level scaled by the range (maximum minus minimum) of the seasonal cycle of SLA. The third and the fourth columns show the ratio of the ranges and the lag of maximum correlation of the seasonal cycle of SLA from ALES and steric sea level.

	Scaled $RMSD_{ALES}$	Scaled $RMSD_{Tide\ gauges}$	$\frac{Range_{Steric}}{Range_{ALES}}$	Lag maximum correlation ALES and steric (months)
Lista (58.12° N, 6.59° E)	16 %	15 %	0.8	1
Indre Utsira (59.50° N, 5.20° E)	21 %	23 %	0.7	1
Ytre Utsira (59.50° N, 5.00° E)	21 %	22 %	0.6	1
Sognesjøen (61.00° N, 4.86° E)	13 %	14 %	0.8	0
Bud (62.90° N, 6.90° E)	12 %	16 %	0.9	0
Skrova (68.15° N, 14.20° E)	18 %	16 %	0.7	0
Eggum (68.30° N, 13.57° E)	19 %	14 %	0.7	0
Ingøy (70.90° N, 23.35° E)	19 %	19 %	0.7	0

considering the halosteric sea-level signals (Fig. 14b). As an example, while the minimum linear correlation coefficient between two adjacent hydrographic stations in Fig. 14a is 0.52, it is only 0.19 in Fig. 14b. We briefly discuss the small spatial-scale variability of the halosteric sea level along the Norwegian coast in the "Discussion and conclusions" section of the paper.

From Fig. 14c, we also note that the values of the correlation matrix of the steric sea level fall between those of the thermosteric and halosteric components. This suggests that the thermosteric and halosteric components of the sea level give a similar contribution to the sea-level variability along the Norwegian coast.

6 Discussion and conclusions

In this paper, we have first assessed the ability of the ALES-reprocessed satellite altimetry dataset to capture the Norwegian sea-level variability over a range of timescales. Then, we have used data from hydrographic stations to quantify the steric contributions to the sea-level variability along the coast of Norway.

Along the Norwegian coast, the sea-level trend from the ALES-reprocessed satellite altimetry dataset is found to be compatible with the estimates from tide gauges. Their difference only ranges between -0.85 and $1.15\,mm\,yr^{-1}$ and is significantly different from zero at the 95 % confidence level at 19 out of 22 tide-gauge locations. Because of this good agreement, the choice of the sea-level dataset (either tide gauges or ALES) has a minimal impact on the estimates of the thermosteric, halosteric, and steric relative contributions to the sea-level trend. Despite the large uncertainties, this result is encouraging since it suggests that the ALES dataset can be used to partition the sea-level variability in regions of the coastal ocean not covered by tide gauges. At the same time, it confirms the validity of previous sea-level studies in the region which only used tide-gauge data (e.g. Richter et al., 2012).

Regarding the comparison between the ALES-retracked and the along-track (L3) conventional altimetry datasets, we find that the former shows, on average, a 6 % improvement, despite it being well within the margins of error. This improvement is most evident at Bodø, Kabelvåg, and Tromsø in northern Norway, where the agreement with the tide gauges improves by 19 %, 23 %, and 24 %, respectively. The use of the ALES retracker for more satellite altimetry missions, in order to have more observations and to cover the period before July 2002, might help reduce the uncertainties and return a more statistically significant result.

A comparison with Breili et al. (2017), wherein an along-track (L3), multi-mission conventional altimetry dataset was used to analyse the sea-level trend along the Norwegian coast, returns comparable results. We cannot, however, di-

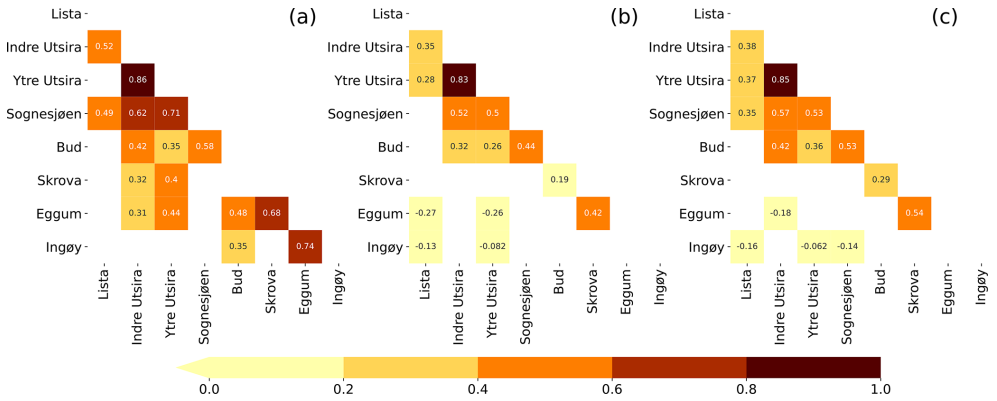

Figure 14. Correlation matrices of the detrended and deseasoned thermosteric **(a)**, halosteric **(b)**, and steric **(c)** components of the sea level at each hydrographic station. Correlation values that are not significant at a 0.05 significance level have been omitted.

rectly compare the linear trends in this work with those in Breili et al. (2017) since they focus on a different period (1993–2016), and the sea-level trend along the Norwegian coast strongly depends on the length of the time window considered (Fig. 10). However, when assessing how the conventional satellite altimetry datasets compare with tide-gauge records in terms of the linear trend computed over a common time window, ALES again shows an improvement in northern Norway between Bodø and Tromsø, where the difference between the linear trend from ALES and the tide gauges is small (up to 0.5 mm yr^{-1}) compared to circa 1 to 3 mm yr^{-1} found by Breili et al. (2017) using a conventional altimetry dataset.

The ALES-retracked satellite altimetry dataset is found to underestimate the amplitude of the annual cycle along large portions of the Norwegian coast (Fig. 7). Even though the difference between the two sets of estimates is not significant at a 95 % significance level (the 95 % confidence interval is approximately twice the standard error), we find this result interesting because of its consistency. We do not expect such a consistency to depend on the ALES retracker since we find a comparable result when we use the along-track (L3) conventional altimetry product (Fig. C3). We rather suspect a dependence of the amplitude of the annual cycle on the bathymetry and, therefore, on the distance from the coast, as shown by Passaro et al. (2015) along the Norwegian sector of the Skagerrak.

A comparison with Volkov and Pujol (2012) shows that the ALES-retracked satellite altimetry better captures the sea-level annual cycle along the coast of Norway with respect to the gridded sea-level altimetry products. In that study, the authors considered six tide gauges along the Norwegian coast, namely Kristiansund, Rørvik, Andenes, Hammerfest, Honningsvåg, and Vardø, to assess the quality of satellite altimetry maps at the northern high latitudes. Except for Andenes, we note that the ALES-reprocessed coastal altimetry dataset allows for more accurate estimates of the sea-level annual cycle, reducing the differences with the in situ sea-level records by a factor of 3 to 6 compared to gridded satellite altimetry products.

We also assess the steric contribution to the seasonal cycle of SLA. Our results show that the steric variations and, in particular, the thermosteric variations considerably contribute to the seasonal cycle of the sea level along the entire Norwegian coast. Moreover, we find that the relative contributions of the thermosteric, halosteric, and steric sea level minimally depend on whether we use tide gauges or satellite altimetry. This is indicative of the large-scale spatial pattern associated with the seasonal cycle of SLA.

The detrended and deseasoned sea-level variability along the Norwegian shelf resembles the along-slope wind index proposed by Chafik et al. (2019). We note that the similarities between the two are stronger along the western and northern coast of Norway than in the south. Indeed, from Oslo to Ålesund, SLA signals depart from the along-slope wind index between 2003 and 2008, probably due to local effects, such as the Baltic outflow. We refer to local effects since Chafik et al. (2019) attributed the inter-annual sea-level variability over the northern European continental shelf to the along-slope winds, which might regulate the exchange of water between the open ocean and the shelf through Ekman transport.

Because the detrended and deseasoned SLA pattern is coherent over large distances along the Norwegian coast (see also Chafik et al., 2017), coastal altimetry observations located a few hundred kilometres apart can be representative of the sea-level variations occurring at a particular tide-gauge location. This explains why we can average the SLA from altimetry over an area a few hundred kilometres wide around each tide-gauge location to maximize the linear correlation coefficient between the detrended and deseasoned SLA from

satellite altimetry and the tide gauges (Sect. 3.2). Moreover, it also partly explains the good agreement between satellite altimetry and tide gauges since, as we average over a large number of satellite altimetry observations, we increase the temporal sampling provided by altimetry, and therefore we reduce the noise in the resulting SLA (Oelsmann et al., 2021).

The small-scale variability of the detrended and deseasoned sea-level halosteric component (Fig. 14) does not reconcile with the good agreement between tide-gauge sea-level signals and the ALES-reprocessed altimetry dataset. Indeed, to compare the two datasets, we have averaged the satellite altimetry observations over an area a few hundred kilometres wide around each tide gauge. However, Fig. 14 suggests that the estimates of the halosteric component can change significantly over an area of this size. Furthermore, while this component has a magnitude comparable to that of the detrended, deseasoned SLA (not shown), it only explains a small fraction (from 3 % to 11 %) of the difference between the sea-level signals from altimetry and the tide gauges.

Future work is thus warranted to understand whether the small-scale variability of the halosteric component of the sea level along the Norwegian coast results from measurement issues. For example, ocean salinity is measured approximately once a week at Skrova and approximately twice a month at the remaining hydrographic stations: this aliases the sub-weekly salinity variations into the lower-frequency components and, consequently, might significantly alter the monthly mean salinity values. A new study, which takes benefit from ships of opportunity as well as synergies between different observational platforms and ocean models, could help clarify this issue.

To conclude, we have demonstrated the advantage of the ALES retracker over the conventional open-ocean retracker along the coast of Norway. The retracking of earlier altimeter missions would, however, be necessary to provide a more accurate estimate of the sea-level variability along the coast of Norway and could possibly be used to understand whether the sea-level rise in the region is accelerating. Still, this paper gives confidence that the ALES-reprocessed altimetry dataset can be fruitfully used to measure coastal sea-level variations in regions poorly covered by tide gauges.

Appendix A

To estimate the uncertainty associated with the sea-level trends derived from tide gauges and the ALES-retracked satellite altimetry dataset (Fig. 9), we need to account for the effective degrees of freedom in the sea-level anomaly time series. Indeed, successive points in the SLA time series might be correlated and, therefore, not drawn from a random sample.

To determine the effective number of degrees of freedom, we produce semi-variograms of the detrended and deseasoned SLA from the tide gauges and the altimetry dataset. The semi-variogram is defined as

$$\gamma(t) = \frac{1}{2} \cdot \mathrm{var}[x(t) - x(t+\tau)], \tag{A1}$$

where $x(t)$ is the time series under study, var stands for variance, and τ is the time lag.

The number of degrees of freedom is obtained by fitting the semi-variograms with a spherical function of the form

$$\begin{cases} c(h) = b + C_0 \cdot \left(1 - \frac{3}{2}\frac{|h|}{a} + \frac{1}{2}\frac{|h|^3}{a^3}\right) & \text{if } h \le a \\ c(h) = b + C_0 & \text{if } h > a, \end{cases} \tag{A2}$$

where h is the fitting parameter, and a is the effective range or, in other words, the lag needed for the semi-variogram to reach a constant value. Semi-variograms are preferred to autocorrelations in geostatistics because they better detect the non-stationarity of time series.

We use the fit to determine the lag at which each semi-variogram reaches a plateau, since it indicates the decorrelation timescale of the time series. The effective number of degrees of freedom corresponds to the ratio between the length of the time series and the lag.

We find that the lag only minimally depends on the tide-gauge location and on whether we consider the detrended and deseasoned SLA from the altimetry dataset or the tide gauges (Figs. A1 and A2). The semi-variograms obtained from both altimetry and the tide gauges return a lag of 2 months at each tide-gauge location, with the exception of three stations in southern Norway (Viker, Oscarborg, and Helgeroa), where the SLA from the tide gauges is characterized by a 3-month lag.

We use the same approach to compute the uncertainty associated with the linear trend of the difference between the SLA from satellite altimetry and the tide gauges, with only one exception. We noticed that the spheric model does not fit the semi-variogram for Trondheim. Therefore, for Trondheim, we opted for an exponential model:

$$\gamma(t) = b + C_0 \left(1 - e^{-\frac{h}{a}}\right), \tag{A3}$$

where h is the fitting parameter, and a is the range parameter. An exponential function is preferred over the spherical function when the time series shows a strong temporal correlation.

The serial correlation is negligible along the entire Norwegian coast with the exception of Viker, Oscarborg, Oslo, and Narvik, where the semi-variograms return a 2-month lag (Fig. A3). At Trondheim, instead, we find a much larger lag (approximately 10 months).

We use the effective number of degrees of freedom when we compute the confidence intervals of the sea-level rates in Fig. 9. We compute the 95 % confidence interval of the linear trend as follows:

$$\mathrm{CI} = t_{0.05/2, N^*-6} \cdot \sqrt{\frac{N-1}{N^*-1}} \cdot \mathrm{SE}, \tag{A4}$$

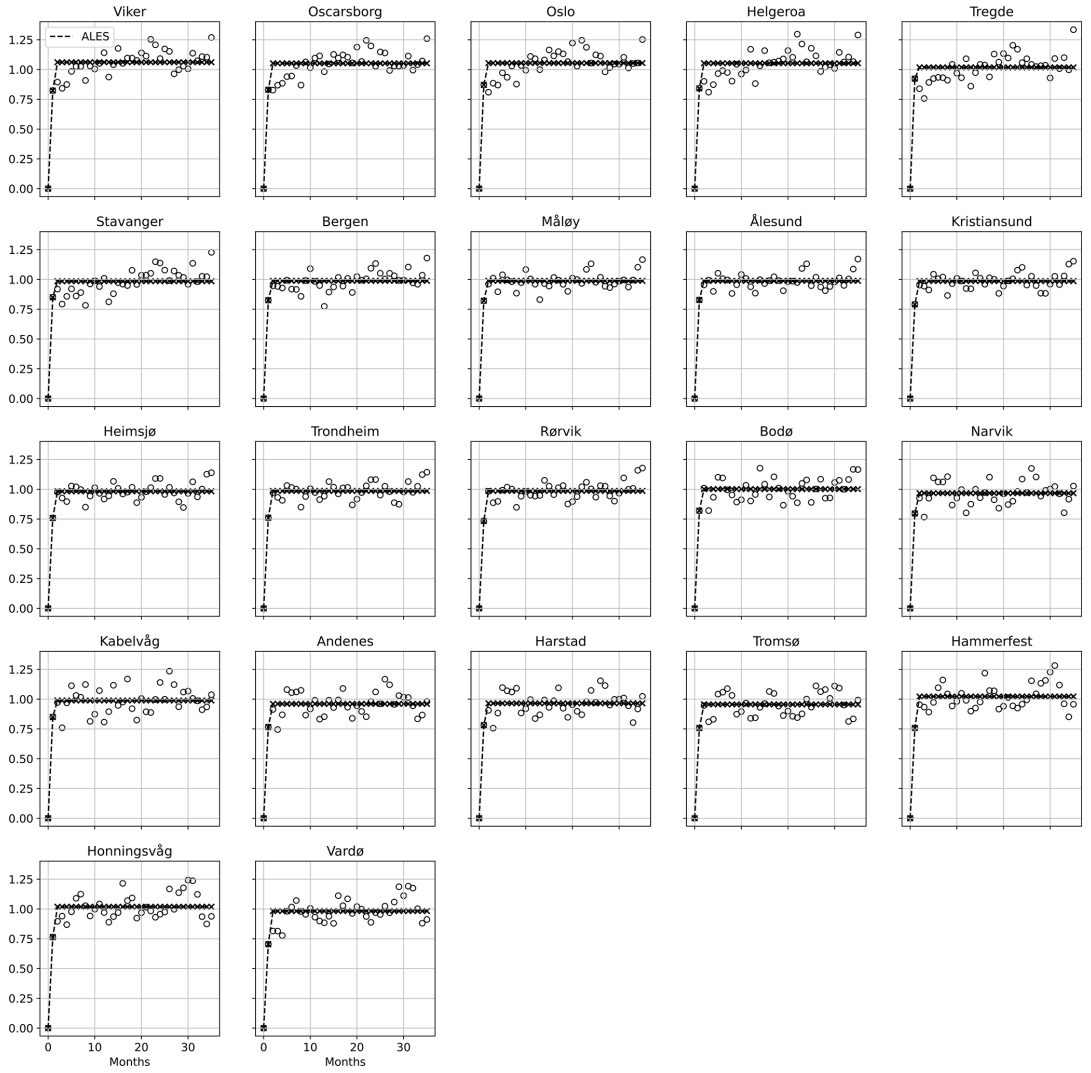

Figure A1. For each tide gauge along the Norwegian coast, semi-variogram of the detrended and deseasoned SLA estimated from the ALES-retracked satellite altimetry (empty circles) and corresponding fit (crosses connected by a dashed line). At each tide-gauge location, we scaled each semi-variogram by the variance of the corresponding detrended and deseasoned SLA for all the plots to have the same limits on the y axis.

where SE is the standard error of the linear trend computed as if $N^* = N$ (the total number of observations in the time series), and $t_{0.05/2,N^*-6}$ represents the t values computed using $N^* - 6$ degrees of freedom at a 0.05 significance level.

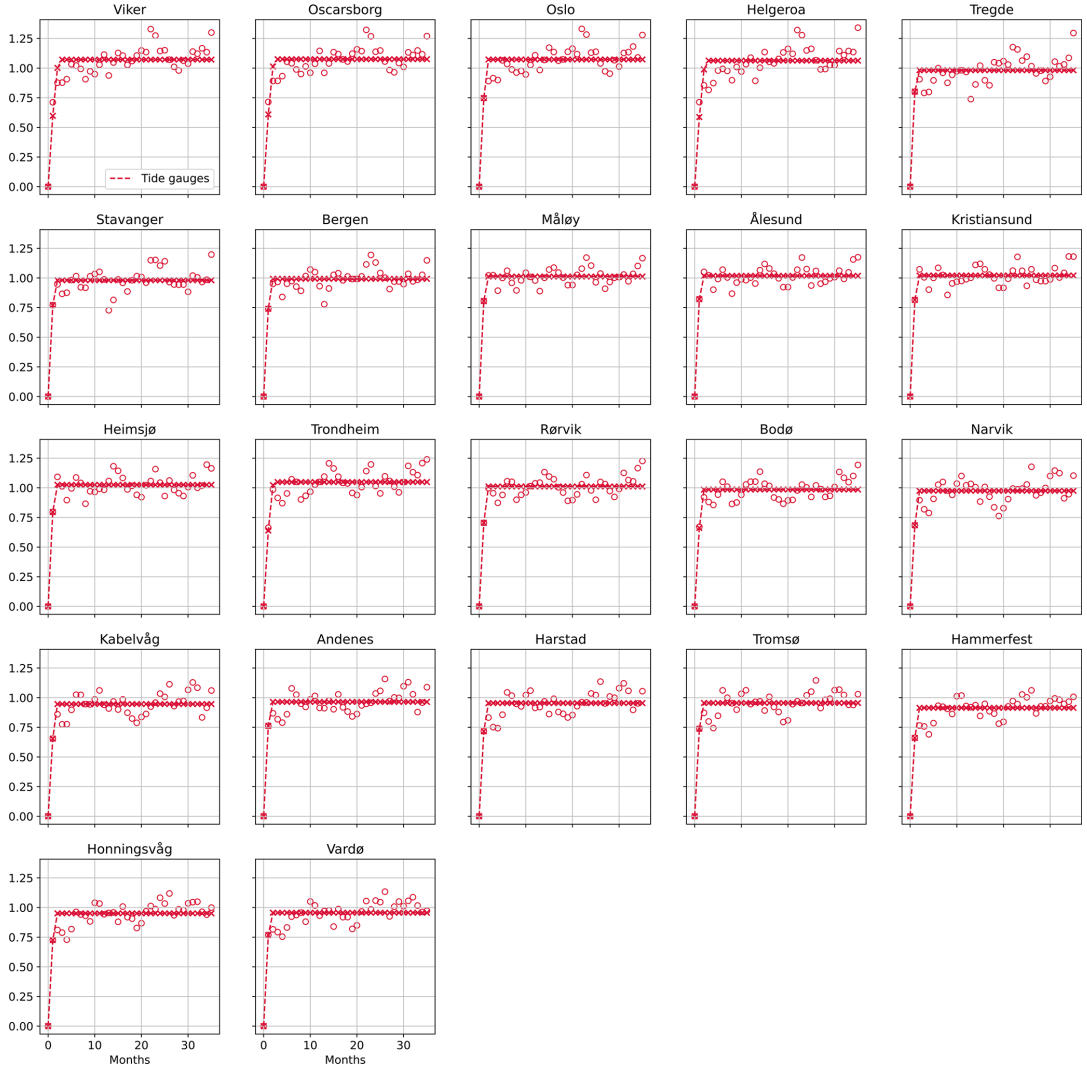

Figure A2. For each tide gauge along the Norwegian coast, semi-variogram of the detrended and deseasoned SLA measured by the tide gauge (empty circles) and corresponding fit (crosses connected by a dashed line). At each tide-gauge location, we scaled each semi-variogram by the variance of the corresponding detrended and deseasoned SLA for all the plots to have the same limits on the y axis.

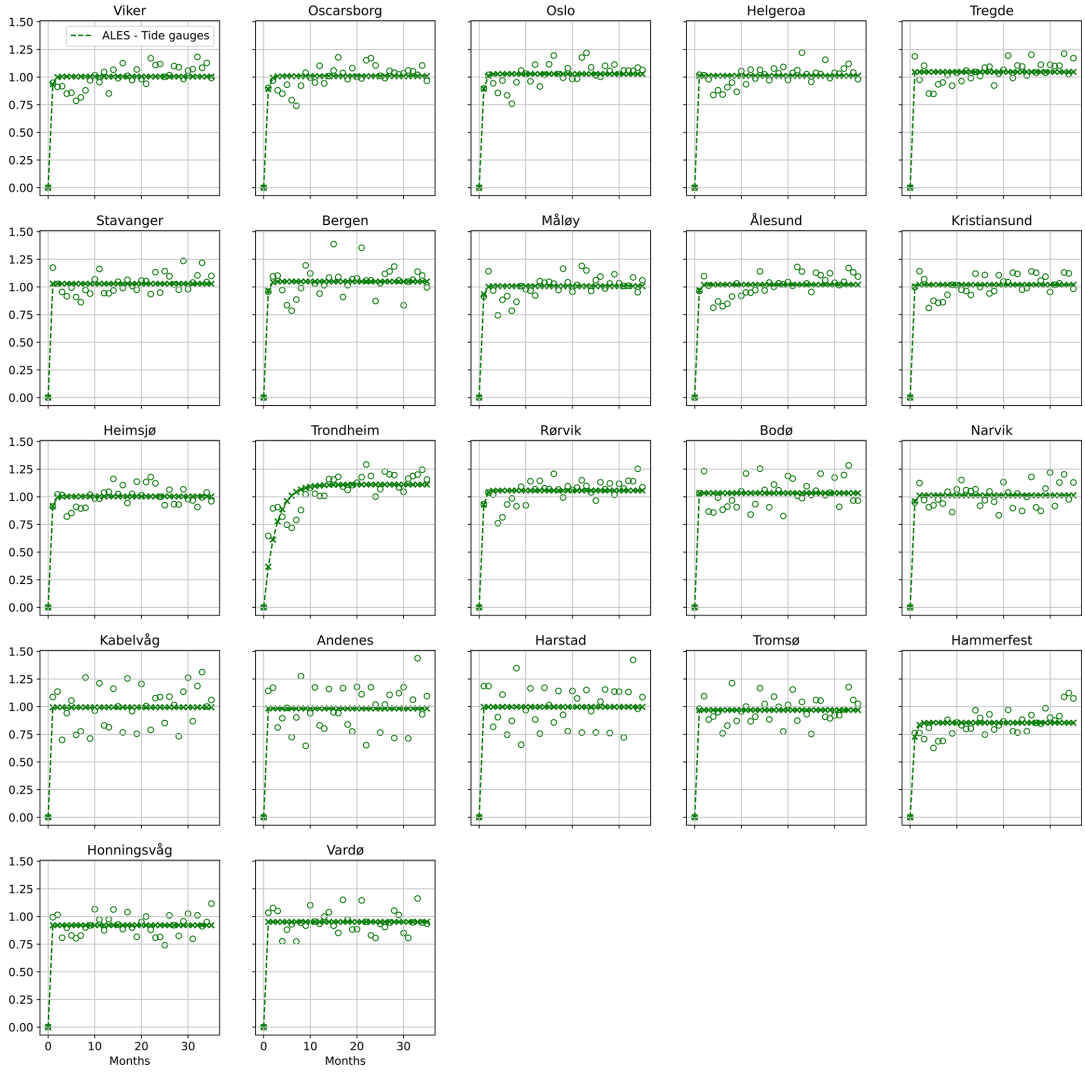

Figure A3. For each tide gauge along the Norwegian coast, semi-variogram of the difference between the detrended, deseasoned SLA estimated from the ALES-retracked satellite altimetry and from the tide gauge (empty circle) along with the corresponding fit (crosses connected by a dashed line). At each tide gauge location, we scaled each semi-variogram by the variance of the corresponding detrended and deseasoned SLA for all the plots to have the same limits on the y axis.

Appendix B

Following the same argument as in Appendix A, to estimate the uncertainty associated with the linear trends of the thermosteric, halosteric, and steric components of the sea level along the Norwegian coast (Fig. 12), we need to account for the effective degrees of freedom in the corresponding time series.

As in Appendix A, to determine the effective number of degrees of freedom, we first produce semi-variograms of the detrended and deseasoned thermosteric, halosteric, and steric components of the sea level at each hydrographic station. Then, we determine the time needed by the semi-variogram's fit to approximately reach a plateau, adopting an exponential function (see Appendix A).

The thermosteric sea level (Fig. B1) shows the strongest serial correlation. The semi-variogram of the thermosteric sea level returns lags ranging from 3 months at Indre Utsira to around 20 months at Skrova. In general, the thermosteric component of the sea level in northern Norway has fewer degrees of freedom than in the south.

The halosteric (Fig. B2) and the steric (Fig. B3) components show a similar pattern, with the number of effective degrees of freedom being smaller in the north than in the south. However, both components show a weaker serial correlation when compared to the thermosteric component of the sea level. Indeed, the semi-variograms return lags between 3 and 9 months for both components of the sea level.

Similarly to Appendix A, we use Eq. (A4) to compute the 95 % confidence interval of the linear trend of the SLA and of the thermosteric, halosteric, and steric components of the sea level at each hydrographic station. With respect to Eq. (A4), though, here we only consider $N^* - 2$ degrees of freedom since the linear model that we use to fit the time series has only two parameters (the offset and the angular coefficient of the straight line).

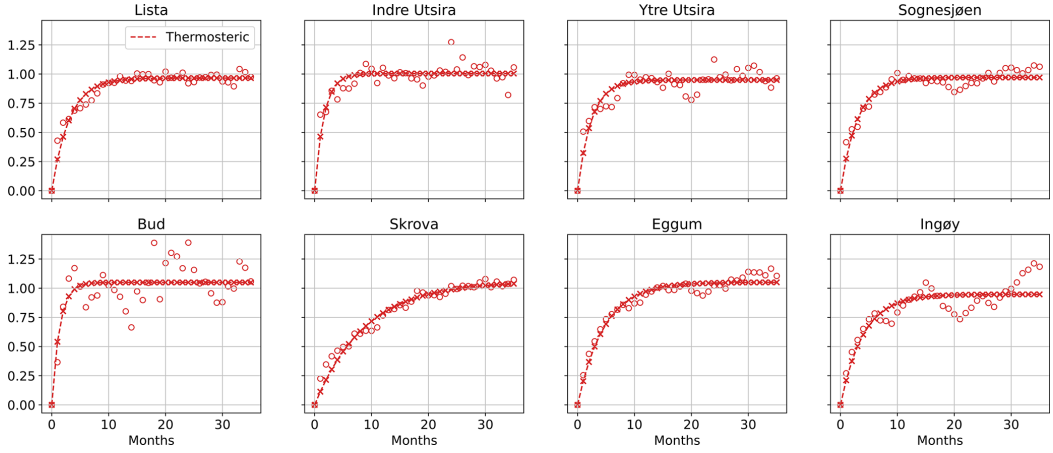

Figure B1. For each hydrographic station along the Norwegian coast, semi-variogram of the detrended and deseasoned thermosteric component of the sea-level variability (empty circles) and corresponding fit (crosses connected by a dashed line). At each hydrographic station location, we scaled each semi-variogram by the variance of the corresponding detrended and deseasoned thermosteric component of the sea level for all the plots to have the same limits on the y axis.

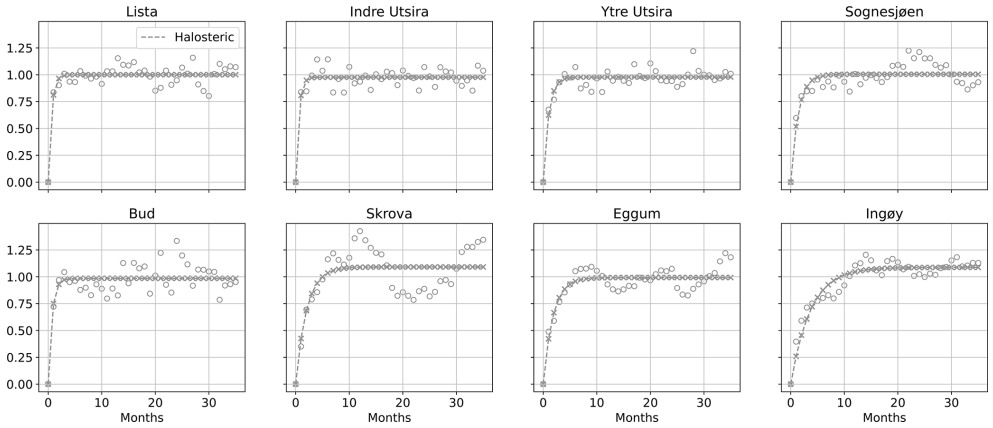

Figure B2. For each hydrographic station along the Norwegian coast, semi-variogram of the detrended and deseasoned halosteric component of the sea-level variability (empty circles) and corresponding fit (crosses connected by a dashed line). At each hydrographic station location, we scaled each semi-variogram by the variance of the corresponding detrended and deseasoned halosteric component of the sea level for all the plots to have the same limits on the y axis.

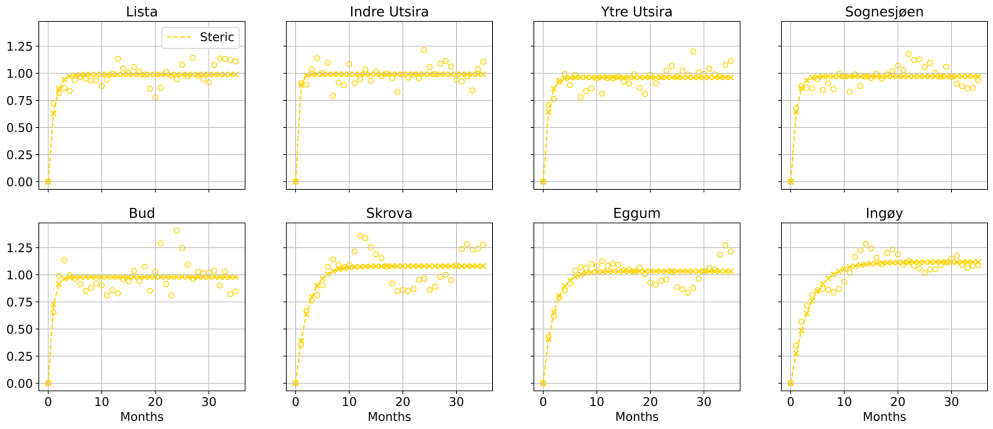

Figure B3. For each hydrographic station along the Norwegian coast, semi-variogram of the detrended and deseasoned steric component of the sea-level variability (empty circles) and corresponding fit (crosses connected by a dashed line). At each hydrographic station location, we scaled each semi-variogram by the variance of the corresponding detrended and deseasoned steric component of the sea level for all the plots to have the same limits on the y axis.

Appendix C

To compare the performance of the ALES-retracked and the conventional satellite altimetry dataset (Figs. C1, C2, C3, C4, and C5), we have downloaded the along-track L3 satellite altimetry missions provided on the Copernicus website: https://resources.marine.copernicus.eu/product-download/SEALEVEL_GLO_PHY_L3_REP_OBSERVATIONS_008_062 (last access: 2 September 2021). We should remember that the discrepancy between the two datasets might result not only from the different retrackers, but also from the different geophysical corrections applied to the data.

We select the same satellite altimetry missions that have been reprocessed with the ALES retracker, and we make sure that both satellite altimetry datasets cover the same period.

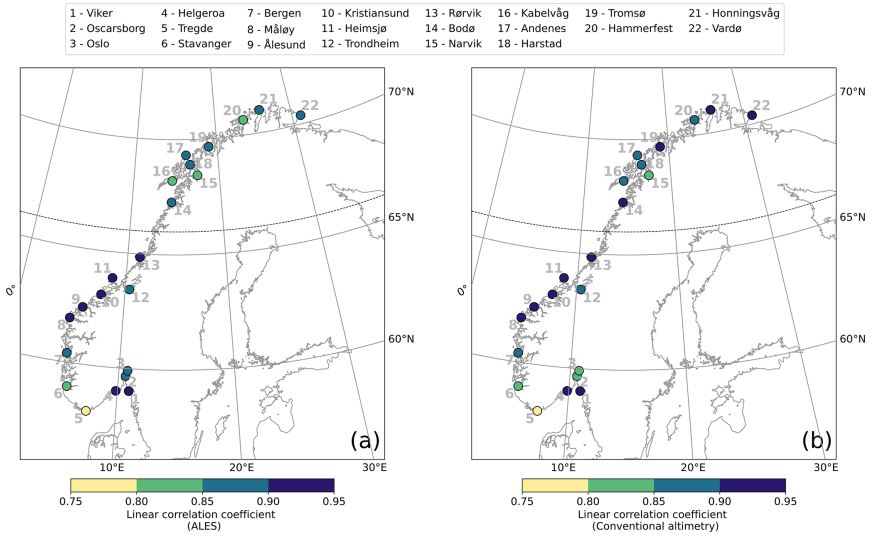

Figure C1. At each tide gauge location, linear correlation coefficient between the detrended, deseasoned monthly mean SLA estimated from the ALES-reprocessed satellite altimetry dataset and from the tide gauge **(a)**, as well as from the conventional altimetry dataset and from the tide gauge **(b)**. The black dashed line indicates the 66° N parallel.

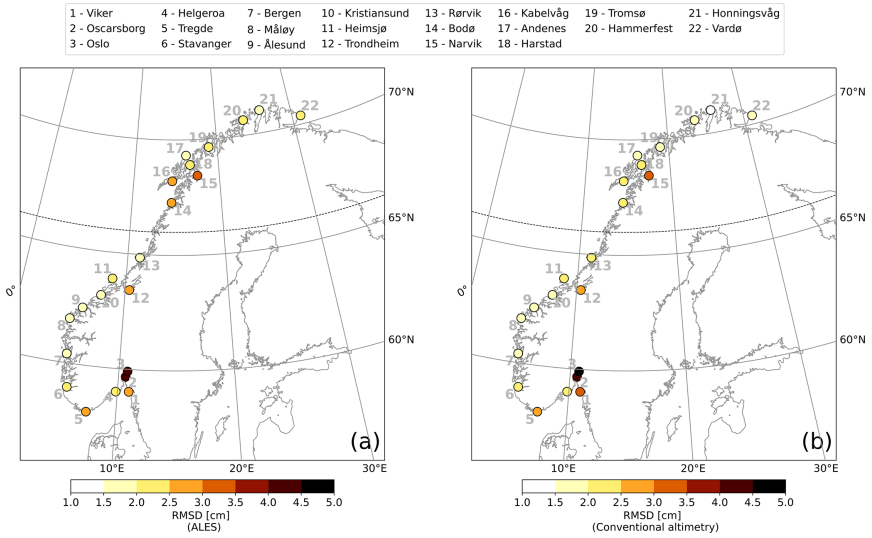

Figure C2. At each tide gauge location, RMSD of the detrended, deseasoned monthly mean SLA estimated from the ALES-reprocessed satellite altimetry dataset and from the tide gauge **(a)**, as well as from the conventional altimetry dataset and from the tide gauge (**b**). The black dashed line indicates the 66° N parallel.

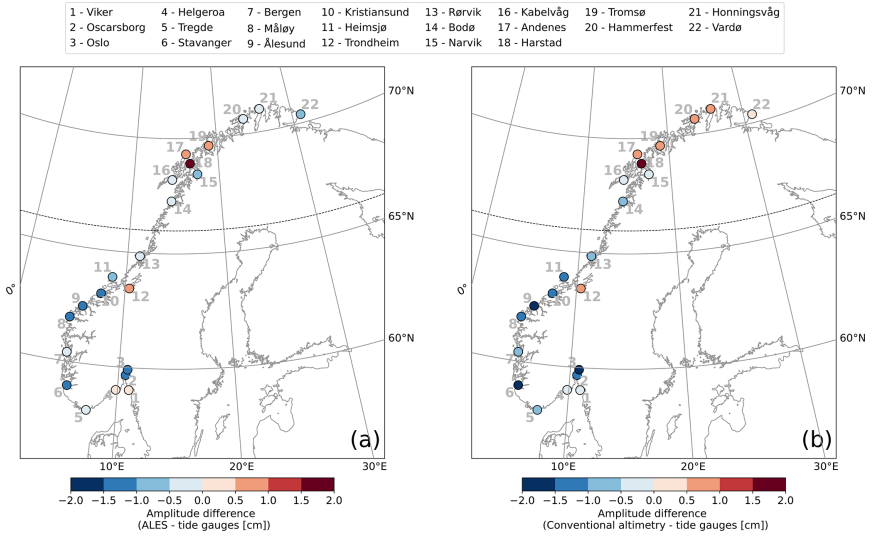

Figure C3. At each tide gauge location, difference between the amplitude of the sea-level annual cycle estimated from the ALES-reprocessed satellite altimetry dataset and from the tide gauge **(a)**, as well as from the conventional altimetry dataset and from the tide gauge (**b**). The black dashed line indicates the 66° N parallel.

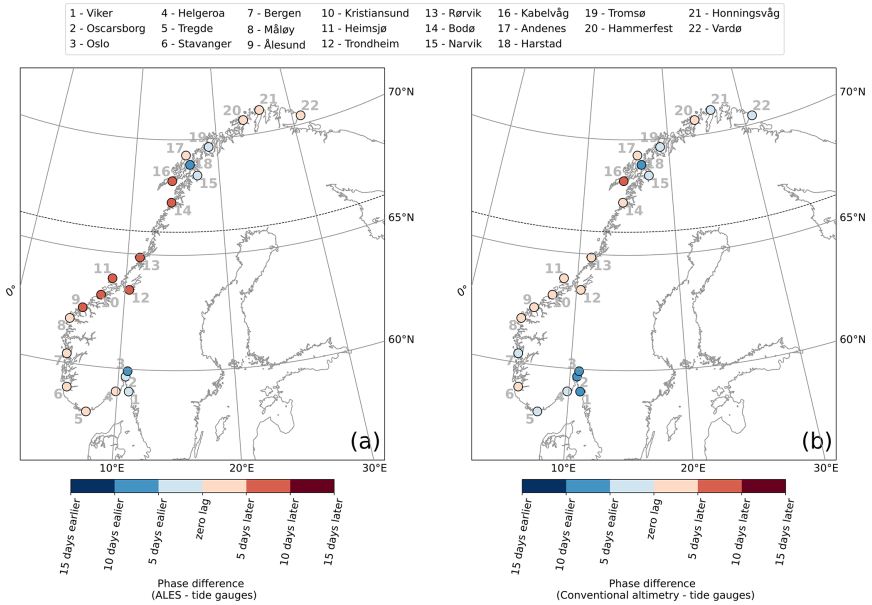

Figure C4. At each tide gauge location, difference between the phase of the sea-level annual cycle estimated from the ALES-reprocessed satellite altimetry dataset and from the tide gauge **(a)**, as well as from the conventional altimetry dataset and from the tide gauge (**b**). The black dashed line indicates the 66° N parallel.

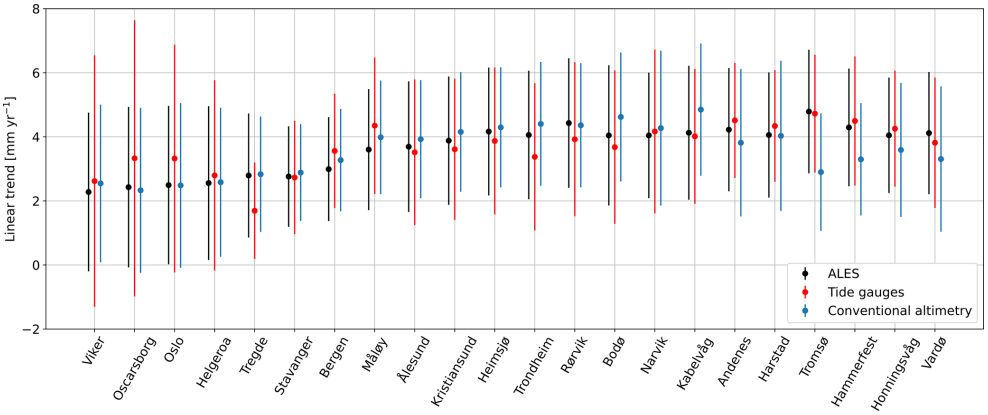

Figure C5. At each tide-gauge location, the linear trend of the SLA from the ALES-reprocessed altimetry dataset (black dots), the conventional altimetry dataset (cyan dots), and tide gauges (red dots). The error bars show the 95th confidence intervals of the sea-level trend at each tide-gauge location.

Data availability. The tide gauges are available and distributed by the Norwegian Mapping Authority, Hydrographic Service (https://www.kartverket.no/en/api-and-data/tidal-and-water-level-data; last access: on 28 April 2021). The ALES-retracked satellite altimetry dataset was produced by DGFI-TUM and distributed via OpenADB (https://openadb.dgfi.tum.de; last access: 22 July 2020). More information on the ALES retracker and the dataset is available in Passaro et al. (2014, 2015, 2017). The conventional altimetry dataset can be accessed from the Copernicus website at https://resources.marine.copernicus.eu/product-download/SEALEVEL_GLO_PHY_L3_REP_OBSERVATIONS_008_062 (last access: 2 September 2021). The hydrographic station datasets (Aure and Østensen, 1993), obtained from the Institute of Marine Research in Bergen, are updated and available at https://www.imr.no/forskning/forskningsdata/stasjoner/index.html (last access: 11 November 2020).

Author contributions. FM, AB, LC, and LB designed the research study. JEØN removed the geophysical signal from the sea level measured by the tide gauges. FM wrote the code to analyse the data. All authors contributed to the analysis of the results and to the writing and editing of the paper.

Competing interests. The contact author has declared that neither they nor their co-authors have any competing interests.

Disclaimer. Publisher's note: Copernicus Publications remains neutral with regard to jurisdictional claims in published maps and institutional affiliations.

Acknowledgements. We would like to thank the two reviewers, who helped significantly improved this paper. All products are computed based on altimetry missions operated by NASA/CNES (Jason-1), ESA (Envisat, Cryosat-2), CNES/NASA/Eumetsat/NOAA (Jason-2, Jason-3), and ISRO/CNES (SARAL). The original datasets are disseminated by AVISO, ESA, NOAA, and PODAAC. Michael Hart-Davis (TUM) is kindly acknowledged for providing the EOT11a tidal model data and Kristian Breili (Norwegian Mapping Authority) for providing the GIA data. Léon Chafik acknowledges support from the Swedish National Space Agency (Dnr: 133/17, 204/19) and the UK Natural Environmental Research Council (NERC) under UK-OSNAP (Overturning in the Subpolar North Atlantic Programme; NE/T00858X/1).

Financial support. This research has been supported by the Swedish National Space Agency (FiNNESS (grant no. 133/17), OCASES (grant no. 204/19)), the UK Natural Environmental Research Council (NERC) under UK-OSNAP (Overturning in the Subpolar North Atlantic Programme; NE/T00858X/1), and the Norges Forskningsråd (grant no. 272411).

Review statement. This paper was edited by Mario Hoppema and reviewed by three anonymous referees.

References

Abulaitijiang, A., Andersen, O. B., and Stenseng, L.: Coastal sea level from inland CryoSat-2 interferometric SAR altimetry, Geophys. Res. Lett., 42, 1841–1847, https://doi.org/10.1002/2015GL063131, 2015.

Aure, J. and Østensen, Ø.: Hydrographic normals and long-term variations in Norwegian coastal waters, Fisken og Havet, 6, 75 pp., https://resources.marine.copernicus.eu/product-download/SEALEVEL_GLO_PHY_L3_REP_OBSERVATIONS_008_062 (last access: 2 September 2021), 1993.

Bartlett, M. S.: Some Aspects of the Time-Correlation Problem in Regard to Tests of Significance, J. R. Stat. Soc., 98, 536–543, https://doi.org/10.2307/2342284, 1935.

Benveniste, J., Birol, F., Calafat, F., Cazenave, A., Dieng, H., Gouzenes, Y., Legeais, J. F., Léger, F., Niño, F., Passaro, M., Schwatke, C., and Shaw, A.: Coastal sea level anomalies and associated trends from Jason satellite altimetry over 2002–2018, Sci. Data, 7, 1–17, https://doi.org/10.1038/s41597-020-00694-w, 2020.

Bonaduce, A., Pinardi, N., Oddo, P., Spada, G., and Larnicol, G.: Sea-level variability in the Mediterranean Sea from altimetry and tide gauges, Clim. Dynam., 47, 2851–2866, https://doi.org/10.1007/s00382-016-3001-2, 2016.

Breili, K., Simpson, M. J. R., and Nilsen, J. E. Ø.: Observed sea-level changes along the Norwegian coast, J. Mar. Sci. Eng., 5, 1–19, https://doi.org/10.3390/jmse5030029, 2017.

Carrère, L. and Lyard, F.: Modeling the barotropic response of the global ocean to atmospheric wind and pressure forcing – Comparisons with observations, Geophys. Res. Lett., 30, 1275, https://doi.org/10.1029/2002GL016473, 2003.

Cazenave, A., Palanisamy, H., and Ablain, M.: Contemporary sea level changes from satellite altimetry: What have we learned? What are the new challenges?, Adv. Space Res., 62, 1639–1653, https://doi.org/10.1016/j.asr.2018.07.017, 2018.

Chafik, L., Nilsson, J., Skagseth, Ø., and Lundberg, P.: On the flow of Atlantic water and temperature anomalies in the Nordic Seas toward the Arctic Ocean, J. Geophys. Res.-Oceans, 120, 7897–7918, https://doi.org/10.1002/2015JC011012, 2015.

Chafik, L., Nilsen, J. E. Ø., and Dangendorf, S.: Impact of North Atlantic teleconnection patterns on northern European sea level, J. Mar. Sci. Eng., 5, 1–23, https://doi.org/10.3390/jmse5030043, 2017.

Chafik, L., Nilsen, J. E. Ø., Dangendorf, S., Reverdin, G., and Frederikse, T.: North Atlantic Ocean Circulation and Decadal Sea Level Change During the Altimetry Era, Sci. Rep., 9, 1–9, https://doi.org/10.1038/s41598-018-37603-6, 2019.

Cipollini, P., Benveniste, J., Bouffard, J., Emery, W., Fenoglio-Marc, L., Gommenginger, C., Griffin, D., Høyer, J., Kuparov, A., Madsen, K., Mercier, F., Miller, L., Pascual, A., Ravichandran, M., Shillington, F., Snaith, H., Sturb, P. T., Vandemark, D., Vignudelli, S., Wilkin, J., Woodworth, P., and Zavala-Garay, J.: The Role of Altimetry in Coastal Observing Systems, in: Proceedings of OceanObs'09: sustained ocean observations and information for society, vol. 2, edited by: Hall,

J., Harrison, D. E., and Stammer, D., 21–25 September 2009, Venice, Italy, European Space Agency, WPP-306, 181–191, https://doi.org/10.5270/oceanobs09.cwp.16, 2010.

Cipollini, P., Benveniste, J., Birol, F., Joana Fernandes, M., Obligis, E., Passaro, M., Ted Strub, P., Valladeau, G., Vignudelli, S., and Wilkin, J.: Satellite altimetry in coastal regions, in: Satellite Altimetry Over Oceans and Land Surfaces, Surv. Geophys., 38, 33–57, https://doi.org/10.1201/9781315151779, 2017.

Frederikse, T., Jevrejeva, S., Riva, R. E. M., and Dangendorf, S.: A consistent sea-level reconstruction and its budget on basin and global scales over 1958–2014, J. Climate, 31, 1267–1280, https://doi.org/10.1175/JCLI-D-17-0502.1, 2018.

Frederikse, T., Landerer, F., Caron, L., Adhikari, S., Parkes, D., Humphrey, V. W., Dangendorf, S., Hogarth, P., Zanna, L., Cheng, L., and Wu, Y. H.: The causes of sea-level rise since 1900, Nature, 584, 393–397, https://doi.org/10.1038/s41586-020-2591-3, 2020.

Gill, A. E. and Niiler, P. P.: The theory of the seasonal variability in the ocean, Deep Sea Res. Oceanogr. Abstr., 20, 141–177, https://doi.org/10.1016/0011-7471(73)90049-1, 1973.

Gómez-Enri, J., Vignudelli, S., Quartly, G. D., Gommenginger, C. P., Cipollini, P., Challenor, P. G., and Benveniste, J.: Modeling Envisat RA-2 waveforms in the coastal zone: Case study of calm water contamination, IEEE Geosci. Remote S., 7, 474–478, https://doi.org/10.1109/LGRS.2009.2039193, 2010.

Hermans, T. H. J., Gregory, J. M., Palmer, M. D., Ringer, M. A., Katsman, C. A., and Slangen, A. B. A.: Projecting Global Mean Sea-Level Change Using CMIP6 Models, Geophys. Res. Lett., 48, e2020GL092064, https://doi.org/10.1029/2020GL092064, 2021.

Ji, M., Reynolds, R. W., and Behringer, D. W.: Use of TOPEX/Poseidon sea level data for Ocean analyses and ENSO prediction: Some early results, J. Climate, 13, 216–231, https://doi.org/10.1175/1520-0442(2000)013<0216:UOTPSL>2.0.CO;2, 2000.

Lichter, M., Vafeidis, A. T., Nicholls, R. J., and Kaiser, G.: Exploring data-related uncertainties in analyses of land area and population in the "Low-Elevation Coastal Zone" (LECZ), J. Coastal Res., 27, 757–768, https://doi.org/10.2112/JCOASTRES-D-10-00072.1, 2011.

Liebmann, B., Dole, R. M., Jones, C., Bladé, I., and Allured, D.: Influence of choice of time period on global surface temperature trend estimates, B. Am. Meteorol. Soc., 91, 1485–1491, https://doi.org/10.1175/2010BAMS3030.1, 2010.

Madsen, K. S., Høyer, J. L., Suursaar, Ü., She, J., and Knudsen, P.: Sea Level Trends and Variability of the Baltic Sea From 2D Statistical Reconstruction and Altimetry, Front. Earth Sci., 7, 243, https://doi.org/10.3389/feart.2019.00243, 2019.

Nerem, R. S., Chambers, D. P., Choe, C., and Mitchum, G. T.: Estimating Mean Sea Level Change from the TOPEX and Jason Altimeter Missions, Mar. Geod., 33, 435–446, https://doi.org/10.1080/01490419.2010.491031, 2010.

Nicholls, R. J.: Planning for the Impacts of Sea Level Rise, Oceanography, 24, 144–157, 2011.

Oelsmann, J., Passaro, M., Dettmering, D., Schwatke, C., Sánchez, L., and Seitz, F.: The zone of influence: matching sea level variability from coastal altimetry and tide gauges for vertical land motion estimation, Ocean Sci., 17, 35–57, https://doi.org/10.5194/os-17-35-2021, 2021.

Passaro, M., Cipollini, P., Vignudelli, S., Quartly, G. D., and Snaith, H. M.: ALES: A multi-mission adaptive subwaveform retracker for coastal and open ocean altimetry, Remote Sens. Environ., 145, 173–189, https://doi.org/10.1016/j.rse.2014.02.008, 2014 (https://openadb.dgfi.tum.de, last access: 22 July 2020).

Passaro, M., Cipollini, P., and Benveniste, J.: Annual sea level variability of the coastal ocean: The Baltic Sea-North Sea transition zone, J. Geophys. Res.-Oceans, 120, 3061–3078, https://doi.org/10.1002/2014JC010510, 2015 (https://openadb.dgfi.tum.de, last access: 22 July 2020).

Passaro, M., Dinardo, S., Quartly, G. D., Snaith, H. M., Benveniste, J., Cipollini, P., and Lucas, B.: Cross-calibrating ALES Envisat and CryoSat-2 Delay-Doppler: A coastal altimetry study in the Indonesian Seas, Adv. Space Res., 58, 289–303, https://doi.org/10.1016/j.asr.2016.04.011, 2016.

Passaro, M., Smith, W., Schwatke, C., Piccioni, G., and Dettmering, D.: Validation of a global dataset based on subwaveform retracking: improving the precision of pulse-limited satellite altimetry, OSTST Meeting 2017, 23–27 October 2017, Miami, USA, 2017 (https://openadb.dgfi.tum.de, last access: 22 July 2020).

Passaro, M., Rose, S. K., Andersen, O. B., Boergens, E., Calafat, F. M., Dettmering, D., and Benveniste, J.: ALES+: Adapting a homogenous ocean retracker for satellite altimetry to sea ice leads, coastal and inland waters, Remote Sens. Environ., 211, 456–471, https://doi.org/10.1016/j.rse.2018.02.074, 2018.

Passaro, M., Müller, F. L., Oelsmann, J., Rautiainen, L., Dettmering, D., Hart-Davis, M. G., Abulaitijiang, A., Andersen, O. B., Høyer, J. L., Madsen, K. S., Ringgaard, I. M., Särkkä, J., Scarrott, R., Schwatke, C., Seitz, F., Tuomi, L., Restano, M., and Benveniste, J.: Absolute Baltic Sea Level Trends in the Satellite Altimetry Era: A Revisit, Front. Mar. Sci., 8, 647607, https://doi.org/10.3389/fmars.2021.647607, 2021.

Picaut, J., Hackert, E., Busalacchi, A. J., Murtugudde, R., and Lagerloef, G. S. E.: Mechanisms of the 1997–1998 El Niño–La Niña, as inferred from space-based observations, J. Geophys. Res., 107, 3037, https://doi.org/10.1029/2001jc000850, 2002.

Raj, R. P., Andersen, O. B., Johannessen, J. A., Gutknecht, B. D., Chatterjee, S., Rose, S. K., Bonaduce, A., Horwath, M., Ranndal, H., Richter, K., Palanisamy, H., Ludwigsen, C. A., Bertino, L., Nilsen, J. E. Ø., Knudsen, P., Hogg, A., Cazenave, A., and Benveniste, J.: Arctic sea level budget assessment during the grace/argo time period, Remote Sens., 12, 2837, https://doi.org/10.3390/rs12172837, 2020.

Richter, K., Nilsen, J. E. Ø., and Drange, H.: Contributions to sea level variability along the Norwegian coast for 1960–2010, J. Geophys. Res., 117, C05038, https://doi.org/10.1029/2011JC007826, 2012.

Richter, K., Meyssignac, B., Slangen, A. B. A., Melet, A., Church, J. A., Fettweis, X., Marzeion, B., Agosta, C., Ligtenberg, S. R. M., Spada, G., Palmer, M. D., Roberts, C. D., and Champollion, N.: Detecting a forced signal in satellite-era sea-level change, Environ. Res. Lett., 15, 094079, https://doi.org/10.1088/1748-9326/ab986e, 2020.

Rose, S. K., Andersen, O. B., Passaro, M., Ludwigsen, C. A., and Schwatke, C.: Arctic ocean sea level record from the complete radar altimetry era: 1991–2018, Remote Sens., 11, 1672, https://doi.org/10.3390/rs11141672, 2019.

Siegismund, F., Johannessen, J., Drange, H., Mork, K. A., and Korablev, A.: Steric height variability in

the Nordic Seas, J. Geophys. Res., 112, C12010, https://doi.org/10.1029/2007JC004221, 2007.

Simpson, M. J. R., Nilsen, J. E. Ø., Ravndal, O. R., Breili, K., Sande, H., Kierulf, H. P., Steffen, H., Jansen, E., Carson, M., and Vestøl, O.: Sea Level Change for Norway Past and Present Observations and Projections to 2100, Tech. rep., Norwegian Centre for Climate Services report 1/2015, ISSN 2387–3025, 156 pp., 2015.

Simpson, M. J. R., Ravndal, O. R., Sande, H., Nilsen, J. E. Ø., Kierulf, H. P., Vestøl, O., and Steffen, H.: Projected 21st century sea-level changes, observed sea level extremes, and sea level allowances for Norway, J. Mar. Sci. Eng., 5, 36, https://doi.org/10.3390/jmse5030036, 2017.

Stammer, D., Cazenave, A., Ponte, R. M., and Tamisiea, M. E.: Causes for contemporary regional sea level changes, Annu. Rev. Mar. Sci., 5, 21–46, https://doi.org/10.1146/annurev-marine-121211-172406, 2013.

Volkov, D. L. and Pujol, M. I.: Quality assessment of a satellite altimetry data product in the Nordic, Barents, and Kara seas, J. Geophys. Res., 117, C03025, https://doi.org/10.1029/2011JC007557, 2012.

Wackernagel, H.: Multivariate Geostatistics, 3rd edn., Springer, Berlin, Heidelberg, 388 pp., https://doi.org/10.1007/BF02769635, 2003.

Woodworth, P. L.: A note on the nodal tide in sea level records, J. Coastal Res., 28, 316–323, https://doi.org/10.2112/JCOASTRES-D-11A-00023.1, 2012.

Xu, X.-Y., Xu, K., Xu, Y., and Shi, L.-W.: Coastal Altimetry: A Promising Technology for the Coastal Oceanography Community, in: Estuaries and Coastal Zones – Dynamics and Response to Environmental Changes, Surv. Geophys., 40, 1351–1397, https://doi.org/10.5772/intechopen.89373, 2019.

Zhang, Z., Lu, Y., and Hsu, H.: Detecting ocean currents from satellite altimetry, satellite gravity and ocean data, in Dynamic Planet, International Association of Geodesy Symposia, edited by: Tregoning, P. and Rizos, C., Springer, Berlin, https://doi.org/10.1007/978-3-540-49350-1_3, 2007.

Graphic design: Communication Division, UiB / Print: Skipnes Kommunikasjon AS

uib.no

ISBN: 9788230846902 (print)
9788230854365 (PDF)